MODELING AND SIMULATION OF A NAVIGATION SYSTEM WITH AN IMU AND A MAGNETOMETER

A THESIS SUBMITTED TO
THE GRADUATE SCHOOL OF NATURAL AND APPLIED SCIENCES
OF
THE MIDDLE EAST TECHNICAL UNIVERSITY

BY

UĞUR KAYASAL

IN PARTIAL FULFILLMENT OF THE REQUIREMENTS
FOR
THE DEGREE OF MASTER OF SCIENCE
IN
MECHANICAL ENGINEERING

SEPTEMBER 2007

Approval of the thesis :

MODELING AND SIMULATION OF NAVIGATION SYSTEM WITH AN IMU AND A MAGNETOMETER

Submitted by **UĞUR KAYASAL** in partial fulfillment of the requirements for the degree of **Master of Science in Mechanical Engineering Department, Middle East Technical University by,**

Prof. Dr. Canan ÖZGEN _____
Dean, Graduate School of **Natural and Applied Sciences**

Prof. Dr. KEMAL İDER _____
Head of the Department, **Mechanical Engineering**

Prof. Dr. M. Kemal ÖZGÖREN _____
Supervisor, **Mechanical Engineering Dept., METU**

Dr. Osman MERTTOPÇUOĞLU _____
Co-Supervisor, **Chief Engineer, ROKETSAN**

Examining Committee Members

Prof. Dr. Bülent E. PLATIN _____
Mechanical Enginering Dept., METU

Prof. Dr. M. Kemal ÖZGÖREN _____
Mechanical Enginering Dept., METU

Prof. Dr. Reşit SOYLU _____
Mechanical Enginering Dept., METU

Prof. Dr. Ozan TEKİNALP _____
Mechanical Enginering Dept., METU

Dr. Osman MERTTOPÇUOĞLU _____
Chief Engineer, ROKETSAN

Date: _____

I hereby declare that all information in this document has been obtained and presented in accordance with academic rules and ethical conduct. I also declare that, as required by these rules and conduct, I have fully cited and referenced all material and results that are not original to this work.

Name, Last name : UĞUR KAYASAL

Signature :

ABSTRACT

MODELING AND SIMULATION OF NAVIGATION SYSTEM WITH AN IMU AND A MAGNETOMETER

KAYASAL, UĞUR
M.S., Department of Mechanical Engineering
Supervisor: Prof. Dr. M. Kemal ÖZGÖREN
Co-Supervisor: Dr. Osman MERTTOPÇUOĞLU
September 2007, 173 pages

In this thesis, the integration of a MEMS based inertial measurement unit and a three axis solid state magnetometer are studied.

It is a fact that unaided inertial navigation systems, especially low cost MEMS based navigation systems have a divergent behavior. Nowadays, many navigation systems use GPS aiding to improve the performance, but GPS may not be applicable in some cases. Also, GPS provides the position and velocity reference whereas the attitude information is extracted through estimation filters. An alternative reference source is a three axis magnetometer, which provides direct attitude measurements.

In this study, error propagation equations of an inertial navigation system are derived; measurement equations of magnetometer for Kalman filtering are

developed; the unique method to self align the MEMS navigation system is developed. In the motion estimation, the performance of the developed algorithms are compared using a GPS aided system and magnetometer aided system. Some experiments are conducted for self alignment algorithms.

Keywords: Inertial navigation system, magnetometer, MEMS, Kalman filter

ÖZ

AÖB VE MANYETOMETRELİ BİR SEYRÜSEFER SİSTEMİNİN MODELLENMESİ VE BENZETİMİ

KAYASAL, Uğur
Yüksek Lisans, Makina Mühendisliği Bölümü
Tez Yöneticisi: Prof. Dr. M. Kemal ÖZGÖREN
Ortak Tez Yöneticisi: Dr. Osman MERTTOPÇUOĞLU

Eylül 2007, 173 sayfa

Bu tezde, MEMS tabanlı bir ataletsel ölçüm birimi ile üç eksenli bir manyetometrenin tümleştirilmesi üzerinde çalışılmıştır.

Bilindiği gibi desteklenmeyen ataletsel seyrüsefer sistemlerinin, özellikle ucuz MEMS tabanlı seyrüsefer sistemlerin, ıraksayan bir yapısı vardır. Günümüzde çoğu seyrüsefer sistemi GPS ölçümlerini destek amaçlı olarak kullanmaktadır. Ancak, GPS ölçümlerinin kullanılamadığı durumlar bir çok sistem için mevcuttur. Ayrıca, GPS doğrusal konum ve hız bilgisi sağlarken, açısal konum bilgisi de kestirim filtreleri kullanılarak elde edilir. Alternatif bir destek kaynağı da üç eksenli manyetometre kullanımıdır.

Bu çalışmada, ataletsel seyrüsefer sisteminin hata ilerleme denklemleri çıkartılmış; Kalman filtresinde kullanılmak üzere manyetometre ölçüm denklemleri türetilmiş; kendi kendine ilk hizalama algoritmaları hazırlanmıştır. Hareket halindeki kestirim performansları GPS ve manyetometre desteklemeleri kullanılarak karşılaştırılmıştır. İlk hizalama algoritmaları için deneysel çalışmalar yapılmıştır.

Anahtar kelimeler: Ataletsel seyrüsefer sistemi, manyetometre, MEMS, Kalman filtresi

To my wife Hacer…

ACKNOWLEDGMENTS

I would like to express my gratitude to my supervisor Prof. Dr. M.Kemal Özgören for his never ending guidance, patience, advice, understanding, and support throughout my research.

I would also like to express my appreciation to Dr. Osman Merttopçuoğlu for his guidance, support, patience and encouragement.

I am grateful to my colleagues at ROKETSAN for their invaluable comments and suggestions.

Dr. Sartuk Karasoy and Mr. Bülent Semerci are kindly acknowledged for their support in this thesis.

I would like to thank my family for their support, guidance and encouragement.

Finally, I would like to thank to my wife Hacer for her everlasting support and love. Without her support, this work could not be completed.

ROKETSAN A.Ş. who supported this work is greatly acknowledged.

TABLE OF CONTENTS

LIST OF SYMBOLS AND ABBREVIATIONS

Symbol	Definition
ψ	Azimuth angle
θ	Pitch angle
ϕ	Roll angle
a	Acceleration
w	Angular rates
S_x	Scale factor error in x axis
m_{xy}	Misalignment error between x and y axis
δC_b^n	Error Direction cosine matrix
ω_{ib}^b	Angular rates between body and inertial frame, defined in body frame
ω_{in}^n	Angular rates between navigation and inertial frame, defined in navigation frame
$\delta\omega_{ib}^b$	Error in angular rates between body and inertial frame, defined in body frame
$\delta\omega_{in}^n$	Error in angular rates between navigation and inertial frame, defined in navigation frame
γ^n	Misalignment vector defining the error in DCM
n	Navigation frame
b	Body frame
i	Inertial frame

H^N	Magnetic reference vector defined in navigation frame
B^B	Magnetic measurement vector defined in body frame
ν	Gaussian noise
x_k	State vector
w_k	Process Noise vector
A_k	System matrix
Q_k	Process Noise covariance matrix
v_k	Measurement Noise vector
H_k	Measurement matrix
z_k	Measurement vector
R_k	Measurement Noise covariance matrix
K_k	Kalman Gain
P_k	State Covariance Matrix
Ω	Magnitude of Earth rotation rate
R	The length of semi major axis
r	The length of semi minor axis
f	The flattening of semi minor axis
e	The major eccentricity
L	Latitude
l	Longitude
h	Altitude
g	Gravity vector
V	Velocity
ε	Position errors
$\tilde{w}$	Cross product matrix form

Abbreviation	Definition
INS	Inertial Navigation System
IMU	Inertial Measurement Unit
GPS	Global Positioning System
TAM	Three Axis Magnetometer
FOG	Fiber Optic Gyro
RLG	Ring Laser Gyro
MEMS	Micro Electro Mechanical System
TERCOM	Terrain Contour Matching
DSMAC	Digital Scene Matching Area Correlation
WMM	World Magnetic Model
RMS	Root Mean Square

Throughout the text,

Numbers in brackets	DENOTE	References
Numbers in parenthesis		Equations

CHAPTER 1

INTRODUCTION

1.1 Motivation

Inertial Navigation systems are widely used in several areas, (especially in military areas, e.g. guided munitions) since WW2. The high accuracy inertial navigation systems (e.g. dynamically tuned gyros, pendulous accelerometers, fiber optic gyros (FOG), ring laser gyros (RLG)) have high accuracy, but these systems are very expensive. (~10k$-100k$) [1].

MEMS (Micro Electro Mechanical System) technology is being widely used for the last ten years in inertial measurement systems. Nowadays, MEMS accelerometers are used in tactical grade systems. These sensors have high accuracies such as 0.01 m/s^2 bias and they are very cheap (~1k$) relative to accelerometers with older technologies (~5-10k$). MEMS gyros are also widely used in many areas, they provide a cheap solution to inertial sensing, but unfortunately they are not mature enough to provide tactical grade (~1deg/hr bias) accuracy, where RLGs or FOGs can have such accuracy. MEMS gyros have high bias values (100-1000 deg/hr) and high noise (1-10deg/√hr), which results in cumulative errors in attitude solution [2]. Therefore, these gyros need some kind of aiding to preserve accuracy.

1.2 Current Applications and Drawbacks

There are different aiding alternatives to aid MEMS IMUs. Most navigation systems use GPS as an aiding source, which provides position and velocity to the estimation filter. Attitude errors are indirect observables in these systems, requiring more time to have the errors to be converged in the estimation filter. [1, 3]

Magnetometers are generally used as a reference system for North finding purposes. In satellite attitude determination and control systems, magnetometers are used as measurement in estimation filters, in which attitude dynamics are used as the main system [4, 5, and 6]. In most of the military navigation systems, attitude dynamics cannot be modeled accurately enough to be used in Kalman Filter as these dynamics are very complex to be modeled in a linear filter [6]. Generally, attitude kinematics is modeled rather than the attitude dynamics. Therefore, main system states, the navigation errors and sensor errors are derived from inertial navigation systems.

1.3 Objectives of the Thesis

In this thesis, magnetometers are proposed as an aiding source to the low cost MEMS IMUs. In the proposed system, the inertial navigation system error propagation models are used as the system model. Nonlinear error models are developed; these models are linearized to be used in the estimation filter with appropriate assumptions. Magnetometers provide attitude data with the help of the reference magnetic field model. In this thesis, World Magnetic Model 2005 [7], which is the most recent magnetic model is used as the reference magnetic model of the world. This model is being widely used in satellite attitude determination systems.

In the proposed system, there are two modes of operation; namely alignment mode and navigation mode. High accuracy navigation systems can make self alignment, by using gravity vector and earth rotation rate as reference information [6]. In the low cost IMUs, the gravity vector may be used as reference but low accuracy gyros prevent the use of earth rate data, because these gyros have high bias values greater than the earth rotation rate, which make this rate unobservable. For low cost systems, there are different alignment algorithms. Transfer alignment requires a reference (master) navigation system (either an INS or GPS), which may not be used some cases, such as where there is no host system for transfer alignment, or where GPS signals are not available. [7].

In this thesis, a new alignment method is proposed. Instead of earth rotation rate, magnetometer measurements are used. In the alignment mode, the gravity vector and magnetometer measurements are used in an analytical method, known as coarse alignment, therefore reduce the attitude errors in a quick manner. After the alignment mode, the navigation system can proceed into navigation mode. In the navigation mode, the INS uses only magnetometers as an aiding source. Magnetometers provide measurement data for attitude errors and angular rate errors. Thus, velocity, position errors and accelerometer error states are not observable. But the main disturbing factor in the navigation solution, the gyro based errors are estimated. As the system is aligned before entering into navigation mode, the initial attitude errors are small enough (even only coarse alignment is completed), thus linear error models can be used. The system performance is demonstrated by Monte Carlo simulations.

1.4 Outline of the Thesis

Chapter 1 gives an introduction and brief information about this thesis study.

In Chapter 2, fundamental information about Inertial navigation systems are presented. Inertial navigation mechanization equations, linear error model of inertial navigation and inertial measurement systems are given.

In Chapter 3, magnetometer technology is introduced. Brief information about reference magnetic field, magnetometer types and error behavior of magnetometers are presented.

In Chapter 4, Kalman filter and its implementation techniques are given. Advantages and disadvantages of the Kalman Filter is discussed.

In Chapter 5, attitude determination with vector measurement algorithms are derived. Classical attitude determination algorithm with two vector measurements is given. Measurement equations for Kalman filter implementation are derived. A novel analytical solution with one vector measurement and two gyros is introduced.

In Chapter 6 and 7, the simulation studies are carried out. An alignment method for MEMS IMUs is tested by Monte Carlo simulations and experiments. Dynamic performance of the developed algorithms is simulated in an air defense missile case.

In chapter 8, the summary of this study is given. Conclusions and recommendations for future works are presented in this chapter.

CHAPTER 2

STRAPDOWN INERTIAL NAVIGATION SYSTEMS

This chapter presents the fundamentals of strapdown inertial navigation systems (SINS). The inertial measurement unit is defined and the error sources of inertial sensors are given. Kinematic equations that are used in a strapdown inertial navigation system are derived. The linear error propagation model of SINS is derived with some appropriate assumptions.

2.1 Inertial Measurement Unit

An inertial measurement unit (IMU) is a closed system that is used to detect attitude, location, and motion. Typically installed on aircraft or missiles, it normally uses a combination of accelerometers and angular rate sensors (gyroscopes) to track how the craft is moving and where it is. The term IMU is widely used to refer to a box, containing 3 accelerometers and 3 gyroscopes. The Accelerometers and gyros are placed such that their measuring axes are orthogonal to each other. They measure the so-called "specific forces [1, 2, and 3].

Typically, an IMU detects the current acceleration and rate of change in attitude (i.e. pitch, roll and yaw rates) and then integrates them to find the total change from the initial position. IMUs typically suffer from the accumulated error. Because an IMU is continually adding detected changes to the current position, any error in the measurement is accumulated.

An IMU is a self sufficient, autonomous system; that is, it does need any external electromagnetic signal to be operational, thus it can work in almost all environments (e.g. , underwater, indoor, and underground. Also, an IMU cannot be jammed like GPS. Unlike GPS, an IMU can provide very high data output rates (~1 kHz), which makes it possible to track high dynamic maneuvers [3].

IMU errors result in cumulative navigation errors. High quality inertial sensors provide a more stable navigation solution with a burden in cost. On the other hand, low cost inertial sensors are cheap but suffer in accuracy. Other systems such as GPS (used to correct for long term drift in position), a barometric system (for altitude correction), or as proposed in this thesis, a magnetometer (for attitude correction) compensate for the limitations of an IMU. Of course, only attitude correction is not sufficient for high accuracy navigation, but this will improve the performance in a good manner as the main driving factor in a navigation error is attitude performance[1]. Note that most other systems have their own shortcomings which are mutually compensated for.

Another shortcoming of IMUs is the initial alignment requirement. An inertial navigation system is a deduced reckoning navigation system, it integrates ordinary differential equations to obtain position, velocity and attitude data. Without the knowledge of the initial conditions, it is not possible to have acceptable navigation solutions. Several kinds of initial alignment algorithms depending on the platform of navigation system can be found in the literature [8, 9, 10].

2.1.1 IMU Technologies

The basic sensors of an INS are configured in either of two ways [1, 2, 8, and 11]:

• Isolated from the vehicle rotations on servo controlled gimbals (“stabilized gimbals”);
• Mounted directly to the vehicle (“strapdown”).

In stabilized systems, which are not widely used recently, inertial sensors are mounted on a stable platform with three or two gimbals that is kept either non rotating with respect to an inertial frame or is rotated with a known rate to establish a reference frame. The outputs of the gyroscopes, which are angular rates of the body with respect to the inertial frame, are sent to torque motors commanding them to maintain the platform fixed with respect to a reference frame. Thus, the accelerometers on that stable platform provide the specific force of the body with respect to the reference frame. Since the accelerometers measure the specific force, which is the difference between the acceleration with respect to inertial frame and the acceleration due to gravitation, the local gravity should be calculated and added to the sensor outputs. The compensated outputs are integrated twice to provide the velocity and position of the body in the reference frame. Moreover, the gimbal angles provide the attitude of the body with respect to the reference frame. In strapdown inertial navigation systems (SINS), the inertial sensors are rigidly attached to the body. An analytical platform is established in a computer. The measurements provided by the gyroscopes are used to calculate mathematically the attitude of the body with respect to the reference frame then the attitude of the host platform is used to resolve gravity compensated accelerometer outputs. Then they are integrated twice to obtain velocity and position of body. The advantages of the SINS compared to stabilized inertial navigation systems are reduced cost, weight, and mechanical complexity. However, an increase in computing complexity occurs. Due to advances in computer technology this is not a disadvantage anymore. In this work, a strapdown inertial navigation system is considered.

Strapdown systems appeared in the mid 70's when the computation power became sufficient to compute a virtual reference frame in real-time. Strapdown systems are typically more reliable and lower cost than gimbaled systems.

Accelerometers fall into two main categories:

• Force feedback or pendulous rebalanced accelerometers; and
• Vibrating beam accelerometers.

Gyroscopes are more diverse:
• Earlier designs consisted of metal wheels spinning in ball or gas bearings;
• Optical gyros were developed later and have counter-rotating laser beams either in an evacuated cavity (RLG: Ring Laser Gyro) or in an optical fiber (FOG: Fiber Optic Gyro); and
• Other designs use resonators of different shapes (bars, cylinders, rings, hemispheres) and are known under the generic name of Coriolis vibrating gyros.

Currently, the most advanced such technique uses micro electro mechanical systems (MEMS) technology, enabling true solid-state sensors. MEMS offer the promise of a complete sensor and supporting electronics on a single integrated circuit chip. The basic materials often used by this technology are silicon or quartz.

Sensors are often compared on the basis of certain performance factors, such as bias and scale-factor stability and repeatability or noise (random walk) [12]. The sensor selection is made difficult by the fact that many different sensor technologies offer a range of advantages and disadvantages while offering similar performances. Nearly all new applications are strapdown (rather than gimbaled) and this places significant performance demands upon the gyroscope (specifically: gyro scale-factor stability, maximum angular rate capability, minimum g-sensitivity, high bandwidth). For many applications, an improved accuracy/performance is not necessarily the driving issue, but meeting the

performance at a reduced cost and size is. In particular, a small sensor size allows the introduction of guidance, navigation, and control into applications previously considered out of reach (e.g., artillery shells, 30-mm bullets). Many of these newer applications require production in much larger quantities at much lower cost. In recent years, three major technologies in inertial sensing have enabled advances in military (and commercial) capabilities. These are the ring laser gyro (since ~1975), fiber optic gyros (since ~1985), and MEMS (since ~1995). The RLG moved into a market dominated by spinning mass gyros such as rate gyros, single-degree-of-freedom integrating gyros, and dynamically (or dry) tuned gyros, because it is ideal for strapdown navigation. The RLG was thus an enabling technology for high dynamic environmental military applications. Fiber Optic Gyros (FOGs) were developed primarily as a lower-cost alternative to RLGs, with expectations of leveraging technology advances from the telecommunications industry. FOGs are now beginning to match and even beat RLGs in performance and cost, and are very competitive in many military and commercial applications. However, apart from the potential of reducing the cost, the FOG did not really enable the emergence of any new military capabilities beyond those already serviced by RLGs. Efforts to reduce size and cost resulted in the development of small-path-length RLGs and short-fiber-length FOGs. MEMS Inertial sensors have the potential to be an extreme enabling technology for new military applications. Small size, extreme ruggedness, and potential for very low-cost means that numerous new applications will be able to incorporate inertial guidance, a situation unthinkable before MEMS [11].

2.1.2 Error Model of IMU

In the literature, more than 20 different types errors are defined for IMU outputs [10, 11]. However, for the system point of view, most of these errors are out of concern. This is because, during the field use of an IMU, the combined effect of most errors can not be separated by just observing the raw IMU outputs. To localize each error sources, some specialized test methodologies (like Allen variance tests) should be incorporated and obviously this is not possible during an

active operation. Therefore, in this study, actual IMU errors are grouped according to their effects on the raw IMU outputs. Errors which represent similar output characteristics are modeled using just a single model based on the dominant error source belonging to that group. For instance, the quantization error of sensors was ignored and their effects on sensor outputs were represented by adjusting random walk variance in constructing models. This is because, it is impossible to distinguish these two errors by using sensor outputs recorded at a constant rate.

The bias and scale factor error are the major error sources for inertial sensors. According to IEEE standards, the inertial sensor bias is defined as the average of the sensor output over a specified time measured at specified operating conditions that are independent of input acceleration or rotation. A scale factor is the ratio of a change in output to a change in the input to be measured. Both errors include some or all of the following components: fixed terms, temperature induced variations, turn-on to turn-on variations and in-run variations. The fixed component of the error is present each time when the sensor is turned on and is predictable. A large extent of the temperature induced variations can be corrected with suitable calibration. The turn-on errors vary from sensor turn-on to turn-on but remain constant without power-off. Therefore, they can be obtained from laboratory calibrations or estimated during the navigation process. Sensitive to dynamics changes and vibrations, the in-run random errors are unpredictable and vary throughout the periods when the sensor is powered on. The in-run random errors therefore cannot be removed from measurements using deterministic models and should be modeled by a stochastic process such as random walk process or Gaussian Markov process.

The cross-coupling error is the error due to sensor sensitivity to inputs about axes normal to an input reference axis. Such an error arises through non-orthogonality of the sensor triad and is usually expressed as parts per million (ppm). For a low-cost MEMS INS, the cross-coupling error is relatively small and negligible compared to other error sources.

The bias for a gyro/accelerometer is the average of accelerometer/gyro output over a specified time measured at specified operating conditions that have no correlation with input acceleration or rotation. The gyro bias is typically expressed in degree per hour (^{o}/h) or radian per second (rad/s) and the accelerometer bias is expressed in meter per second square (m/s^2 or g). The bias generally consists of two parts: a deterministic part called bias offset and a random part. The bias offset, which refers to the offset in the measurement provided by the inertial sensor, is deterministic in nature and can be determined by calibration. The random part is called as bias drift, which refers to the rate at which the error in an inertial sensor accumulates with time. The bias drift and the sensor output uncertainty are random in nature and they should be modeled as a stochastic process. Bias errors can be reduced from the reference values, but their specific amount is range and type dependent.

In addition to the above, there are two other characteristics used to describe the sensor bias. The first is the bias asymmetry (for gyro or accelerometer), which is the difference between the bias for positive and negative inputs, typically expressed in degree per hour (deg/h) or meter per second square [m/s^2, g]. The second is the bias instability (for gyro or accelerometer), which is the random variation in the bias as computed over specified finite sample time and averaging time intervals. This non-stationary (evolutionary) process is characterized by a 1/f power spectral density. It is typically expressed in degree per hour (deg/h) or meter per second square [m/s^2, g], respectively.

The scale factor is the ratio of a change in the input intended to be measured. The Scale factor is generally evaluated as the slope of the straight line that can be fit by the method of least squares to input-output data. The scale factor error is deterministic in nature and can be determined by calibration. The scale factor asymmetry (for gyro or accelerometer) is the difference between the scale factor measured with positive input and that measured with negative input, specified as a fraction of the scale factor measured over the input range. A scale factor

asymmetry implies that the slope of the input-output function is discontinuous at zero input. It must be distinguished from other nonlinearities. In some inertial sensor designs, the scale factor itself is not a constant for all ranges of applied acceleration. For example, a nonlinear spring might cause the scale factor itself to vary with acceleration. This type of error is known as scale factor non-linearity, and if not compensated can lead to errors in indicated acceleration/angular rate which are proportional to the square (or higher power) of the actual acceleration/angular rate.

The scale factor stability, which is the capability of the inertial sensor to accurately sense angular velocity (or acceleration) at different angular rates (or at different accelerations), can also be used to describe the scale factor. The Scale factor stability is presumed to mean the variation of scale factor with temperature and its repeatability, which is expressed as part per million (ppm). Deviations from the theoretical scale are due to system imperfections.

The axes misalignment is an error resulting from the imperfection of mounting the sensors. It usually results in a non-orthogonality of the axes defining the INS body frame. As a result, each axis is affected by the measurements of the other two axes in the body frame. The axes misalignment can, in general, be compensated or modeled in the INS error equation.

The noise is an additional signal resulting from the sensor itself or other electronic equipment that interferes with the output signals trying to measure. The noise is in general non-systematic and therefore cannot be removed from the data using deterministic models. It can only be modeled by stochastic process. The random noise is an additional signal resulting from the sensor itself or other electronic equipments that interfere with the output signals being measured. It is often considered time-uncorrelated with zero mean and modeled by a stochastic process. The INS noise level can be characterized by the average of the standard deviation of static measurements over few seconds.

Of above error sources, the bias has the largest impact on the INS navigation performance after a mechanization process [11, 12 and 13]. The accelerometer bias will result in a position error drifting with the square of time while the gyro bias will lead to a position error drifting with the cube of time.

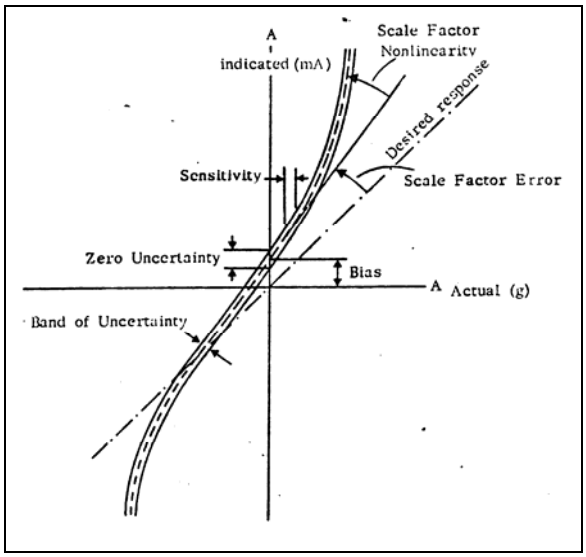

Figure 2.1 Typical IMU Error Behavior [13]

The relation between true and actual IMU outputs can be represented as follows:

$$\begin{bmatrix} a_x^{acc} \\ a_y^{acc} \\ a_z^{acc} \end{bmatrix} = \begin{bmatrix} S_x^{acc}+1 & 0 & 0 \\ 0 & S_y^{acc}+1 & 0 \\ 0 & 0 & S_z^{acc}+1 \end{bmatrix} \left(\begin{bmatrix} m_{xx}^{acc} & m_{xy}^{acc} & m_{xz}^{acc} \\ m_{yx}^{acc} & m_{yy}^{acc} & m_{yz}^{acc} \\ m_{zx}^{acc} & m_{zy}^{acc} & m_{zz}^{acc} \end{bmatrix} \begin{bmatrix} a_x^T \\ a_y^T \\ a_z^T \end{bmatrix} + \begin{bmatrix} \delta a_x^{bias} \\ \delta a_y^{bias} \\ \delta a_z^{bias} \end{bmatrix} + \begin{bmatrix} \delta a_x^{rnd} \\ \delta a_y^{rnd} \\ \delta a_z^{rnd} \end{bmatrix} \right) \quad (2.1)$$

$$\begin{bmatrix} \omega_x^{gyr} \\ \omega_y^{gyr} \\ \omega_z^{gyr} \end{bmatrix} = \begin{bmatrix} S_x^{gyr}+1 & 0 & 0 \\ 0 & S_y^{gyr}+1 & 0 \\ 0 & 0 & S_z^{gyr}+1 \end{bmatrix} \left(\begin{bmatrix} m_{xx}^{gyr} & m_{xy}^{gyr} & m_{xz}^{gyr} \\ m_{yx}^{gyr} & m_{yy}^{gyr} & m_{yz}^{gyr} \\ m_{zx}^{gyr} & m_{zy}^{gyr} & m_{zz}^{gyr} \end{bmatrix} \begin{bmatrix} \omega_x^T \\ \omega_y^T \\ \omega_z^T \end{bmatrix} + \begin{bmatrix} \delta\omega_x^{bias} \\ \delta\omega_y^{bias} \\ \delta\omega_z^{bias} \end{bmatrix} + \begin{bmatrix} \delta\omega_x^{rnd} \\ \delta\omega_y^{rnd} \\ \delta\omega_z^{rnd} \end{bmatrix} \right) \quad (2.2)$$

S= Scale factor errors

m= Misalignment errors

Bias =Constant errors

Rnd= Random noise errors

In the above equations, a^{acc} and ω^{gyr} represent the actual IMU outputs whereas, a^T and ω^T denotes true values. Take notice that this error model is in a simplified form which otherwise can be written in nonlinear form and can include some other terms, such as scale factor nonlinearities, g^2 dependent terms etc.

2.2 Inertial Navigation System

An inertial navigation system is a unit which gets inertial data (angular rate and acceleration) from an IMU, calculates position, velocity and attitude information with respect to a known grid system or reference frame by utilizing 6 degree of freedom kinematics equations. Basically, an INS continuously integrates acceleration and angular rates to obtain velocity, position, and angular position. Generally, inertial navigation systems have high bandwidth, high data output rate and high accuracy in short duration.

An attitude-heading reference is a dead-reckoning system which provides continuous attitude, heading, position, and velocity information. It is neither a slaved directional gyrocompass system nor a vertical gyroscope, but a compromise to both that provides low-accuracy position and velocity (but with unbounded errors) information. Advanced AHRS systems in use today employ strapdown ring laser gyros (RLG) and/or fiber-optic gyros; that is, the sensors are "bolted" to the aircraft structure and not isolated using gimbals.

Due to its nature, an INS/AHRS suffers from stability. Accelerometers and gyros have different kind of errors (bias, noise etc.). When an INS integrates inertial data, all errors in the inertial sensors accumulate, resulting in a performance decrease in long term. Also, any error in gravity and world shape models result in errors similar to sensor errors. However, an INS is perfect for short term navigation requirements. A navigation system designer should choose IMU performance specifications according to the following criteria;

- Accuracy requirements
- Dynamics of the host system

The primary object is to determine the position and attitude accuracy requirements. Choosing a suitable set of inertial sensors is accomplished by optimizing between price and performance. Through the integration process, all inertial sensor errors accumulate, thus as the total integration time increases, navigation errors accumulate. The dynamics of the platform (e.g. manoeuvres done by the host platform) excites some of the inertial sensor errors (scale factor errors, g dependent errors etc.).

Nowadays, many integrated systems use GPS, TERCOM, DSMAC, star sensors etc. to have a stable position and velocity solution. [3, 11].

2.2.1 Inertial Navigation Mechanization Equations

In this part of the thesis, basic components of inertial navigation kinematics will be introduced.

2.2.1.1 Reference Coordinate Frames

Many reference frames are defined in inertial navigation systems. The IMU outputs (acceleration and rotational rates) are expressed in body coordinates, but

the velocity is generally expressed in navigation frames. In this section, the fundamental reference frames that are used in navigation systems are defined [19]

2.2.1.1.1 Inertial Frame

The inertial frame (denoted as i frame), is an ideal coordinate frame, where the coordinate frame itself has no acceleration or rotational rates, in other words an ideal IMU gives zero output if it attached to an inertial frame. Unfortunately, an inertial frame is difficult to express in real world, so a quasi inertial frame is generally used. This quasi inertial frame has its origin at the centre of the Earth and axes that are non-rotating with respect to distant stars. Z axis is along the spin axis of the Earth, x axis points towards the mean vernal equinox, and y axis completes the famous right hand rule.

2.2.1.1.2 Earth frame

The Earth (e) frame has its origin at the centre of the Earth and axes fixed with respect to the Earth. X axis points toward the mean meridian of Greenwich in equatorial plane, Z axis is parallel to mean spin axis of the Earth and again Y axis completes the right hand rule.

Earth frame continuously rotates with respect to inertial frame with an angular velocity of;

$$\omega_{ie}^{e} = [0 \quad 0 \quad \Omega] \tag{2.3}$$

Here, Ω is the angular speed of the earth. Its value is;

Ω =7.2921158 rad/day

In the Earth frame, the position of the host platform is expressed in terms of its latitude, longitude, and altitude.

2.2.1.1.3 Navigation frame

The navigation frame is a local geodetic frame which has its origin coinciding with that of the IMU, with x axis pointing toward geodetic North, its z axis orthogonal to the reference ellipsoid pointing downward, and again y axis complies the right hand rule. The Navigation frame is also known as North East down (NED) frame.

2.2.1.1.4 Computer frame

The computer frame is the frame that is used by the navigation computer. With an ideal inertial navigation system (no IMU errors, no computational errors etc.), the computer frame is exactly the same as the navigation frame. In the real world, there is a difference between the navigation and computer frames.

The transformation matrix between computer and navigation frames is expressed in navigation error equations.

2.2.1.2 Coordinate Transformation

A coordinate transformation is used to express the components of a vector in a different coordinate frame. Coordinate transformation matrices are orthogonal matrices and their determinants are equal to one provided that right-handed Cartesian coordinate systems are used. There are different methods to transform a vector between different coordinate frames, such as direction cosine matrix,

quaternion etc. In this thesis, direction cosine matrices that are obtained by successive Euler rotations are used.

2.2.1.3 Earth Shape Model

In order to determine position on the Earth using inertial measurements, it is necessary to make some assumptions regarding the shape of the Earth. Owing to the slight flattening of the Earth at the poles, Earth is modeled as a reference ellipsoid which approximates more closely to the true geometry. Generally, WGS84 model [1, 2, 3 and 8] is used as the earth shape model. In this model, following parameters are introduced;

R: The length of the semi major axis (~6378 km)

$r = R(1 - f)$: The length of the semi minor axis (~6356 km)

$f = (R - r)/R$: The flattening of the ellipsoid (~1/298.25)

$e = \sqrt{f(2 - f)}$: The major eccentricity of the ellipsoid (~0.08188)

With these parameters defined, the meridian radius of curvature (R_N) and the transverse radius of curvature (R_E) may be derived as;

$$R_N = \frac{R(1-e^2)}{(1-e^2 \sin^2 L)^{\frac{3}{2}}} \tag{2.4}$$

$$R_E = \frac{R}{(1-e^2 \sin^2 L)^{\frac{1}{2}}} \tag{2.5}$$

Here, L is latitude.

2.2.1.4 Gravitational Acceleration Model

As mentioned earlier, an accelerometer can only measure the difference between the gravitational acceleration and the acceleration of the body with respect to the inertial frame. In order to obtain the velocity and position data, an accurate model of the gravitational field is needed. In the related literature, there are different gravity models that are used in navigation applications. Ideally, the gravity vector is assumed to be acting vertically downwards to the reference ellipsoid, which is not the case in the real world due to anomalies. In this thesis, the model given in [11] is used. In this model, gravity at the surface of the reference ellipsoid (zero altitude) is given as;

$$g(0) = 9.7803267714(1 + 5.3024.10^{-3}.\sin^2 L - 5.9.10^{-6}.\sin 2L) \tag{2.6}$$

And the change of magnitude of gravity with respect to altitude is given as;

$$g(h) = \frac{g(0)}{(1 + h/R)^2} \tag{2.7}$$

Here, h is gathered from INS outputs.

2.2.1.5 Inertial Frame mechanization

Dominant INS errors are caused by imperfect knowledge of initial conditions (for example, those existing after alignment) and by error propagation in time. The nine, nonlinear differential navigation equations (3 velocity, 3 position, 3 attitude equation) can be perturbed by a wide variety of error sources, not only those resulting from incorrect initial conditions. The perturbations of these equations, when kept small, can be shown to result in a linear set of differential equations. The most popular set of these equations is called the Pinson error model, named after the man who derived it [14, 15, 16].

Remember that errors are both deterministic and statistical, and the statistical errors can only be estimated. Investigating the propagation of deterministic errors may provide a useful insight into system performance, but there is such a wide variety of error sources that one is never totally sure which ones are dominating the error response curves.

In this system, it is required to calculate the vehicle speed with respect to earth, the ground speed, in inertial axes, denoted by v_e^i. The differential equations for velocity, position and attitude can expressed as follows;

$$\dot{v}_e^n = C_b^n.a^b - (2.\omega_{ie} + \omega_{en}) \times v_e^n + g_p \tag{2.8}$$

$$\dot{L} = \frac{V_N}{R_N + h} \tag{2.9}$$

$$\dot{l} = \frac{V_E \sec(L)}{R_N + h} \tag{2.10}$$

$$\dot{h} = -V_D \tag{2.11}$$

$$\dot{C}_b^n = C_b^n(\tilde{\omega}_{nb}^b) \tag{2.12}$$

where;

v_e^n: velocity of the host platform

L: latitude

l: longitude

C_b^n : direction cosine matrix relating body and navigation frame.

h: altitude

a^n : acceleration to which the inertial measurement unit is subjected

ω_{en} :Transport rate, whic can be expressed as;

$$\omega_{en}^n = [V_E/(R_e + h) \quad -V_N/(R_n + h) \quad -V_E.\tan(L)/(R_e + h)] \tag{2.13}$$

ω_{ie} : Earth rotation rate

g_p : Gravity vector

ω_{nb}^b :The angular rate of the body with respect to the navigation frame

ω_{nb}^b can be expressed as the measured body rates (ω_{ib}^b) and estimates of the components of the navigation frame rate ($\omega_{in} = \omega_{ie} + \omega_{en}$) ;

$$\omega_{nb}^b = \omega_{ib}^b - C_b^n.(\omega_{ie}^n + \omega_{en}^n) \tag{2.14}$$

Detailed derivation of the navigation mechanization equations are given in Appendix C.

2.2.2 Error Model of Inertial Navigation Systems

The navigation computer of an INS is essentially a differential equation solver. The navigation mechanization equations represent a nonlinear, time varying system. This system is unstable in the sense of Liapunov. Therefore, every disturbance that affects the system causes the output errors to grow unbounded. The rate at which errors grow are determined by the source of error and the trajectory that system follows. For the INS systems, major error sources can be classified into 3 groups [10, 15]:

1. IMU Errors (Input Errors)

2. Initialization Errors (Initial state Errors)

3. Computation Errors

The discrete and quantized nature of navigation processors tends to produce some computational errors on navigation solution. This situation arises especially in high vibratory environments. The importance of this kind of error depends on the fact that this error can neither be estimated nor compensated. Therefore this error sets a lower limit in the accuracy of inertial navigation system. For the real implementation (when real IMU increments are used), with the use of appropriate conning and sculling algorithms and sufficient processing frequency, computational errors can be reduced to very low levels. However, one should be very careful when designing a simulation environment in computer. In a computer simulation implementation, calculating simulated velocity and angle increments instead of acceleration and rotation rate can be very difficult under vibratory environments (i.e. vibrations in the host platform). Usually, this difficulty is handled by simply taking Euler integration of the calculated acceleration and rotation rate to obtain associated increments. However, such an operation causes computational errors to grow significantly. Therefore, when developing a

simulation environment in computer, this point should always be considered, and necessary precautions should be taken to reduce the effect of computational errors during simulations.

As the navigation mechanization equations are nonlinear, they cannot be applied to a linear estimation filter, namely Kalman filter. That's why the error model of navigation states. The error propagation equations are derived by first order perturbations assuming small attitude errors. The error model of attitude, velocity and position is expressed as follows;

$$\dot{\gamma}^n = -C_b^n.\delta\omega_{ib}^b - \omega_{in}^n \times \gamma^n + \delta\omega_{in}^n \tag{2.15}$$

$$\begin{aligned}\delta\dot{v}_e^n &= (C_b^n.a^b)\times\gamma^n + C_b^n.\delta a^b - v_e^n \times (2.\omega_{ie}^n \times \varepsilon^n + \delta\omega_{en}^n) \\ &-(2.\omega_{ie}^n + \omega_{en}^n)\times\delta v_e^n + \delta g_p\end{aligned} \tag{2.16}$$

$$\delta\dot{h} = \delta V_D \tag{2.17}$$

$$\delta\dot{L} = \delta V_N /(R_n + h) - V_N.\delta h/(R_n + h) \tag{2.18}$$

$$\begin{aligned}\delta\dot{l} &= \delta V_E.\sec(L)/(R_e + h) + \delta V_E.\sec(L).\tan(L).\delta L/(R_e + h) \\ &-\delta V_E.\sec(L).\delta h/(R_e + h)\end{aligned} \tag{2.19}$$

γ^n: Error misalignment vector that relates navigation and computer frame

δL: Error in latitude

δl: Error in longitude

δV : Velocity error vector

$\delta \dot{h}$: Altitude error

$\delta \omega_{ib}^{b}$: Errors in gyro measurements

$\delta \omega_{in}^{n}$: Errors in ω_{in}^{n}, which is expressed as;

$$\delta \omega_{in}^{n} = \delta \omega_{ie}^{n} + \delta \omega_{en}^{n} \tag{2.20}$$

$$\delta \omega_{en}^{n} = \begin{bmatrix} \dfrac{\delta V_E}{R_E + h} - \dfrac{V_E \delta h}{R_E + h} \\ \dfrac{\delta V_N}{R_N + h} - \dfrac{V_N \delta h}{(R_N + h)^2} \\ \dfrac{-\delta V_N . \tan(L)}{R_E + h} + \dfrac{V_N . \tan(L) \delta h}{(R_E + h)^2} - \dfrac{-V_N .}{(R_E + h)(\cos(L))^2} \end{bmatrix} \tag{2.21}$$

$$\delta \omega_{ie}^{n} = [-\Omega \sin(L) \delta L \quad 0 \quad -\Omega \cos(L) \delta L]^T \tag{2.22}$$

The detailed derivation of the linear error equations are given in Appendix D.

CHAPTER 3

MAGNETOMETERS

3.1 World Magnetic Model

World magnetic model (WMM)[7] is a tool to obtain the Earth's ideal magnetic field model at any point on the Earth. WMM gives the model in terms of spherical harmonic series. The coefficients of the model is updated every five years. The outputs of the model are magnetic field values in NED components. The details of WMM 2005 is given in Appendix A

3.1.1 Alternative Magnetic Field Model

World magnetic field model is global model that is the model theoretically works in any point of the world, but having some problems An alternative model is proposed with the following assumptions;

- Magnetic field is approximately constant in a local field, i.e., the horizontal position change is limited to 10km, and vertical position change is limited to 1km.
- The sensor errors are negligible.

The mathematical relation between the reference magnetic field and the magnetometer measurements is as bellows;

$$B^N = \hat{C}_B^N . (B^B) \quad (3.1)$$

Where

B^N = Reference Magnetic field given by WMM2005

B^B = Magnetic field measurement by magnetometer

$\hat{C}_B^N$ = Direction Cosine matrix relating navigation and body frames.

If attitude information of the host platform ($\hat{C}_B^N$) and magnetometer measurements (B^B) are known, it is possible to find the reference magnetic field vector in every navigated point. In this alternative model, two error sources occur;

- INS errors (gyro errors especially)
- Magnetometer errors

INS errors can be minimized by using multiple aiding sources (DGPS, DSMAC, TERCOM etc.). As it will be explained in this chapter, magnetometer errors are negligible.

This method has two deficiencies arising from its assumptions. The developed method only works in a local navigation case (short range missiles, UAVs, mobile robots). On the other hand, neither the magnetometer nor the gyros are perfect sensors; the sensor errors will affect the magnetic field solution. High accurate gyros (e.g., Ring laser or fiber optic gyros) and magnetometers must be used.

Although this method has some advantages to the WMM, it must be experimentally proven before it can be used. Difficulties in this process are as follows;

- High Accuracy Magnetometer Requirement: In order to have an accurate model, the magnetometer should have high accuracy,

- DGPS aided navigation unit: As it can be seen from equation 3.1, the accuracy of the resultant magnetic field model depends on the accuracy of the attitude information. High accuracy, navigation grade (e.g.., RLG, FOG) gyros must be used to have an accurate model.

Any error in attitude and magnetic field measurements will result in error in the resultant model, so the magnetometers and gyros should have very high accuracy. As these units are very expensive, the accuracy of this magnetic model could not be proven in this study. Thus, WMM 2005 will be used in this thesis.

3.2 Magnetometer Types

Magnetic sensors differ from most other detectors in that they do not directly measure the physical property of interest [24]. Devices that monitor properties such as temperature, pressure, strain, or flow provide an output that directly reports the desired parameter. Magnetic sensors, on the other hand, detect changes, or disturbances, in magnetic fields that have been created or modified, and from them derive information on properties such as direction, presence, rotation, angle, or electrical currents. The output signal of these sensors requires some signal processing for translation into the desired parameter. Although magnetic detectors are somewhat more difficult to use, they do provide accurate and reliable data — without physical contact [24].

Magnetic sensors can be classified according to low-, medium-, and high-field sensing range. In this study, devices that detect magnetic fields <1 μG (micro Gauss) are considered low-field sensors; those with a range of 1 μG to 10 G are Earth's field sensors; and detectors that sense fields >10 G are referred to as bias magnet field sensors.

A magnetic field is a vector quantity with both magnitude and direction. The scalar sensor measures the field's total magnitude but not its direction. The omni directional sensor measures the magnitude of the component of magnetization that lies along its sensitive axis. The bidirectional sensor includes direction in its

measurements. The vector magnetic sensor incorporates two or three bidirectional detectors. Some magnetic sensors have a built-in threshold and produce an output only when it is surpassed.

3.3 Magnetometer Error Sources

Magnetometer accuracy is affected by [25]:

1. Magnetic sensor errors
2. Temperature effects
3. Nearby ferrous materials
4. Variation of the earth's field

Solid state magneto-resistive (MR) sensors available today can reliably resolve <0.07 mgauss fields. This is more than a five times margin over the 0.39 mgauss field required to achieve 0.01° resolution. Other magnetic sensor specifications should support field measurement certainty better than 0.005° to maintain an overall 0.01° heading accuracy. These include the sensor noise, linearity, hysteresis, and repeatability errors. Any gain and offset errors of the magnetic sensor will be compensated for during the hard iron calibration (discussed later) and will not be considered in the error budget. MR sensors can provide a total error of less than 0.1 mgauss [24, 25].

The temperature coefficient of the sensor will also affect the heading accuracy. There are two characteristics of temperature to consider—the offset drift with temperature and the sensitivity temperature coefficient. The sensitivity temperature coefficient will appear as a change in output gain of the sensor over temperature (Figure 3.1). MR sensors generally have sensitivity temperature coefficients that are well correlated, or matched—especially sensors with two (X, Y) axes in the same package. The matching temperature coefficients imply that

the output change over temperature of the X axis will track the change in output of the Y axis. This effect will cancel itself since it is the *ratio* of Y over X that is used in the heading calculation [Azimuth = arcTan(Y/X)]. For example, as the temperature changes the Y reading by 12%, it also changes the X reading by 12% and the net change is canceled. The only consideration is then the dynamic input range of the A/D converter. The magnetic sensor offset drift with temperature is not correlated and may in fact drift in opposite directions. This will have a direct affect on the heading and can cause appreciable errors. There are many ways to compensate for temperature offset drifts using digital and analog circuit techniques. A simple method to compensate for temperature offset drifts in MR sensors is to use a switching technique referred to as set/reset switching. This technique cancels the sensor temperature offset drift, and the dc offset voltage as well as the amplifier offset voltage and its temperature drift. The transfer curves for a MR magnetic sensor after it has been set, and then reset, are shown in Figure 3.2. The set/reset modes are achieved by using an ac coupled driver to generate a bi-directional current

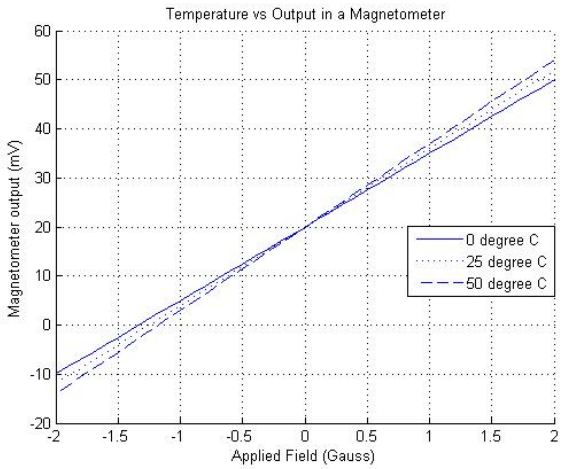

Figure 3.1Magnetic sensor output temperature variation

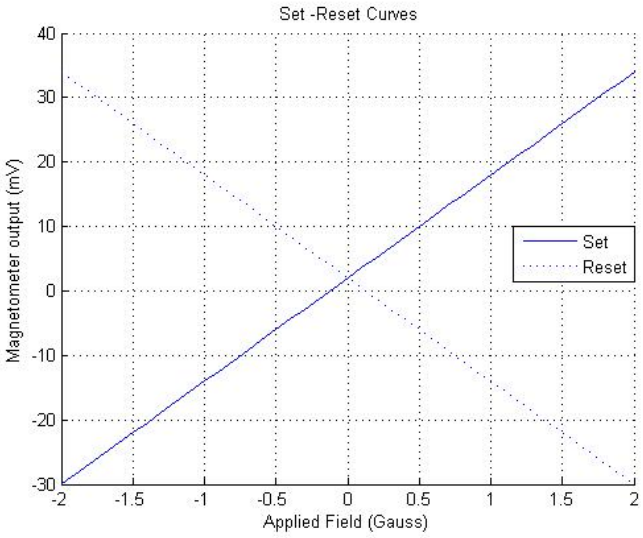

Figure 3.2 Set and reset output transfer curves.

The two curves result from an inversion of the gain slope with a common crossover point at the offset voltage. For the sensor in Figure 3.2, the sensor offset is –3 mV. This offset is not desirable and can be eliminated using the set/reset switching technique described below. Other methods of offset compensation are described in [6]. The sensor offset (Vos) can be eliminated by using a simple subtraction technique. First apply a set pulse, measure $H_{applied}$ and store it as V_{set}— Figure 3.3. Then apply a reset pulse and store that reading as V_{reset}. Subtract these two readings to eliminate V_{os}:

$$V_{set} = S * H_{applied} + V_{os} \quad (3.2)$$

$$V_{reset} = -S * H_{applied} + V_{os} \quad (3.3)$$

$$V_{set} - V_{reset} = S * 2 * H_{applied} \quad (3.4)$$

The sensor sensitivity (S) is expressed in mV/gauss. Note that equation (3.4) has no V_{os} term. This method also eliminates the amplifier offset as well. Another benefit is that the temperature drift of the sensor offset and the amplifier is eliminated. Now, a low cost amplifier can be used without concern for its offset

effects. This is a powerful technique and is easy to implement if the readings are controlled by a low cost microprocessor. Using this technique to reduce temperature effects can drop the overall variation in magnetic readings to less than 0.01%/°C. This amounts to less than 0.29° effect on the heading accuracy over a 50°C temperature change [25].

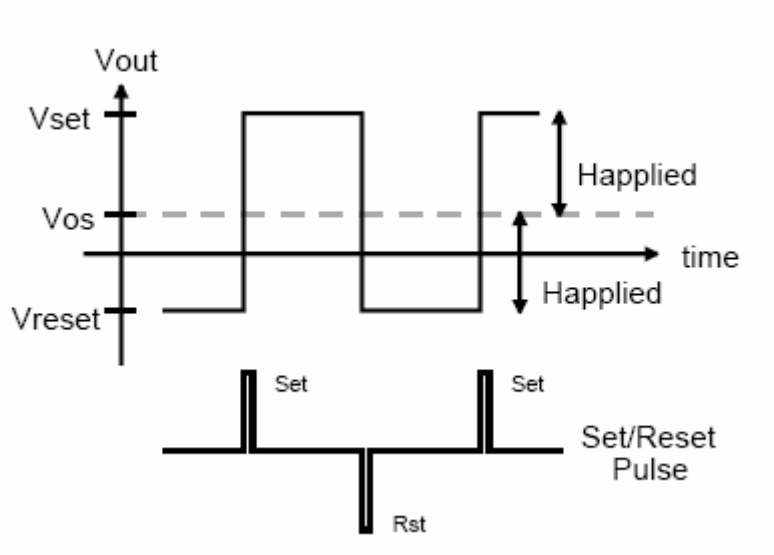

Figure 3.3 Set and reset effect on sensor output (Vout) [25]

Another consideration for heading accuracy is the effects of nearby ferrous materials on the earth's magnetic field. Since heading is based on the direction of the earth's horizontal field (Xh,Yh), the magnetic sensor must be able to measure this field without influence from other nearby magnetic sources or disturbances. The amount of disturbance depends on the material content of the platform and connectors as well as ferrous objects moving near the magnetometer. When a ferrous object is placed in a uniform magnetic field it will create disturbances as shown in Figure 3.4. This object could be a steel bolt or bracket near the magnetometer or an iron door latch close to the magnetometer. The net result is a characteristic distortion, or anomaly, to the earth's magnetic field that is unique to

the shape of the object. Before looking at the effects of nearby magnetic disturbances, it is beneficial to observe an ideal output curve with no disturbances. When a two-axis (X,Y) magnetic sensor is rotated in the horizontal plane, the output plot of Xh vs. Yh will form a circle centered at the (0,0) origin (see Figure 3.5). If a heading is calculated at each point on the circle, the result will be a linear sweep from 0° to 360°.

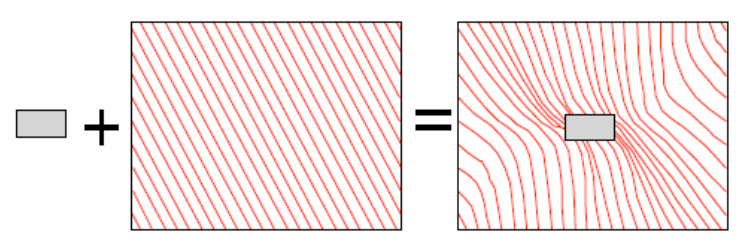

Figure 3.4 Ferrous object disturbance in uniform field.

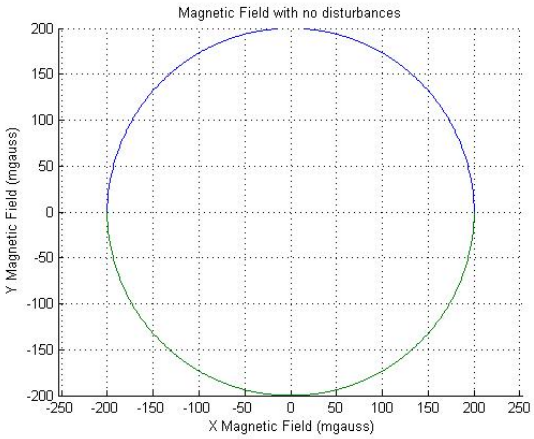

Figure 3.5 Magnetic sensor outputs (X,Y) rotated horizontally in the earth's field with no disturbances.

The effect of a magnetic disturbance on the heading will be to distort the circle shown in Figure 3.6. Magnetic distortions can be categorized as two types—hard iron and soft iron effects. Hard iron distortions arise from permanent magnets and magnetized iron or steel on the magnetometer platform. These distortions will remain constant and in a fixed location relative to the magnetometer for all heading orientations. Hard iron effects add a constant magnitude field component along each axes of the sensor output. This appears as a shift in the origin of the circle equal to the hard iron disturbance in the Xh and Yh axis (see Figure 3.6). The effect of the hard iron distortion on the heading is a one-cycle error and is shown in Figure 3.7. To compensate for hard iron distortion, the offset in the center of the circle must be determined. This is usually done by rotating the magnetometer and platform in a circle and measures enough points on the circle to determine this offset. Once found, the (X,Y) offset can be stored in memory and subtracted from every reading. The net result will be to eliminate the hard iron disturbance from the heading calculation; as if it were not present. The soft iron distortion arises from the interaction of the earth's magnetic field and any magnetically soft material surrounding the magnetometer. Like the hard iron materials, the soft metals also distort the earth's magnetic field lines. The difference is the amount of distortion from the soft iron depends on the magnetometer orientation. Soft iron influence on the field values measured by X and Y sensors are depicted in Figure 3.8. Figure 3.9 illustrates the magnetometer heading errors associated with this effect—also known as a two cycle error.

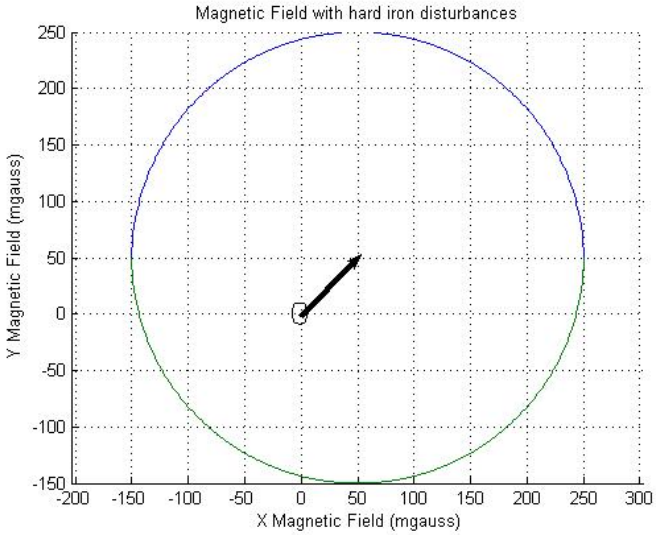

Figure 3.6 Hard iron offsets

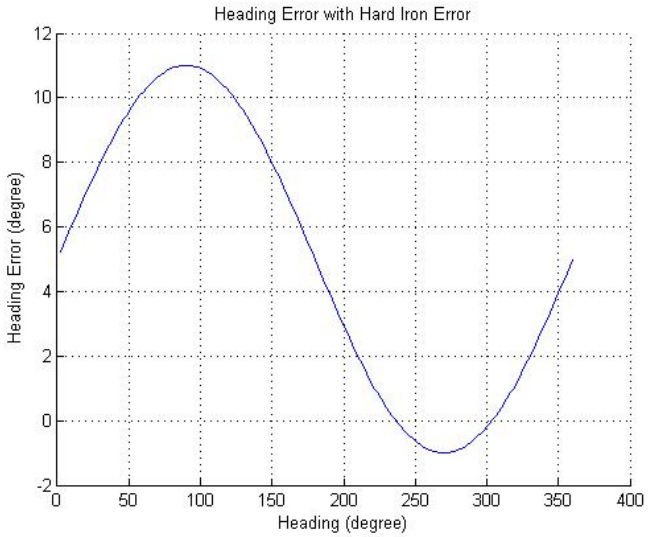

Figure 3.7 Heading error due to hard iron effects

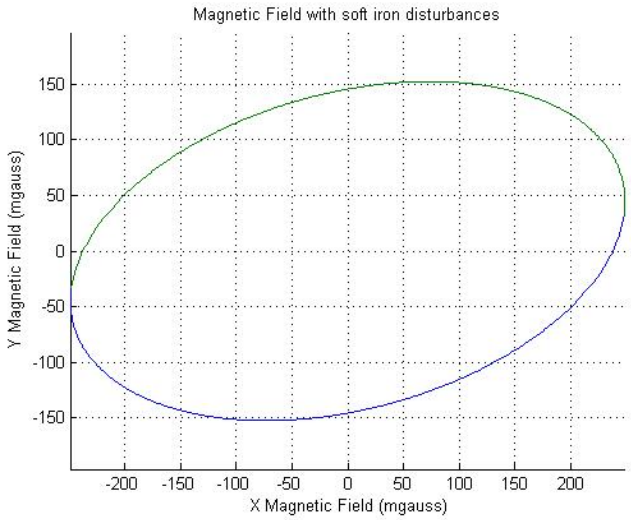

Figure 3.8 Soft iron distortion

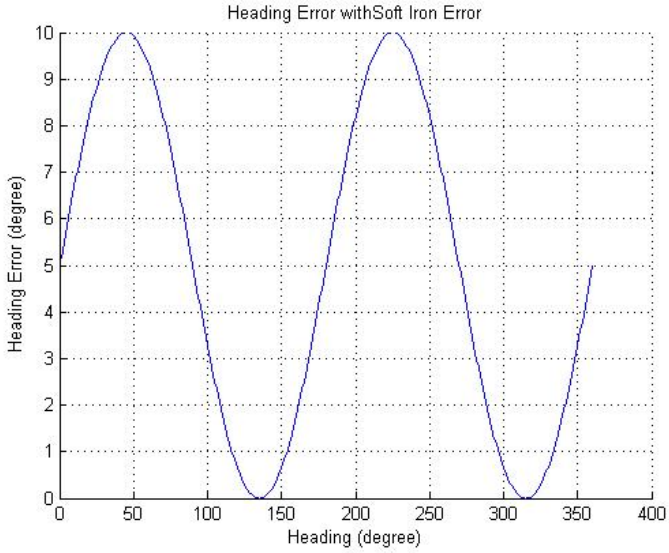

Figure 3.9 Heading error due to soft iron effects

Compensating for soft iron effects is a bit more difficult than for hard iron effects. This involves a bit more calculation than a simple subtraction. One way to remove the soft iron effect is to rotate the reading by 45°, scale the major axis to change

the ellipse to a circle, and then rotate the reading back by 45°. This will result in the desired circular output response shown in Figure 3.9. Most ferrous material in vehicles tends to have hard iron characteristics. The best approach is to eliminate any soft iron materials near the magnetometer and deal with the hard iron effects directly. It is also recommended to degauss the platform near the magnetometer prior to any hard/soft iron compensation. Some magnetometer manufacturers provide calibration methods to compensate for the hard and soft iron effects. Each calibration method is associated with a specified physical movement of the magnetometer platform in order to sample the magnetic space surrounding the magnetometer. The calibration procedure can be as simple as pointing the host in three known directions, or as complicated as moving in a complete circle with pitch and roll, or pointing the host in 24 orientations including variations in tilt. It is impossible for a marine vessel to perform the 24- point calibration, but easy for a hand-held platform. If the magnetometer is only able to sample the horizontal field components during calibration, then there will be uncompensated heading errors with tilt. Heading error curves can be generated for several known headings to improve heading accuracy Hard and soft iron distortions will vary from location to location within the same platform. The magnetometer has to be mounted permanently to its platform to get a valid calibration. A particular calibration is only valid for that location of the magnetometer. If the magnetometer is reoriented in the same location, then a new calibration is required. A gimbaled magnetometer can not satisfy these requirements and hence the advantage of using a strapdown, or solid state, magnetic sensor. It is possible to use a magnetometer without any calibration if the need is only for repeatability and not accuracy.

The final consideration for heading accuracy is the variation, or declination, angle. It is well known that the earth's magnetic poles and its axis of rotation are not at the same geographical location. They are about 11.5° away from each other. This creates a difference between the true north, or grid north, and the magnetic north, or direction a magnetic magnetometer will point. Simply it is the angular difference between the magnetic and true north expressed as an Easterly or

Westerly variation. This difference is defined as the variation angle and is dependent on the magnetometer location—sometimes being as large as 25°. To account for the variation simply add, if Westerly, or subtract, if Easterly, the variation angle from the corrected heading computation. The variation angles have been mapped over the entire globe. For a given location the variation angle can be found by using a geomagnetic declination map or a GPS (Global Positioning System) reading and an IGRF model. The International Geomagnetic Reference Field (IGRF) or World Magnetic Model (WMM) is a series of mathematical models describing the earth's field and its time variation After heading is determined, the variation correction can be applied to find true north according to the geographic region of operation.

The performance of a magnetometer will greatly depend on its installation location. A magnetometer depends on the earth's magnetic field to provide heading. Any distortions of this magnetic field by other sources should be compensated for in order to determine an accurate heading. Sources of magnetic fields include permanent magnets, motors, electric currents—either dc or ac, and magnetic metals such as steel or iron. The influence of these sources on magnetometer accuracy can be greatly reduced by placing the magnetometer far from them. Some of the field effects can be compensated by calibration. However, it is not possible to compensate for time varying magnetic fields; for example, disturbances generated by the motion of magnetic metals, or unpredictable electrical current in a nearby wire. Magnetic shielding can be used for large field disturbances from motors or speakers. The best way to reduce disturbances is distance. Also, never enclose the magnetometer in a magnetically shielded metallic housing.

The effects of nearby magnetic distortions can be calibrated out of the magnetometer readings once it is secured to the platform. Caution must be taken in finding a magnetometer location that is not too near varying magnetic disturbances and soft iron materials. Shielding effects from speakers and high current conductors near the magnetometer may be necessary. Variations in the

earth's field from a true north heading can be accounted for if the geographical location of the magnetometer is known. This can be achieved by using a map marked with the deviation angles to find the correct heading offset variation; or use a GPS system and the IGRF reference model to compute the variation angle. Low cost magnetometeres of the type described here are susceptible to temporary heading errors during accelerations and banked turns. The heading accuracy will be restored once these accelerations diminish. With a strapdown magnetometer there is no accuracy drift to worry about since the heading is based on the true earth's magnetic field. They tend to be very rugged to shock and vibrations effects and consume very low power and are small in size

CHAPTER 4

KALMAN FILTER

Navigation outputs—position, velocity, and attitude (PVA) — must be updated in order to be bounded. Kalman filter provides the manner and the method for combining updates that is practically useful as well as mathematically ingenious. Moreover, this technique can be extended to the integration of outputs from a wide variety of systems and continues to show a high degree of practical utility in navigation applications.

The Kalman filter is a linear filter. Recall that the actual differential equations for INS operation are non-linear, but the error equations are valid for linearized versions of these differential equations. Hence the requirement for the errors themselves to remain small, otherwise a linear analysis is not valid. Kalman filter applications presume that state-space dynamic modeling will be used to implement the algorithm. In the next part of this chapter the discrete Kalman filter in its most universal form will be presented and derived in a straightforward manner. Only those parts of the derivation will be emphasized that have practical significance for flight applications [26, 27, 28, 29].

4.1 Kalman Filter

4.1.1 Motivation for the Kalman Filter for INS

The major problems that exist if one relies on an inertial navigation system in motion:

- How to correct the navigation error equations while flying so that they remain useful even though the initial navigation errors were not known accurately.
- How to deal with noisy measurements from a variety of other systems that are arriving at different times; how to estimate the covariance of the INS output whenever an update could occur to see how much of the measurement should be believed in the presence of noisy system dynamics;
- How to obtain estimates for all navigation outputs even though only one or two is being measured by other means, providing as a result the most probable position.

The Kalman filter can be used to solve all of these problems. The basic procedure is;

- Initialize the filter by providing statistical estimates $\hat{x}_o$ for the initial navigation error states, their covariance $P(t_0)$, and noise covariance Q_0 .
- Propagate both $P(t_0)$ and the $\hat{x}_o$ to time of measurement update t_k before the measurement z_k .
- Note that values before measurement are $P_k(-)$ and $\hat{x}_k(-)$.
- Compute the most probable estimate $\hat{x}_k(+)$ by weighting $\hat{x}_k(-)$ and z_k with the Kalman gains.

If the filter converges, then it is possible to have a useable estimate of all the navigation error states at all discrete times t_k during the motion. Also estimate of

the covariance of the navigation error states are obtained and one can verify that it decreases following a measurement update.

4.1.1.1 Kalman Filter Implementation

In the related literature, two implementation method for Kalman Filter exists, direct (total state space) and indirect (error state space) Kalman Filter. In the direct estimation, the states are attitude, position and velocity, which have high nonlinearities. As the Kalman Filter is a linear filter, this implementation method may not work properly in integrated navigation.

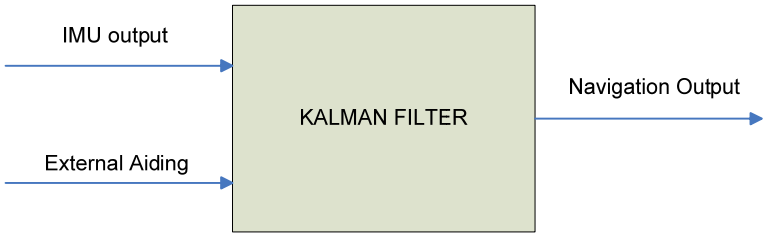

Figure 4.1 Direct Kalman Filter

In the indirect filter, the linearized error navigation states are used, thus the Kalman Filter works properly. The indirect filter has also two types, feedback and feedforward filters. In the feedforward type, the estimated error states are used to correct the INS errors but the INS is unaware of the filter, thus the error states grow and linearity assumption fails. In the feedback type, the estimated errors are fed back to INS thus error states are not allowed to grow unbounded. In this thesis, feedback indirect Kalman Filter is used.

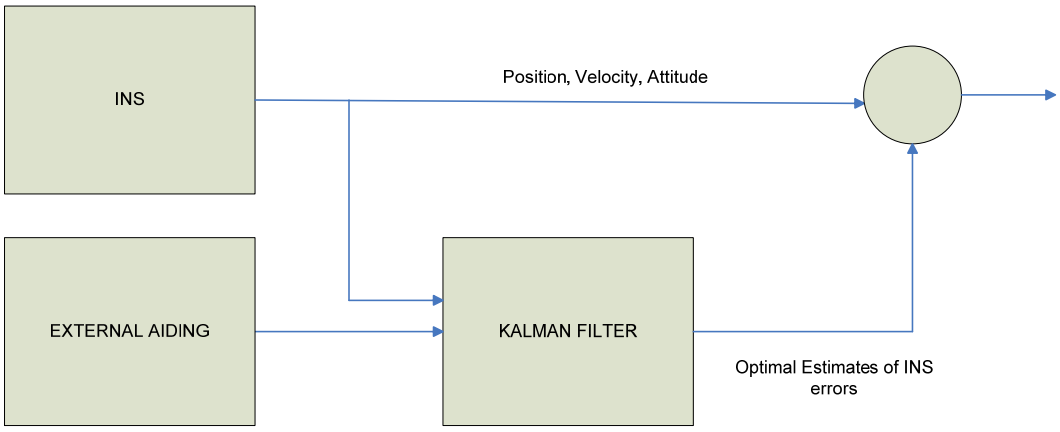

Figure 4.2 Indirect Feedforward Kalman Filter

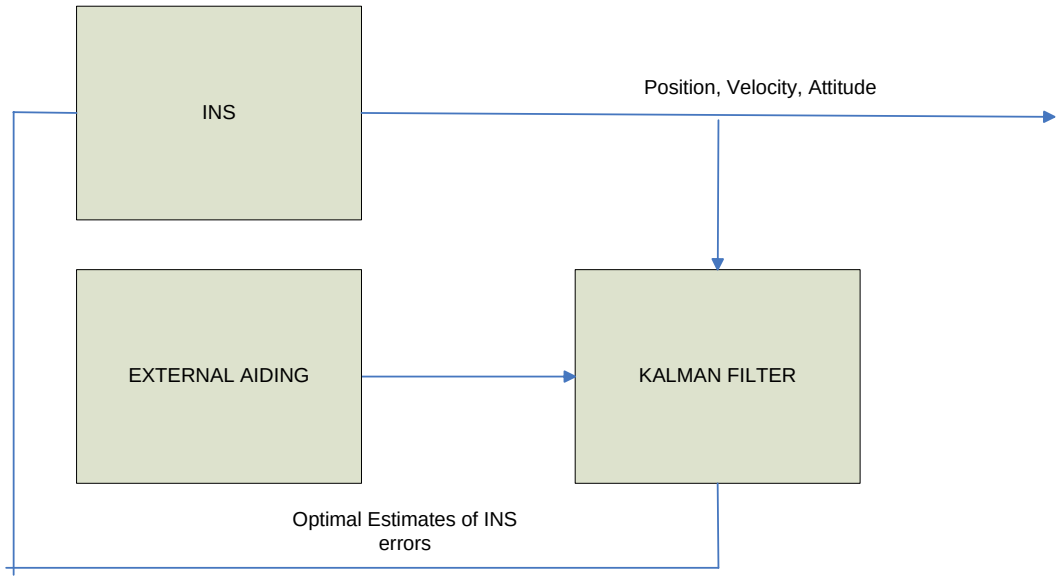

Figure 4.3 Indirect Feedback Kalman Filter

Equations for the Kalman Filter is summarized in table 4.1

Table 4.1 Discrete State-Space System Kalman Filter [26]

Discrete System Equation and Error Source	$x_{k+1} = A_k x_k + w_k$
Noise Covariance of Error Source Noise	$E(w_k w_k^T) = Q_k$
Discrete Measurement Equation	$z_k = H_k x_k + v_k$
Noise Covariance of Measurement	$E(v_k v_k^T) = R_k$
Assumed Form for Estimate of Navigation Error State	$\hat{x}_k(+) = K_k' \hat{x}_k(-) + K_k z_k$ $K_k' = (I - K_k H_k)$
Final Form for Estimate	$\hat{x}_k(+) = \hat{x}_k(-) + K_k[z_k - H_k \hat{x}_k(-)]$ $K_k = P_k(-) H_k^T [H_k P_k(-) H_k^T + R_k]^{-1}$
Covariance of navigation error residual $P_k(+) = E[\tilde{x}_k(+)\tilde{x}_k^T(+)]$	$P_k(+) = (I - K_k H_k) P_k(-)$ $P_k^{-1}(+) = P_k^{-1}(-) + H_k^T R_k^{-1} H_k$
Propagation Equations for Estimate $\hat{x}_{k+1}(-)$ before update z_{k+1} and for its residual covariance $P_{k+1}(-)$	$\hat{x}_{k+1}(-) = A_k \hat{x}_k(+)$ $P_{k+1}(-) = A_k P_k(+) A_k^T + Q_k$ $Q_k = E(w_k w_k^T)$

4.2 Kalman Filter Divergence

4.2.1 Nonlinear System Behavior

Kalman filter is a linear filter in that K_k, the Kalman gain matrix, produces a "weighted linear combination" of old estimates and measurements to produce new estimates. In this thesis, linearized navigation error states and magnetometer measurements are used in a feedback Kalman filter. The feedback in the

estimation filter does not let the unstable system errors grow and the linearity assumption is preserved. [30].

4.2.2 Covariance Matrix Calculations

The problem of Kalman filter divergence caused by covariance calculations, which has been with system developers since the 1960s, is still with the aerospace community. Basically, the covariance matrix $P_k(+)$ becomes too small resulting in a small $K_k = P_k(+)H_k^T R_k^{-1}$ and thus eliminates the weighting on new measurements as can be seen

$$\hat{x}_k(+) = \hat{x}_k(-) + K_k[z_k - H_k x_k(-)] \tag{4.1}$$

This results in the new state estimate after update staying the same as the estimate before update (since K_k approaches zero). This estimate is then propagated forward and the same thing occurs at the next measurement time. The filter, in effect, is rejecting all of the new measurements and relying only on its own propagated values for covariance which keep getting smaller and making things worse. This is a loss of system integrity.

4.2.3 Inaccurate Models

Modeling is the hardest part of the Kalman filtering. This is especially true when there are nonlinearities in the physical equations that must be linearized. As a general rule, a Kalman filter should have models that are simple enough to be implementable, but at the same time it should still represent the physical situation with a reasonable degree of accuracy.

That's why the error propagation model of inertial navigation systems is derived. With the help of these error models, the Kalman filter represents the real world behavior of the navigation system with a simple linear model. Also, the

measurement model of the magnetometer is derived in the same manner, it is linear and accurate.

4.2.4 Measurement Acceptance/Rejection Criteria

If "outlier" measurements cannot be rejected, the navigation error will rapidly grow without bound because the filter equations will ignore its own system equations and become erratic. Measurement rejection criteria are normally based on the "innovations" given by $[\ z_k - H_k \hat{x}_k(-)\ ]$ or the equivalent $[\, z_k - \hat{z}_k(-)\,]$ which represents the "new information" that the measurement z_k is providing relative to what the filter estimates the measurement to be $[\, \hat{z}_k(-) = H_k \hat{x}_k(-)\,]$.

[28] recommends a 3-sigma test for this problem based on the innovations. According to his scheme, if the magnitude of the ratio of the innovation to its standard deviation is larger than 3, it is rejected, otherwise it is accepted. There are no distinct criteria in this area, and once again the Monte Carlo data is invaluable in testing the algorithms before it is in-motion tested. The sigma value of a state is extracted from the related diagonal element of the covariance matrix, $P_k(+)$. The diagonal elements of $P_k(+)$ are the square of sigma (standard deviation) of related states.

CHAPTER 5

ATTITUDE DETERMINATION WITH VECTOR MEASUREMENTS

5.1 Attitude Determination with 2 Vector Sets

Let B represent the body frame and N represent the navigation frame. With a single sensor that gives a vector output (e.g. magnetometer) V^B_{sensor}, it is not possible to find the Euler angles that gives the transformation C^B_{N} between B and N frames;

$$v^B_{\text{sensor}} = C^B_{\text{N}} . v^N_{\text{reference}} \tag{5.1}$$

By a single vector measurement, there exist infinitely many Euler angle solutions [31]. To overcome this problem, a second vector measurement that is also between B and N frame is used. Thus, 2 different vector sets (totally 4 vectors) are ready for the attitude solution;

$$v^B = C^B_{\text{N}} . v^N \qquad u^B = C^B_{\text{N}} . u^N \tag{5.2}$$

By cross product of U and V vectors, W vector is obtained;

$$w^B = u^B \times v^B \qquad w^N = u^N \times v^N \tag{5.3}$$

Using U, V and W, augmented matrix D is obtained;

$$D^B_{3\times3} = [u^B_{3\times1}\ v^B_{3\times1}\ w^B_{3\times1}] \qquad D^N_{3\times3} = [u^N_{3\times1}\ v^N_{3\times1}\ w^N_{3\times1}] \tag{5.4}$$

Finally, C^B_N matrix can obtain as [33];

$$C^B_N = D^B.\ (D^N)^{-1} \tag{5.5}$$

In order to obtain attitude from 5.5, $U^N_{3\times1}$ and $V^N_{3\times1}$ should be non-collinear, otherwise D^N will be singular. For this kind of solution, two different vector measurements are required. In coarse alignment procedure of navigation systems, generally gravity and Earth rotation rates, which are certainly not parallel to each other, are used for vector measurements [8, 32]. To measure the Earth rotation rate (approx. 15deg/hr); the angular rate sensors must have a bias that is far less than 15deg/hr, which is not the case in low cost gyros. To overcome this problem, another kind of vector measurement should be taken. Three axis magnetometer (TAM) is a good candidate for solution. Magnetic field and gravity are certainly not parallel to each other. Thus, one has 4 vectors for attitude determination;

- Earth gravity field vector (defined in navigation frame)
- Accelerometer outputs(defined in body frame)
- Earth magnetic field vector (defined in navigation frame)
- Magnetometer field vector (defined in body frame)

This kind of a solution requires the body to have accelerations except the gravitational acceleration. In accelerating body, it is not possible to use gravity field vector.

5.2 Magnetometer Measurement Models for Kalman Filter

Here we assume that the magnetometer has been calibrated for scale factors, non-orthogonality corrections, and biases using one of the attitude independent calibration algorithms. The body frame observation model of a TAM is similar to a typical vector sensor [6,34,35]

$$B^N = \widehat{C}_B^N.(B^B + \nu_{Mgn}) \tag{5.6}$$

where B^B is the TAM observation, B^N is the reference magnetic field in an Earth-fixed inertial frame corresponding to the specific position and altitude, $\widehat{C}_B^N$ is the ideal direction cosine matrix which is function of Euler angles ϕ, θ, ψ, and finally v_k is the measurement noise that includes both sensor errors and geomagnetic field model uncertainties,. The measurement noise is assumed to be a zero-mean Gaussian process with covariance.

In terms of the DCM of computed navigation frame;

$$B^N = (\delta C_B^N.C_B^N)(B^B + \nu_{Mgn}) \tag{5.7}$$

Replacing δC_B^N with the error misalignment vector,

$$B^N = (I - \tilde{\gamma}^n).C_B^N(B^B + \nu_{Mgn}) \tag{5.8}$$

Rearranging the equation

$$B^N = C_B^N(B^B + \nu_{Mgn}) - \tilde{\gamma}^n.C_B^N(B^B + \nu_{Mgn}) \tag{5.9}$$

$$B^N - C_B^N.B^B = C_B^N.\nu_{Mgn} - \tilde{\gamma}^n.C_B^N.B^B \tag{5.10}$$

$$B^N - C_B^N.B^B = (C_B^N.B^B) \times \gamma^n + C_B^N.\nu_{Mgn} \tag{5.11}$$

Similarly, gravitational acceleration measurement can be written as;

$$g^N = \hat{C}_B^N.(a^B + \delta a^b) \tag{5.12}$$

Where

δa^b : Acceleration errors, such as bias scale factor, noise etc.

Following the same procedure in magnetometer measurements;

$$g^N = (\delta C_B^N + C_B^N)(a^B + \delta a^b) \tag{5.13}$$

$$g^N = (I - \tilde{\gamma}).C_B^C(a^B + \delta a^b) \tag{5.14}$$

$$g^N = C_B^C(a^B + \delta a^b) - \tilde{\gamma}.C_B^C(a^B + \delta a^b) \tag{5.15}$$

$$g^N - C_B^C.a^B = C_B^C.\delta a^b - \tilde{\gamma}.C_B^C.a^B \tag{5.16}$$

$$g^N - C_B^C.a^B = (C_B^C.a^B) \times \gamma + C_B^C.\delta a^b \tag{5.17}$$

In measurement equation (5.1), the states are three Euler angles given in nonlinear form. To obtain a measurement equation which have error states (e.g. states that model attitude errors), the relation between true and erroneous direction cosine matrices are expressed;

A measurement equation directly for angular rates can be written by taking derivative of equation (5.6);

$$\begin{aligned}&\dot{B}^N - \dot{C}_B^N.B^B - C_B^N.\dot{B}^B \\ &= (\dot{C}_B^N.B^B + C_B^N.\dot{B}^B)\times\gamma^n + \\ &(C_B^N.B^B)\times\dot{\gamma}^n + \dot{C}_B^N.\nu_{Mgn} + C_B^N.\dot{\nu}_{Mgn}\end{aligned} \tag{5.18}$$

Replacing $\dot{C}_b^n$ and $\dot{\gamma}^n$ by

$$\dot{C}_b^n = C_b^n.(\tilde{\omega}_{ib}^b) - (\tilde{\omega}_{in}^n).C_b^n \tag{5.19}$$

$$\dot{\gamma}^n = -C_b^n.\delta\omega_{ib}^b - \omega_{in}^n\times\gamma^n + \delta\omega_{in}^n \tag{5.20}$$

$$\begin{aligned}&\dot{B}^N - (C_b^n.(\tilde{\omega}_{ib}^b) - (\tilde{\omega}_{in}^n).C_b^n).B^B - C_B^N.\dot{B}^B = \\ &((C_b^n.(\tilde{\omega}_{ib}^b) - (\tilde{\omega}_{in}^n).C_b^n).B^B + C_B^N.\dot{B}^B)x\gamma^n \\ &+(C_B^N.B^B)x(-C_b^n.\delta\tilde{\omega}_{ib}^b - \tilde{\omega}_{in}^n x\gamma^n + \delta\tilde{\omega}_{in}^n) \\ &+(C_b^n.(\tilde{\omega}_{ib}^b) - (\tilde{\omega}_{in}^n).C_b^n).\nu_{Mgn} + C_B^N.\dot{\nu}_{Mgn}\end{aligned} \tag{5.21}$$

Same procedure can be applied to gravitational measurement equation.

With this equation, it is possible to estimate the angular rates. But, as this equation is based on differentiation, all noisy measurements, magnetometer and gyro outputs, are differentiated, which yields an extremely noisy measurement equation. Magnetometers are generally low noise sensors, but the MEMS gyros (especially MEMS gyros) can be very noisy. This measurement equation may result in bad estimation if it is used in Kalman filter. In order to use these equations, gyros should have low noise characteristics. In this thesis, low accuracy MEMS gyros are taken into consideration, thus equation 5.21 cannot be used in the simulation studies. This equation may be used in a case where low noise gyros (such as RLG or FOG) are used.

5.3 Single Axis Attitude Determination

In spinning missiles, the roll rate can be as high as 7000-8.000 deg/s. Many gyros will saturate in that kind of angular motion. Gyros that have such a measurement range probably will have extremely high prices. As the guidance and autopilot loops need the roll rate, it is crucial to estimate this roll motion.

Before analyzing the equations 5.30-5.36 and 5.41, it is important to note that in a vector measurement equation set, three equations are not independent. Thus, it is not possible to find all three Euler angles or rates analytically by a single vector measurement, which is known as Wahba's problem [31]. With a single vector, only one Euler angle without ambiguity can be obtained provided that the other two Euler angle should be known a priori.

Note that all three Euler angles are coupled to each other, thus if someone does not know one of the angular speeds, it is not possible to calculate the Euler angles due to the couplings. In the proposed algorithm, the following assumptions are taken into consideration.

- The system has only one degree of rotational freedom, thus 2 Euler angles are known a priori.
- If the system has three degree of freedom, then;
    - The algorithm should run in such a high rate that the errors due to Euler angle coupling between time steps are minimized.
    - Three are three gyros, but one of them is saturated (e.g. it measures 1000 deg/s angular speed as 500 deg/s due to its measurement range), thus the coupling errors again minimized.

The flow chart of this algorithm is given in Figure 5.1 .

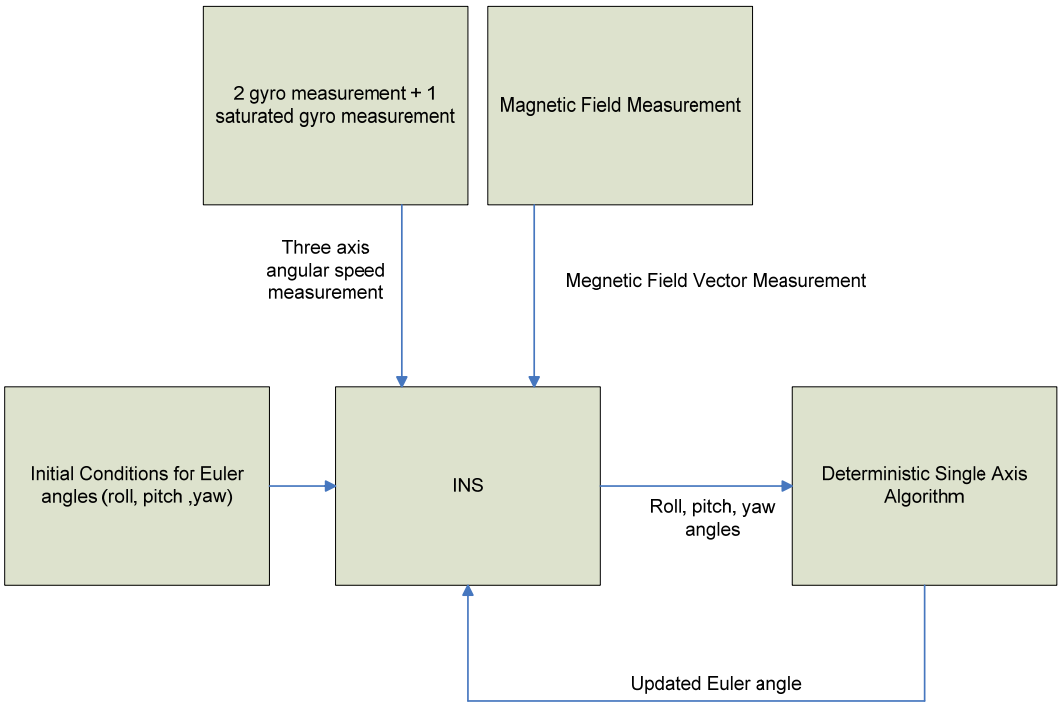

Figure 5.1 Flow diagram of the Single Axis Attitude Determination Algorithm

Remember that a direction cosine matrix can be written as;

$$C_b^n = \begin{pmatrix} \cos(\psi).\cos(\theta) & \cos(\psi).\sin(\theta).\sin(\phi) - \sin(\psi).\cos(\phi) & \cos(\psi).\sin(\theta).\cos(\phi) + \sin(\psi).\sin(\phi) \\ \sin(\psi).\cos(\theta) & \sin(\psi).\sin(\theta).\sin(\phi) + \cos(\psi).\cos(\phi) & \sin(\psi).\sin(\theta).\cos(\phi) - \cos(\psi).\sin(\phi) \\ -\sin(\theta) & \cos(\theta).\sin(\phi) & \cos(\theta).\cos(\phi) \end{pmatrix} \quad (5.22)$$

In an ideal vector measurement;

$$A = C_b^n.B \quad (5.23)$$

Thus, from equation 5.23, it is possible to write 3 equations, but only 2 of them are independent, which means that it is not possible to solve for 3 unknown Euler angles. Besides that, with a vector measurement equation, it is not possible to solve for 2 Euler angles without ambiguity. Note that, the Euler angles in DCM are in sine and cosine form;

$$\sin(\psi) = \pm\sqrt{1-\cos^2(\psi)}$$
$$\sin(\theta) = \pm\sqrt{1-\cos^2(\theta)} \qquad (5.24)$$
$$\sin(\phi) = \pm\sqrt{1-\cos^2(\phi)}$$

To solve equation 5.23 for two unknown Euler angles, basic sine-cosine relation for each Euler should be inserted, but it is not possible to do it with out ambiguity, as it can be seen from equation 5.24.

To find a single Euler angle with a vector measurement, remember the vector-DCM equation;

$$B^N = \underset{321}{\hat{C}}(\psi,\theta,\phi)B^B \qquad (5.25)$$

There are three unknowns and three dependent equations. In the following part, a methodology to find each Euler angle provided that the other two Euler angle is given;

To find the roll angle, provided that pitch and yaw angle is given, write equation 25 as;

$$B^N = \underset{321}{\hat{C}}(\psi,\theta,\phi)B^B = \underset{32}{\hat{C}}(\psi,\theta)\underset{1}{\hat{C}}(\phi)B^B \qquad (5.26)$$

Note that $\underset{1}{\hat{C}}(\phi)B$ can be written as follows with some algebraic manipulations;

$$\underset{1}{\hat{C}}(\phi)B = \begin{bmatrix} 1 & 0 & 0 \\ 0 & \cos\phi & -\sin\phi \\ 0 & \sin\phi & \cos\phi \end{bmatrix}\begin{bmatrix} B_x \\ B_y \\ B_z \end{bmatrix} = \underbrace{\begin{bmatrix} B_x & 0 & 0 \\ 0 & B_y & -B_z \\ 0 & B_z & B_y \end{bmatrix}}_{\hat{B}}\underbrace{\begin{bmatrix} 1 \\ \cos\phi \\ \sin\phi \end{bmatrix}}_{\bar{\phi}} \qquad (5.27)$$

Now insert equation 5.27 into equation 5.26 and solve for

$$B^N = \underset{32}{\hat{C}}\,\hat{B}\overline{\phi} \tag{5.28}$$

And solve for $\overline{\phi}$;

$$\overline{\phi} = \hat{B}^{-1}\,\underset{32}{\hat{C}}^{-1}\,B^N \tag{5.29}$$

Thus, the roll angle can be found as;

$$\phi = \arctan_2\left(\overline{\phi}_3, \overline{\phi}_2\right) \tag{5.30}$$

Similarly, pitch and yaw angles can be found as follows;

To find the pitch angle, rotate the Body vector in roll axis;

$$B^N = \underset{321}{\hat{C}}(\psi,\theta,\phi)B = \underset{32}{\hat{C}}(\psi,\theta)\underbrace{\underset{1}{\hat{C}}(\phi)B}_{B_2} \tag{5.31}$$

$$B^N = \underset{32}{\hat{C}}(\psi,\theta)B_2 = \underset{3}{\hat{C}}(\psi).\underset{2}{\hat{C}}(\theta).B_2 \tag{5.32}$$

With the help of linear algebra;

$$\underset{2}{\hat{C}}(\theta)B_2 = \begin{bmatrix} \cos(\theta) & 0 & \sin(\theta) \\ 0 & 1 & 0 \\ -\sin(\theta) & 0 & \cos(\theta) \end{bmatrix}\begin{bmatrix} B_{2x} \\ B_{2y} \\ B_{2z} \end{bmatrix} = \underbrace{\begin{bmatrix} 0 & B_{2x} & B_{2z} \\ B_{2y} & 0 & 0 \\ 0 & B_{2z} & -B_{2x} \end{bmatrix}}_{\hat{B}_2}\underbrace{\begin{bmatrix} 1 \\ \cos\theta \\ \sin\theta \end{bmatrix}}_{\overline{\theta}} \tag{5.33}$$

$$B^N = \underset{3}{\hat{C}}\,\hat{B}_2\overline{\theta} \tag{5.34}$$

Now solve for pitch angle;

$$\overline{\theta} = \hat{B}_2^{-1} \hat{\underset{3}{C}}^{-1} B^N \tag{5.35}$$

And the pitch angle can be written as;

$$\theta = \arctan_2\left(\overline{\theta}_3, \overline{\theta}_2\right) \tag{5.36}$$

Likewise, to find the yaw angle, rotate the body vector B in roll and pitch axes;

$$B^N = \hat{\underset{321}{C}}(\psi,\theta,\phi)B = \hat{\underset{3}{C}}(\psi)\underbrace{\hat{\underset{2}{C}}(\theta)\hat{\underset{1}{C}}(\phi)B}_{B_3} \tag{5.37}$$

$$\begin{aligned}\hat{\underset{3}{C}}(\psi)B_3 &= \begin{bmatrix}\cos(\psi) & -\sin(\psi) & 0\\ \sin(\psi) & \cos(\psi) & 0\\ 0 & 0 & 1\end{bmatrix}\begin{bmatrix}B_{3x}\\ B_{3y}\\ B_{3z}\end{bmatrix}\\ &= \underbrace{\begin{bmatrix}0 & B_{3x} & -B_{3y}\\ 0 & B_{3y} & B_{3x}\\ B_{3z} & 0 & 0\end{bmatrix}}_{\hat{B}_3}\underbrace{\begin{bmatrix}1\\ \cos\psi\\ \sin\psi\end{bmatrix}}_{\overline{\varphi}}\end{aligned} \tag{5.38}$$

$$B^N = \hat{B}_3\overline{\varphi} \tag{5.39}$$

$$\overline{\varphi} = \hat{B}_2^{-1}B^N \tag{5.40}$$

$$\psi = \arctan_2\left(\overline{\psi}_3, \overline{\psi}_2\right) \tag{5.41}$$

Using equations 5.30, 5.36 and 5.41, one can find the related Euler angle, given that the assumptions mentioned above are valid. Remember that in this method, the main driving factor in the errors is the coupling between the Euler angles. Only one Euler angle is corrected with the help of magnetometers, the other two are stand alone inertial, which means that the accuracy of the aided Euler angle is affected by the errors of these 2 Euler angles.

As this method is an analytical solution, it is not accurate as the Kalman filtered solution. Besides, the cumulative error in the unaided Euler angles will result in high errors in the aided Euler angle. This method can be used only in a short period of time. The main advantage of this algorithm is its computational superiority over Kalman filtered solution.

CHAPTER 6

GROUND ALIGNMENT VIA MEMS IMU + MAGNETOMETER

In a high accuracy IMU, it is possible to align the navigation system by using the inertial measurements, which is also known as self alignment or quasi stationary alignment. This method is generally composed of two main parts [36, 37, and 38];

1. Coarse Alignment
2. Fine Alignment

Where coarse alignment is an analytical solution and the fine alignment is the part that the Kalman filter is used.

The reason for this partition is arising from the nature of estimation algorithms. In most of the navigation system, Kalman filter is used, which is indeed a linear estimation filter. As explained in the previous chapters, the states in the estimation are the navigation and sensor errors. The navigation error equations were derived by using the small attitude error assumption, which is valid up to 20 degree errors. [1, 11, 13, 14]

The coarse alignment phase is an analytic procedure, in which two sets of vector equations are used to find the related direction cosine matrix. In a high accuracy system, gravity and earth rotation rate is used as the vector equations. As it is implied in its name, the solution is "coarse", that is accuracy is only up to 1-0.5 degrees. The main function of the coarse alignment phase is to make the attitude errors as small as possible so that the linearity assumption in the navigation errors is valid. The details of the coarse alignment process were given in the previous chapter.

The fine alignment phase is the part where not only the attitude errors are found with high accuracy, but also the sensor errors may be estimated. In the fine alignment process, following measurements are taken into consideration;

1. Two sets of vector equations
2. Zero velocity
3. Constant Position

As explained above, the ground alignment algorithms use earth rotation rate (~15 deg/hr) and gravity (~9.801 m/s^2) as the vector measurement equations. MEMS accelerometers generally have a bias repeatability in the order of 10 mg, thus they can measure the gravitational acceleration accurate enough such that it may be used as a vector equation. On the other hand, MEMS gyros have a drift repeatability in the order of 100 deg/hr, which is greatly higher than the earth rotation rate. Earth rotation rate can not be used as a vector measurement where MEMS gyros are used.

In the proposed method, the magnetic field is used as a vector measurement equation. The MEMS magnetometers have high accuracy, and the reference magnetic field (world magnetic field) can be modeled very accurately.

The simulations are carried out in Matlab®. The structure of the simulation environment is given as follows;

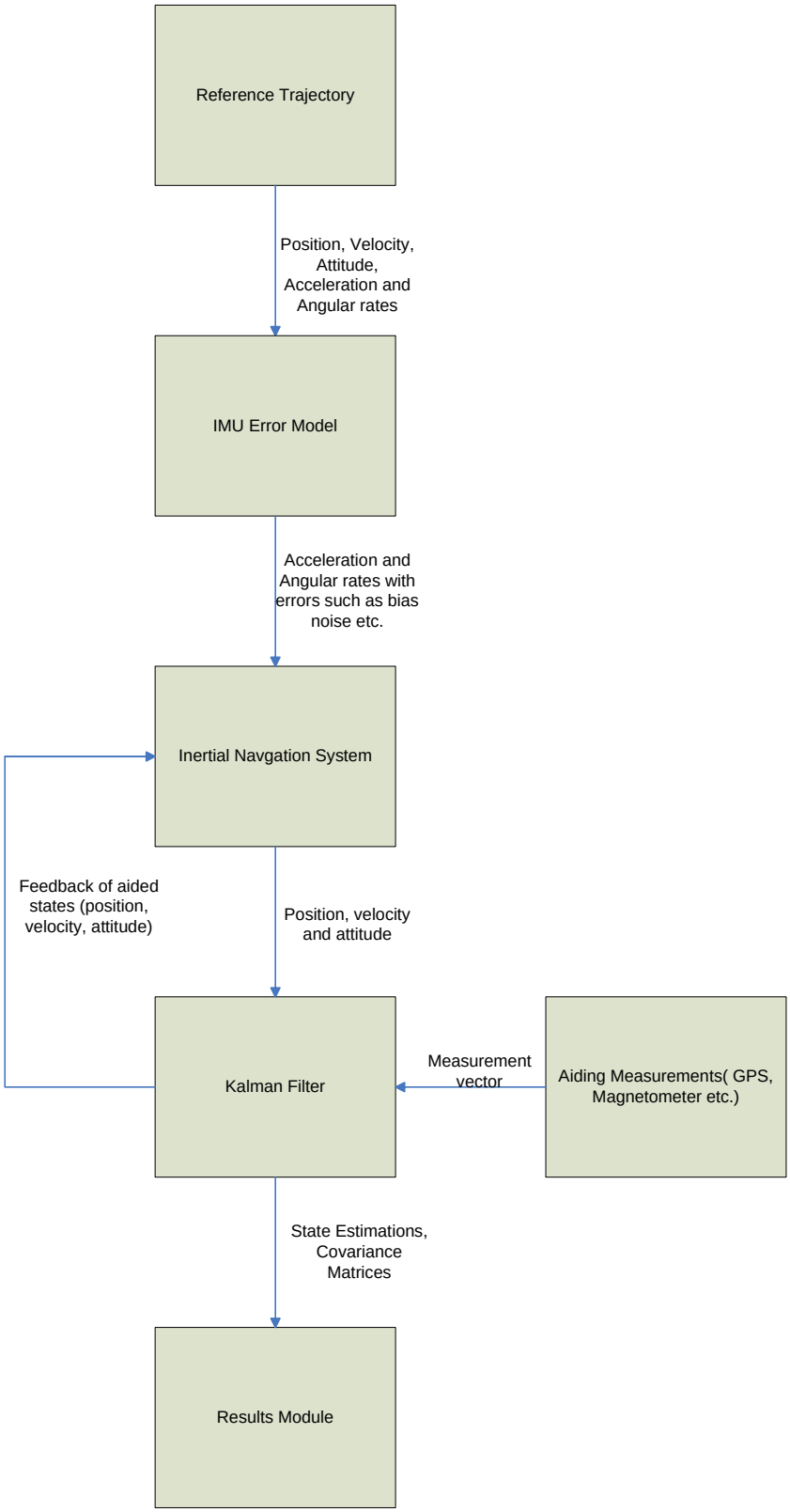

Figure 6.1 Flow diagram of the Simulations

The Matlab®. codes that developed in this thesis are given in Appendix F.

6.1 Coarse Alignment

In the coarse alignment procedure, Equations (5.1)-(5.5) are used, where the gravity and magnetic field are used as vector measurements.

6.1.1 Monte Carlo Simulations

In the simulation and experimental studies process, the following sensor sets are used;

- Colibrys MS8000.C Accelerometer
- Inertial Science RRS01 Gyro
- HMC 1053 Magnetometer

Performance specifications of these sensors are given in the Appendix.

In the Monte Carlo Simulations, following set of random variables is used;

- Gyro Bias Repeatability : 100 deg/hr (1 σ), Normal Distribution
- Gyro Noise: 1 deg/s (1 σ), Normal Distribution
- Gyro Scale Factor Error: 1000 ppm (1 σ), Normal Distribution
- Accelerometer Bias Repeatability 10 mg (1 σ),: Normal Distribution
- Accelerometer Noise : 5 mg (1 σ), Normal Distribution
- Accelerometer Scale Factor Error: 1000 ppm (1 σ), Normal Distribution
- Magnetometer Noise: 5 mGauss (1 σ), Normal Distribution
- Attitude of the Sensor Block (North, East, Down) : Uniform Distribution

Variances of gyro, accelerometer and magnetometer are selected in accordance with the performance specifications of the related sensor, which are given in Appendix B.

The update rate of the inertial navigation module and Kalman filter module are 100 Hz.

Note that, all variables except attitude of the sensor block have normal distribution. Attitude is chosen to have uniform distribution so that the effects of the initial attitude in the simulations are eliminated [37, 38].

The results of the simulations for the pitch roll and azimuth estimations are given in Figure 6-1-6-3. The azimuth and roll attitude errors are approximately 1 degree. The pitch error is relatively smaller (~0.3 degree), which is a results of the accuracy in measuring the gravity vector.

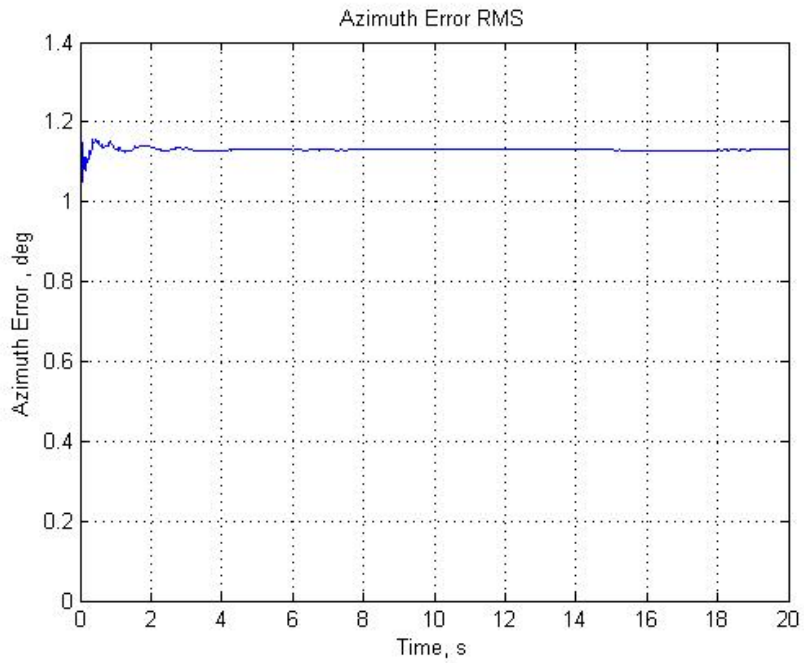

Figure 6.1 Azimuth Error (Root Mean Square Error)

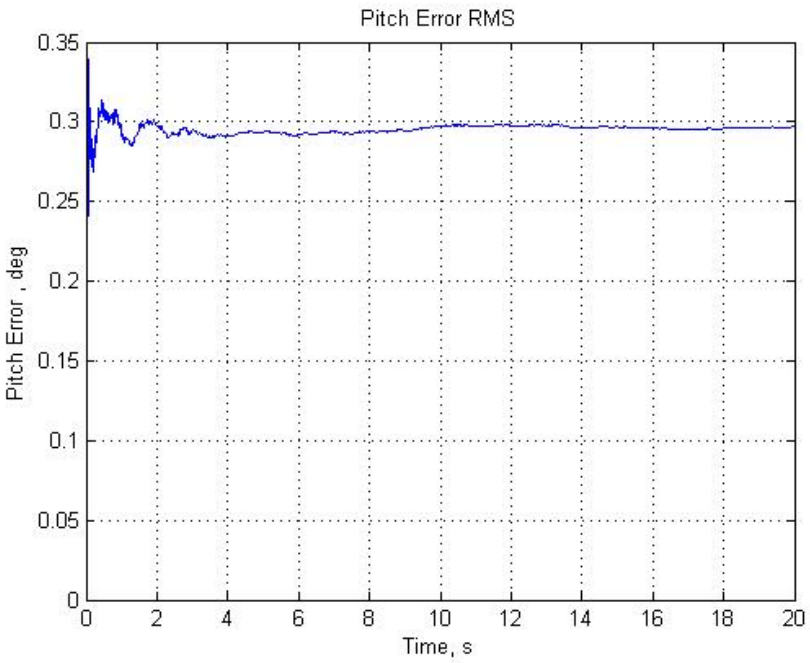

Figure 6.2 Pitch Error (Root Mean Square Error)

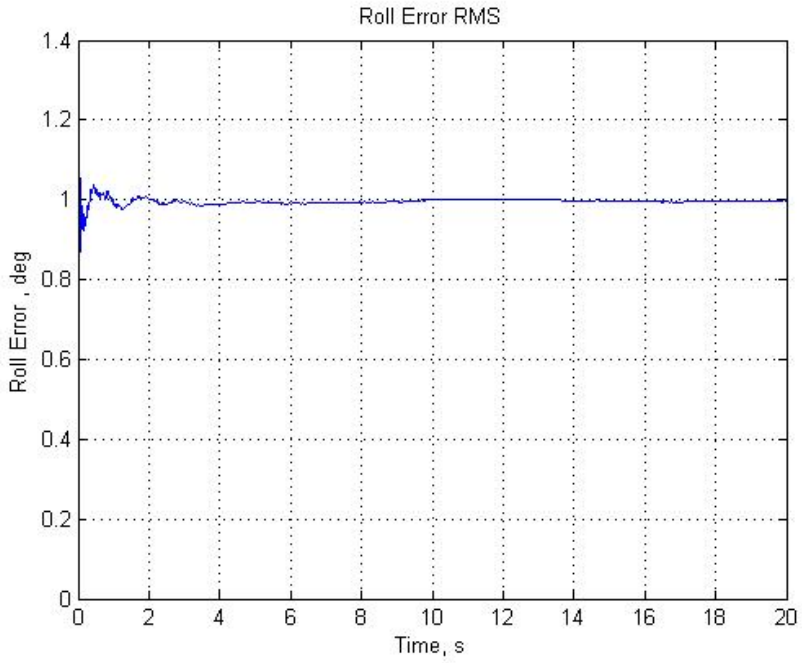

Figure 6.3 Roll Error (Root Mean Square Error)

6.1.2 Coarse Alignment Experiments

The coarse alignment experiment basically consists of an IMU and a magnetometer oriented accurately in a stationary position. The experiments are divided into two parts according to the attitude of the sensor block;

- Set 1: Heading towards North, level to the ground
- Set 2: Heading towards East, level to the ground

6.1.2.1 Coarse Alignment Experiment Set 1

The results of the C/A experiment are given in Figures 6-4-6-6. The azimuth error is relatively larger than pitch and roll errors, which is a result of the errors in the world magnetic field error

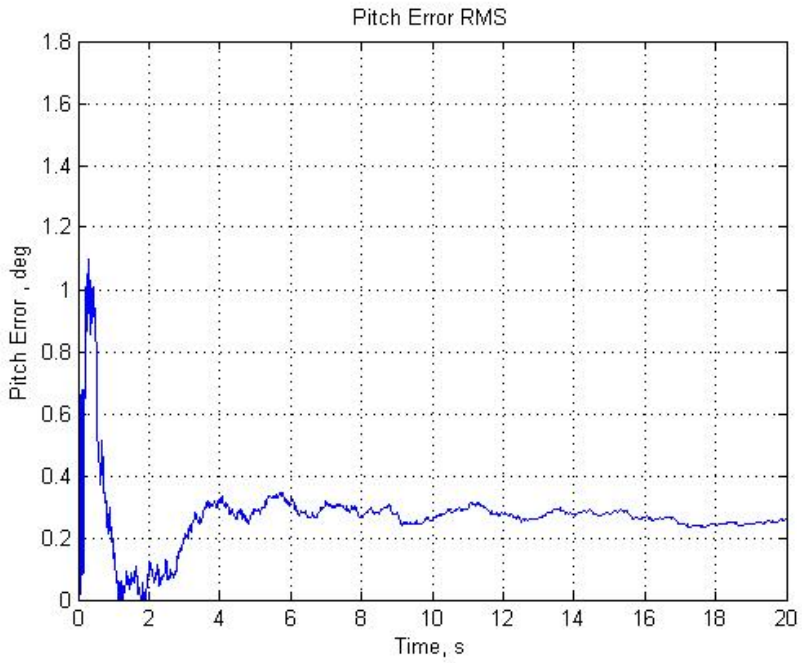

Figure 6.4 Pitch Error (Root Mean Square Error)

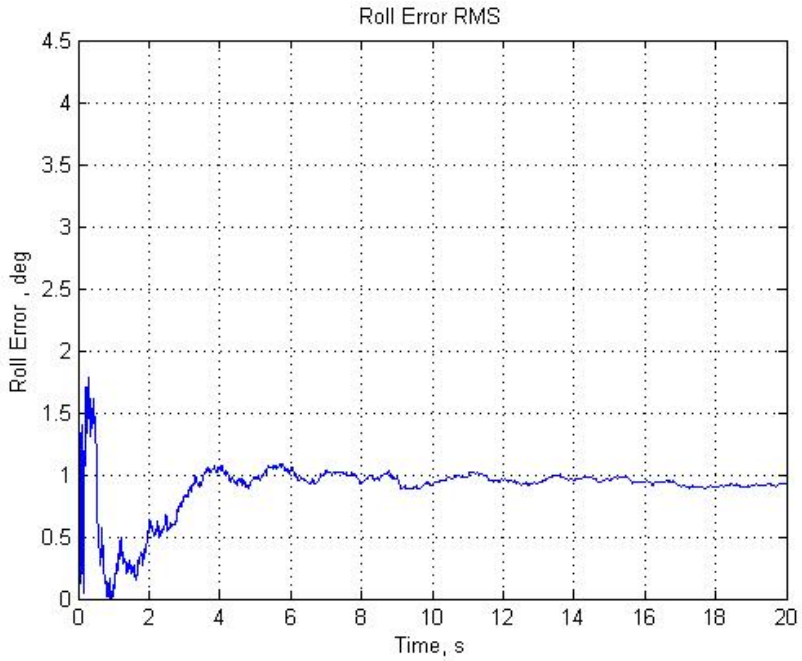

Figure 6.5 Roll Error (Root Mean Square Error)

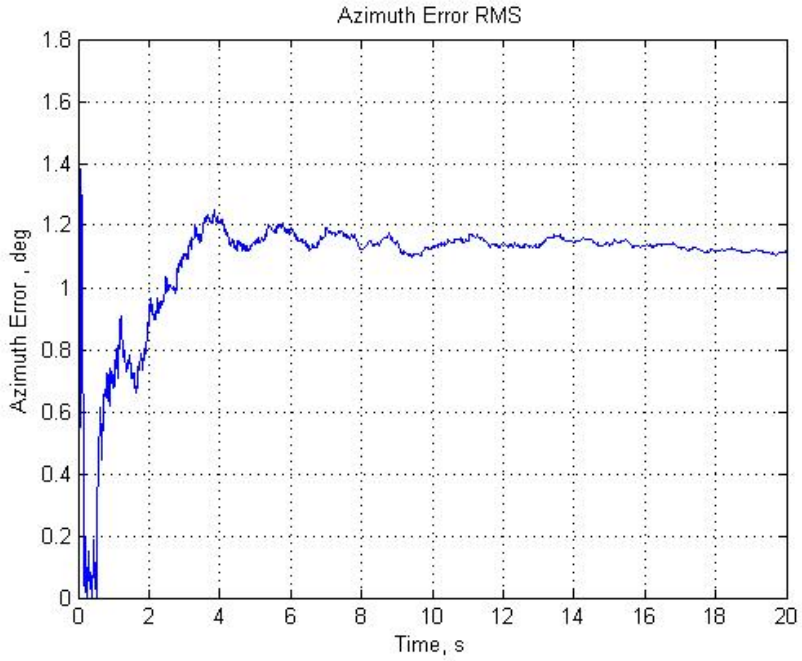

Figure 6.6 Azimuth Error (Root Mean Square Error)

6.1.2.2 Coarse Alignment Experiment Set 2

In the C/A experiment Set 2, again the largest error is seen in the azimuth angle, as a result of the magnetic field modeling errors.

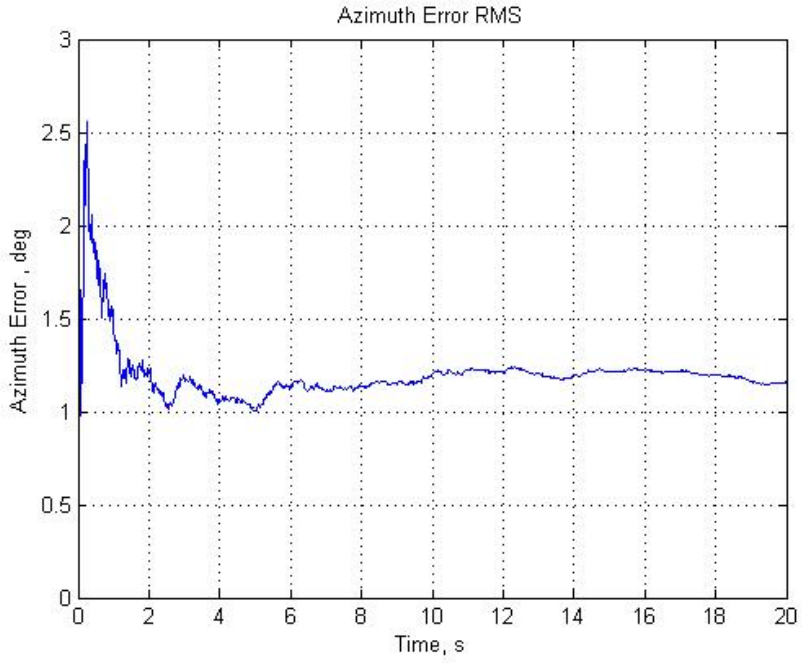

Figure 6.7 Azimuth Error (Root Mean Square Error)

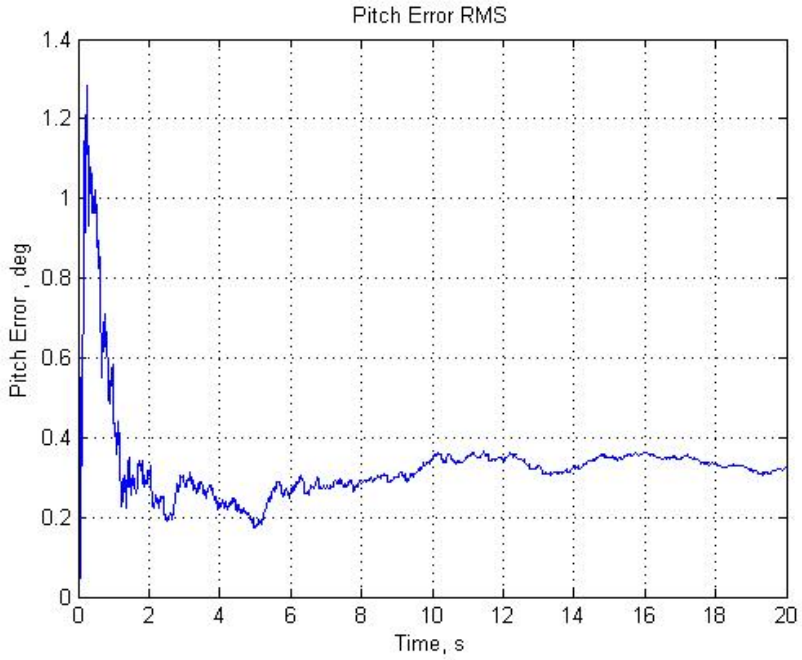

Figure 6.8 Pitch Error (Root Mean Square Error)

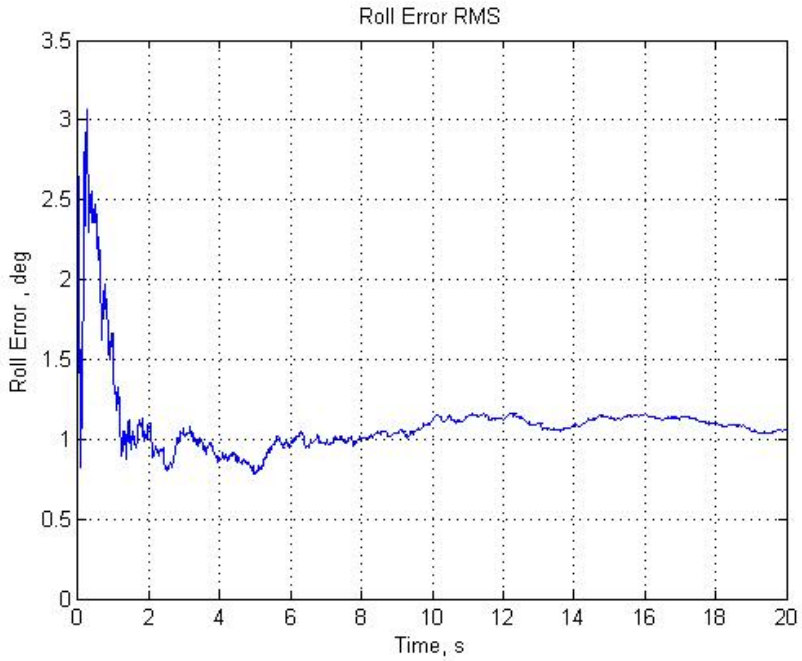

Figure 6.9 Roll Error (Root Mean Square Error)

6.2 Fine Alignment

The fine alignment algorithm is in fact a stochastic estimation. The estimation filter is a linear Kalman filter. As the navigation unit is stationary through the alignment, GPS velocity (quasi stationary velocity) and position (constant position) measurements are used in addition to the accelerometer and magnetometer measurements,

6.2.1 Monte Carlo Simulations

The states of the Kalman filter are;

- 3 states of attitude error
- 3 states of velocity error
- 3 states of position error
- 3 states of gyro bias
- 3 states of accelerometer bias

The attitude, velocity and position errors are modeled with equations given in Chapter 2, where gyro and accelerometer noises are modeled as random constants.

The scale factor error, misalignment errors etc. are not modeled in the estimation filter as these errors are not observable in the MEMS sensors.

The process noises are;

- Accelerometer noises
- Gyro noises

The measurements are;

- Accelerometer measurements
- Magnetometer measurements

- Velocity measurements (zero velocity)
- Position measurements (constant position)

The measurement noises;

- Accelerometer noises
- Magnetometer noises
- Velocity uncertainty
- Position uncertainty

Accelerometer, gyro and magnetometer noises account for all unobservable and negligible sensor errors. Scale factor, cross couplings, g dependent bias etc. are assumed to be pre-calibrated. Initial values for noise covariance matrices are chosen according to the sensor's performance specifications. The velocity and position uncertainties in the measurement noise matrix are chosen as given in the GPS receiver's performance specifications, which also account for the host vehicle vibrations.

Initial states of the covariance values are;

- Attitude error (1σ) : 5 degrees
- Velocity error (1σ) : 0.1 m/s
- Position error (1σ) : 5 m
- Gyro Bias (1σ) : 100 deg/hr
- Accelerometer Bias (1σ) : 10 mg

Process and measurement noise covariance values:

- Gyro noises: 1 deg/s
- Accelerometer noises : 5 mg
- Magnetometer noises: 10 mGauss

- Velocity uncertainty: 0.1 m/s
- Position uncertainty: 5 m

The random variables in the Monte Carlo Simulations are as follows,

- Gyro Bias Repeatability : 100 deg/hr (1 σ), Normal Distribution
- Gyro Noise: 1 deg/s (1 σ), Normal Distribution
- Gyro Scale Factor Error: 1000 ppm (1 σ), Normal Distribution
- Accelerometer Bias Repeatability 10 mg (1 σ), Normal Distribution
- Accelerometer Noise : 5 mg (1 σ), Normal Distribution
- Accelerometer Scale Factor Error: 1000 ppm (1 σ), Normal Distribution
- Magnetometer Noise: 5 mgauss (1 σ), Normal Distribution
- Attitude of the Sensor Block (North, East, Down) : Uniform Distribution
- Velocity uncertainty: 0.1 m/s, (1 σ), Normal Distribution
- Position uncertainty: 5 m, (1 σ), Normal Distribution

The gyro, accelerometer and magnetometer variances are chosen in accordance with their performance specification, given in Appendix B

The primary objective of the fine alignment algorithm is to find the attitude angles in a high accuracy, which can be seen in Figure 6.10-6.12. The secondary objective is to on-line calibrate the IMU. The designed algorithm can estimate the bias errors of the accelerometer and gyros in a fast and accurate manner (Figures 6-10-6-18)

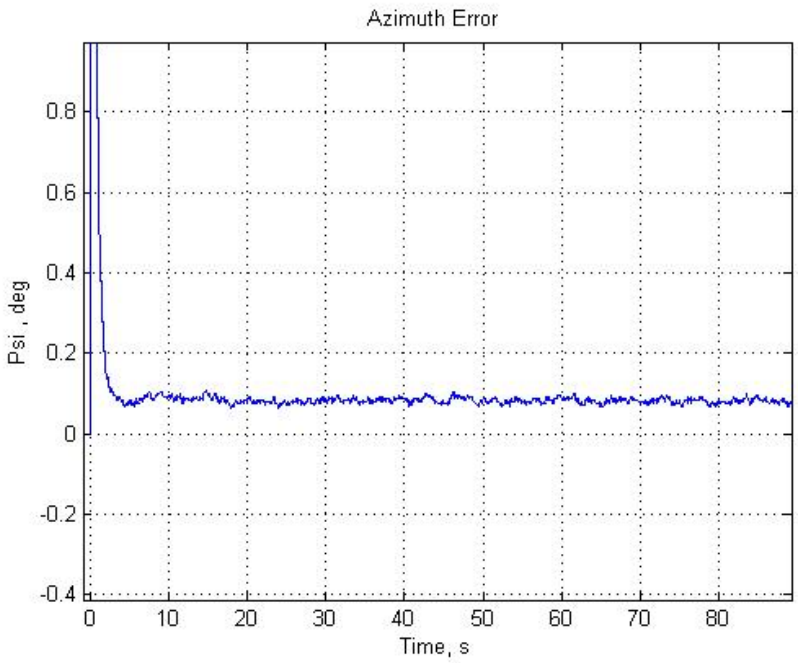

Figure 6.10 Azimuth Error (Root Mean Square Error)

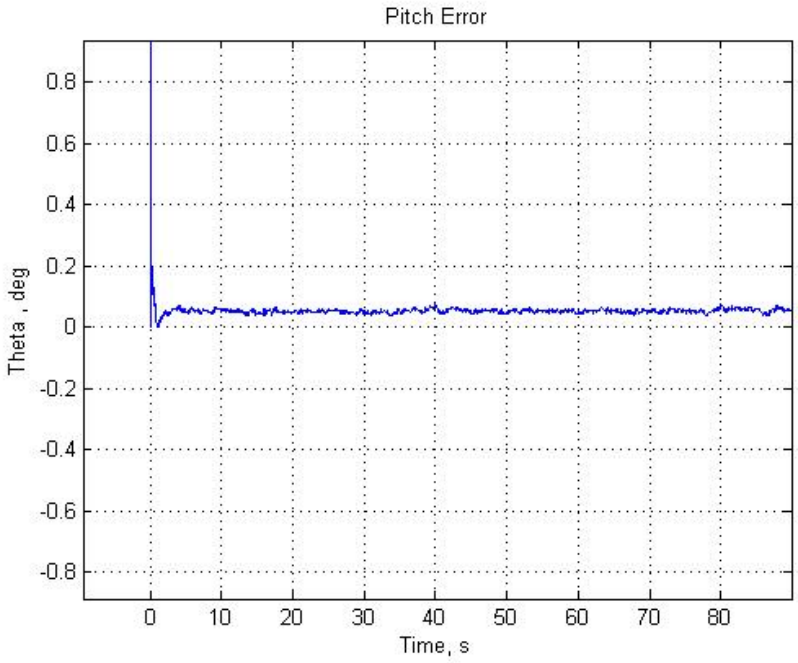

Figure 6.11 Pitch Error (Root Mean Square Error)

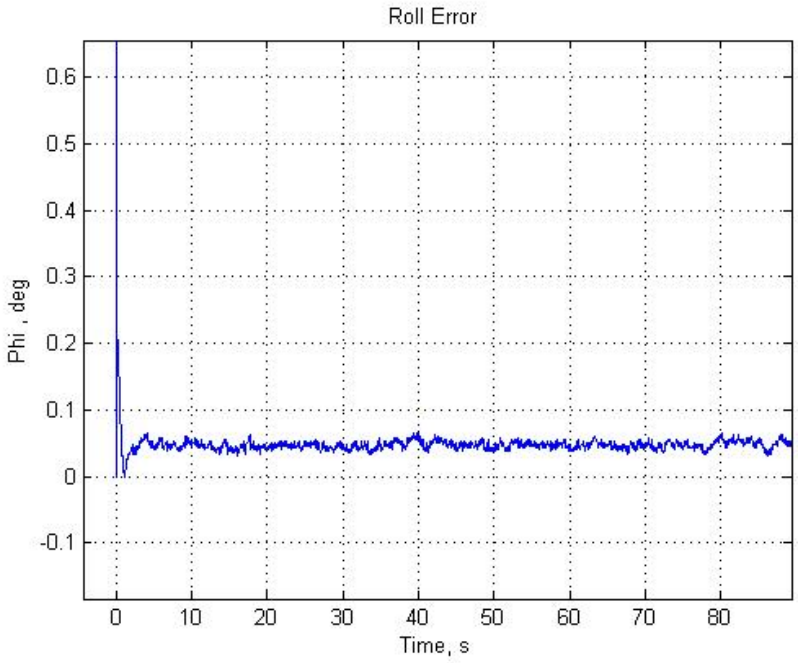

Figure 6.12 Roll Error (Root Mean Square Error)

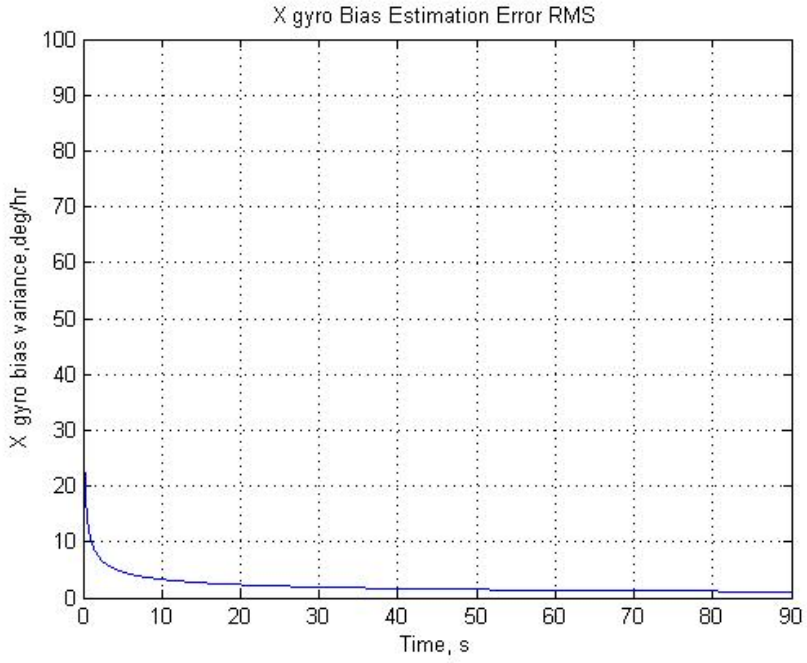

Figure 6.13 X Gyro Bias Estimation Error (Root Mean Square Error)

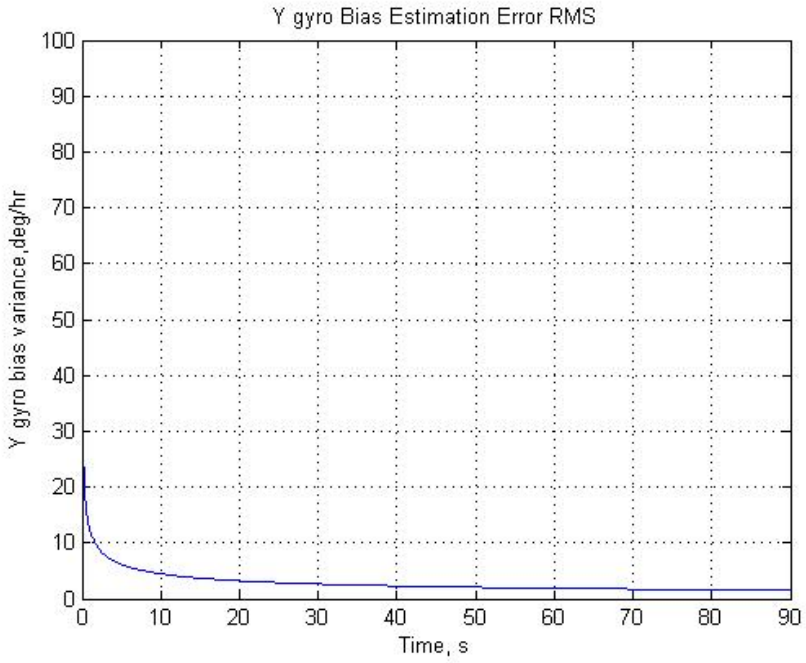

Figure 6.14 Y Gyro Bias Estimation Error (Root Mean Square Error)

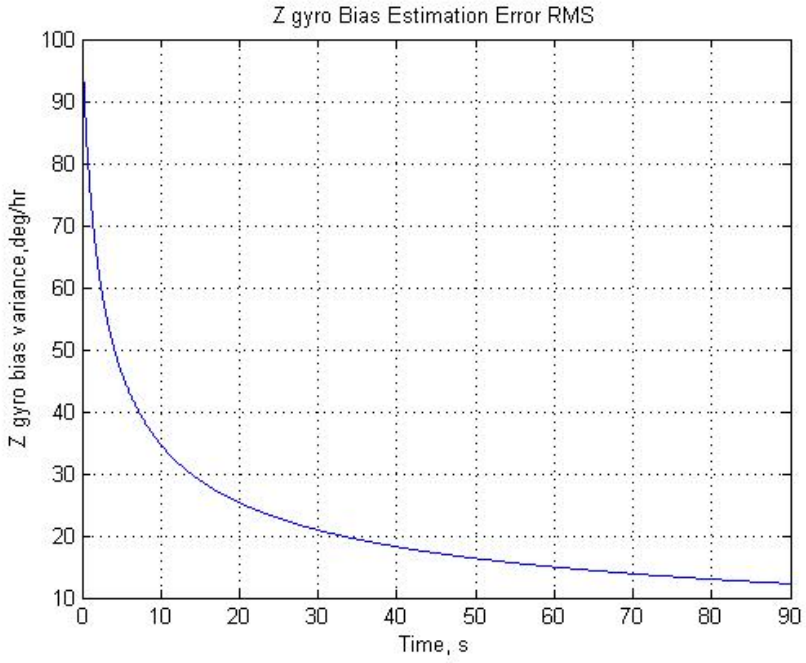

Figure 6.15 Z Gyro Bias Estimation Error (Root Mean Square Error)

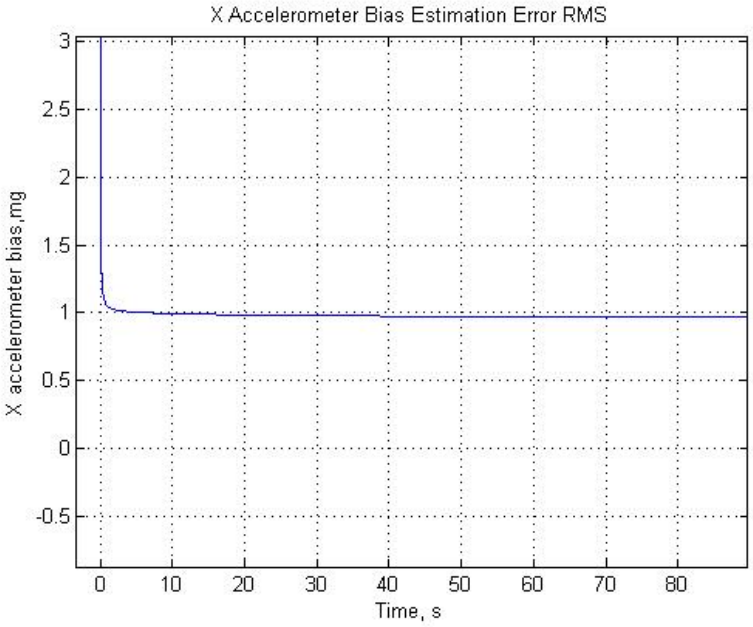

Figure 6.16 X Accelerometer Bias Estimation Error (Root Mean Square Error)

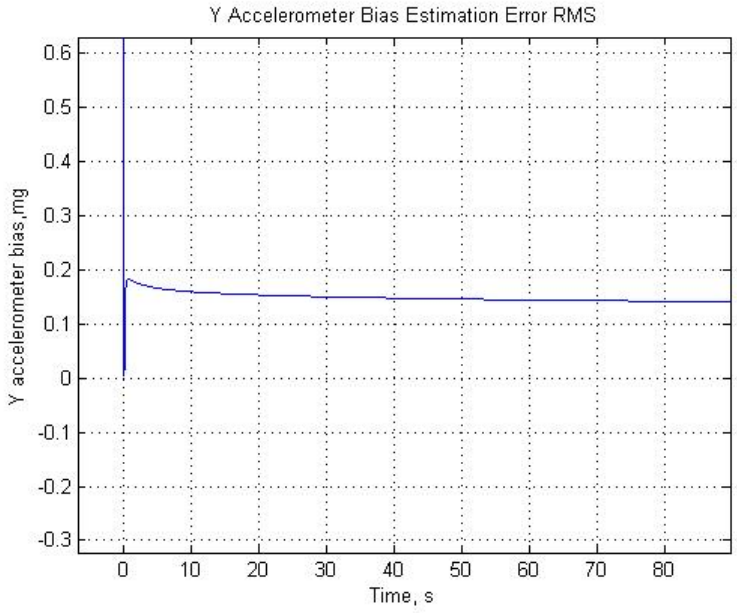

Figure 6.17 Y Accelerometer Bias Estimation Error (Root Mean Square Error)

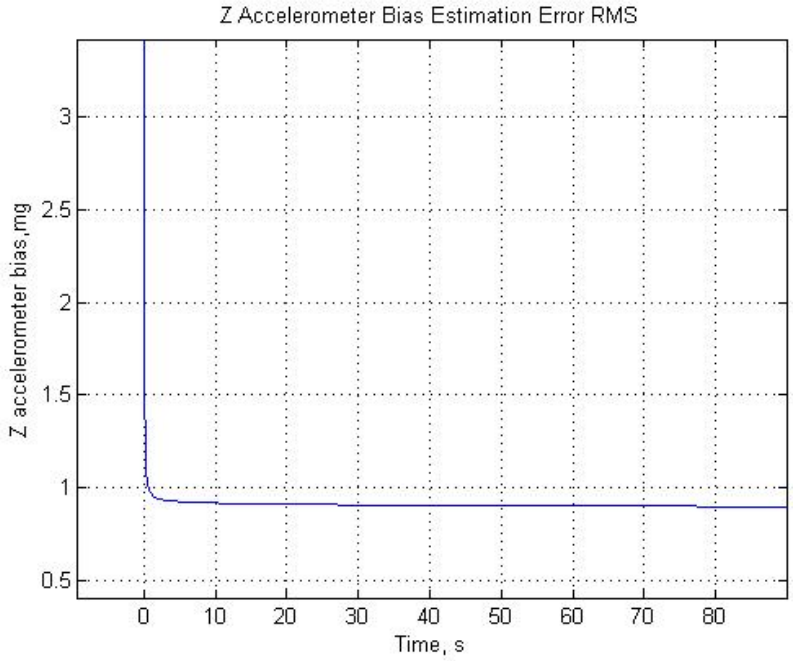

Figure 6.18 Z Accelerometer Bias Estimation Error (Root Mean Square Error)

6.2.2 Fine Alignment Experiments

As in the case in the coarse alignment, the fine alignment experiments are divided into two parts;

- Heading towards North, level to the ground
- Heading towards East, level to the ground

It can be seen from both experiments that the fine alignments has a fast convergence rate with high accuracy. The azimuth error is slightly larger than roll

and pitch errors, which is a result of the WMM 2005 errors, i.e., magnetic anomalies.

6.2.2.1 Fine Alignment Experiment Set 1

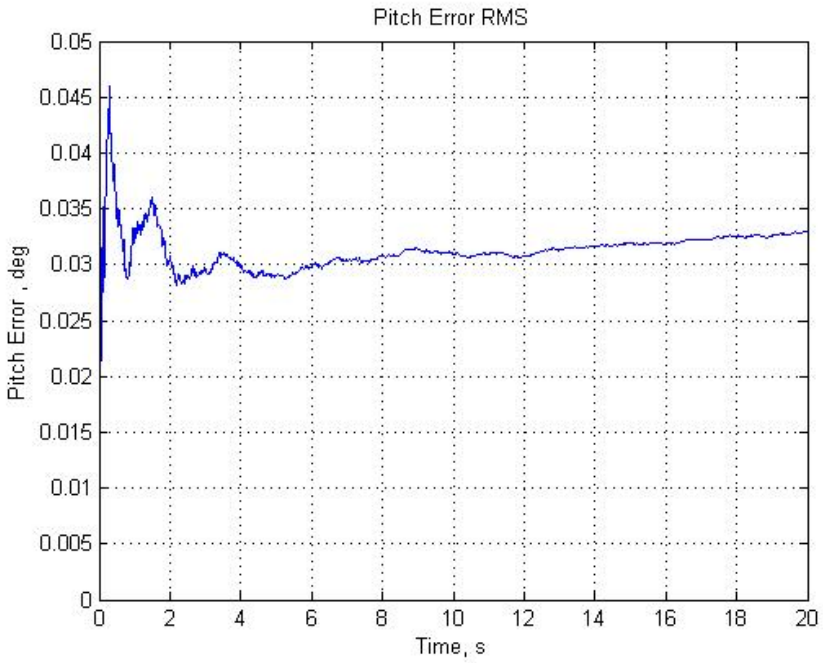

Figure 6.19 Pitch Estimation Error (Root Mean Square Error)

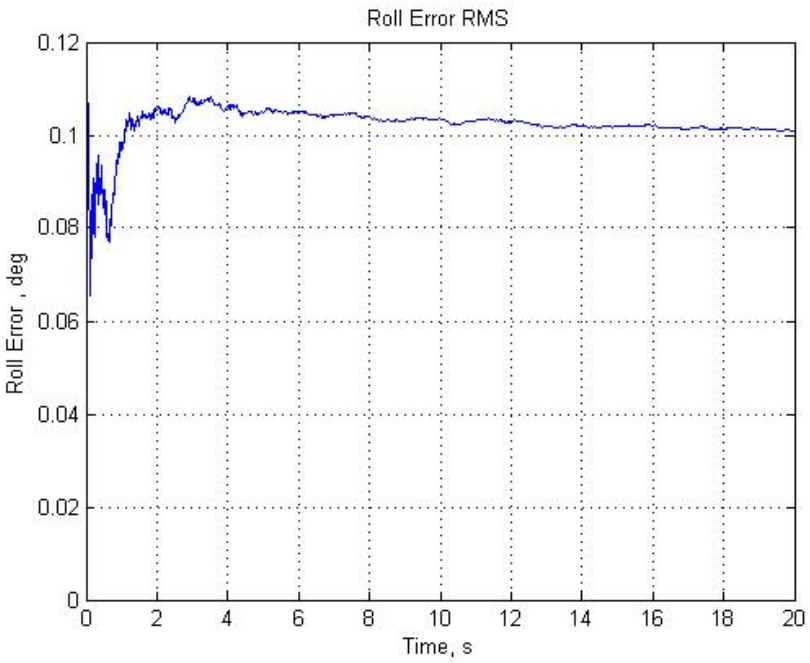

Figure 6.20 Roll Estimation Error (Root Mean Square Error)

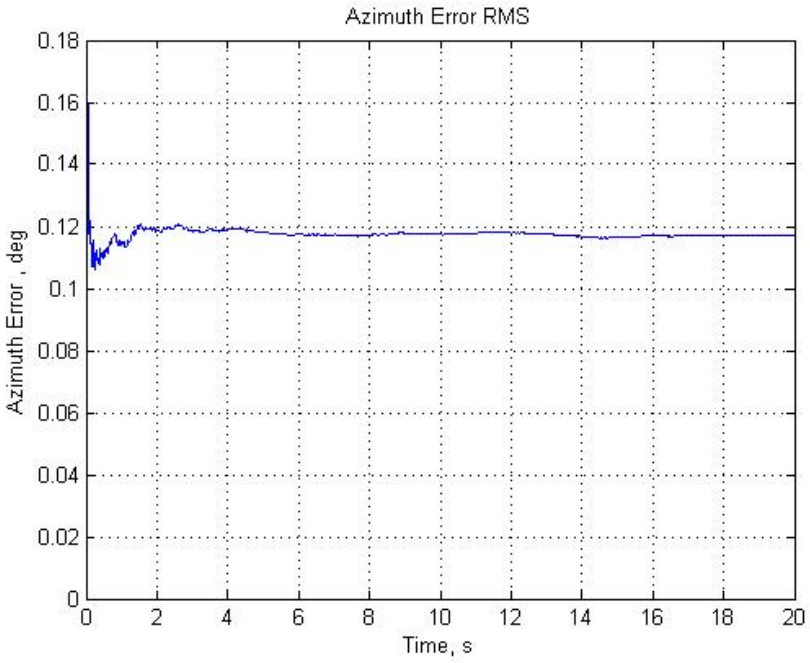

Figure 6.21 Azimuth Estimation Error (Root Mean Square Error)

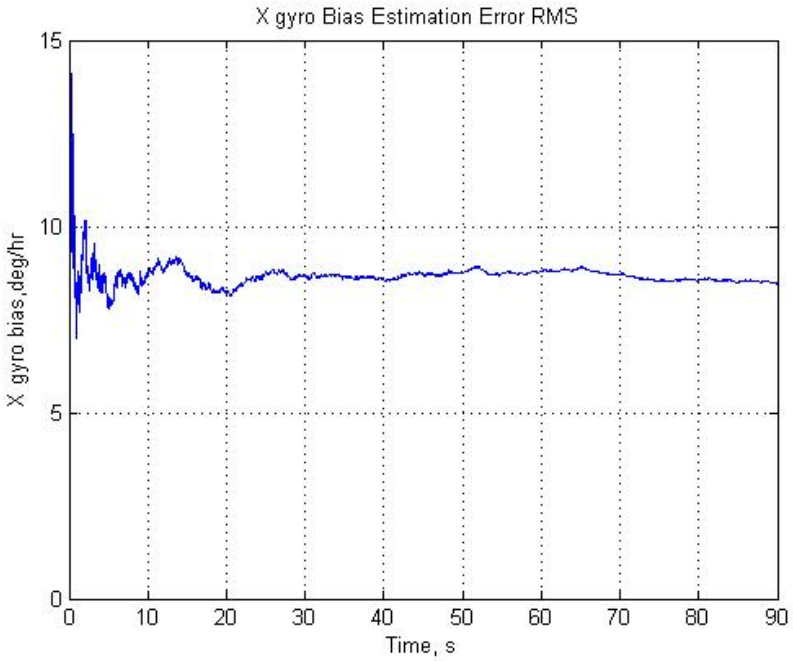

Figure 6.22 X Gyro Bias Estimation Error (Root Mean Square Error)

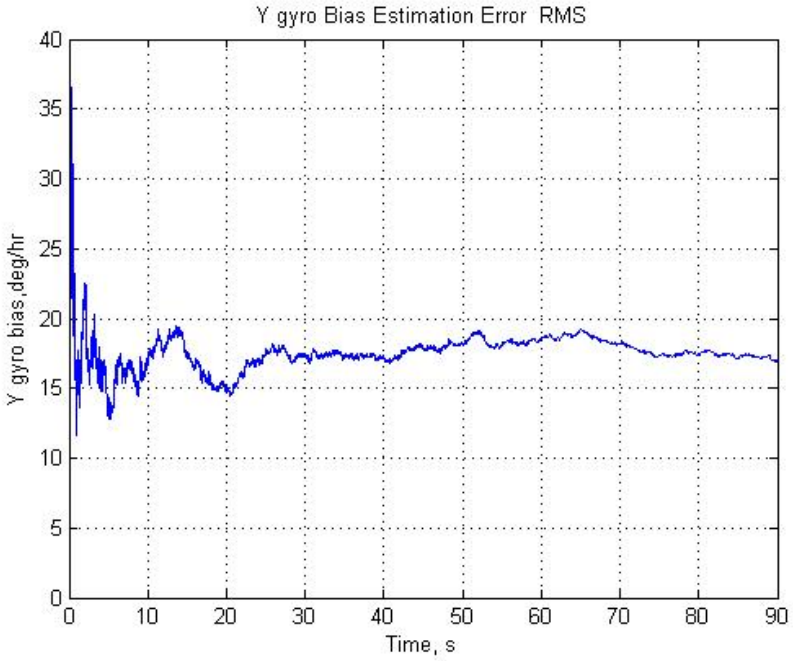

Figure 6.23 Y Gyro Bias Estimation Error (Root Mean Square Error)

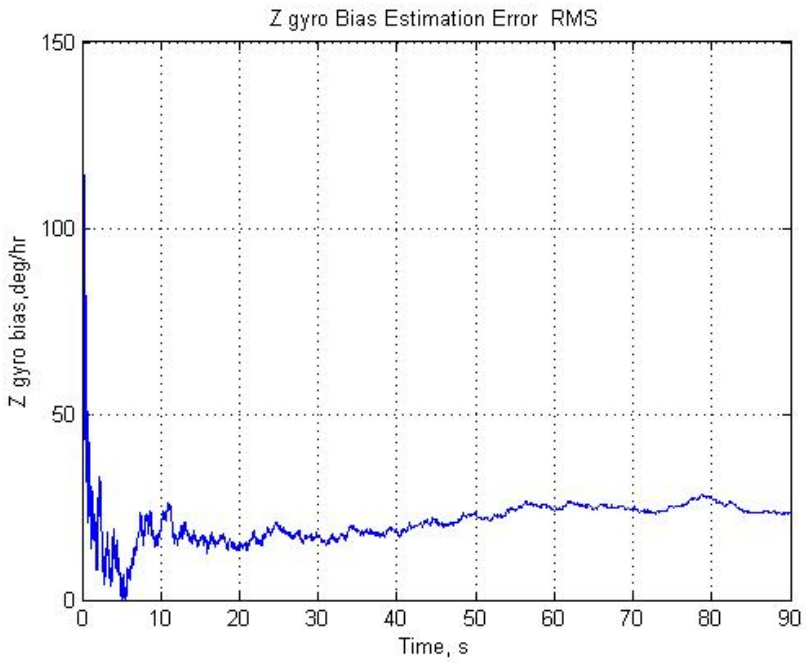

Figure 6.24 Z Gyro Bias Estimation Error (Root Mean Square Error)

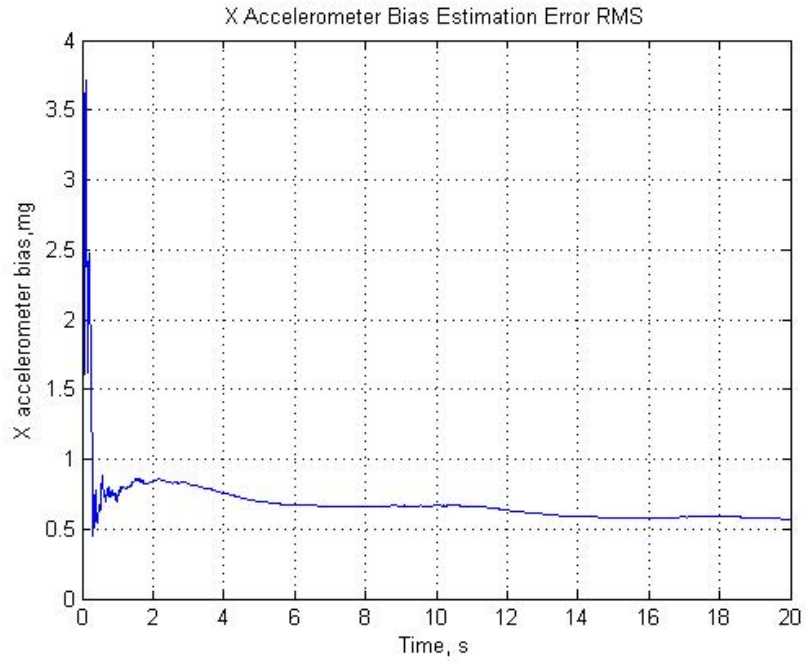

Figure 6.25 X Accelerometer Bias Estimation Error (Root Mean Square Error)

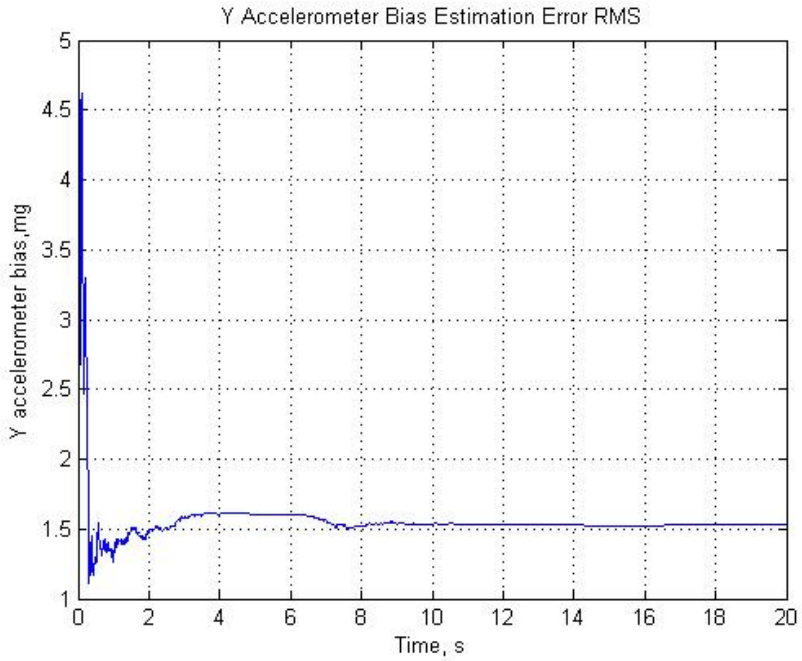

Figure 6.26 Y Accelerometer Bias Estimation Error (Root Mean Square Error)

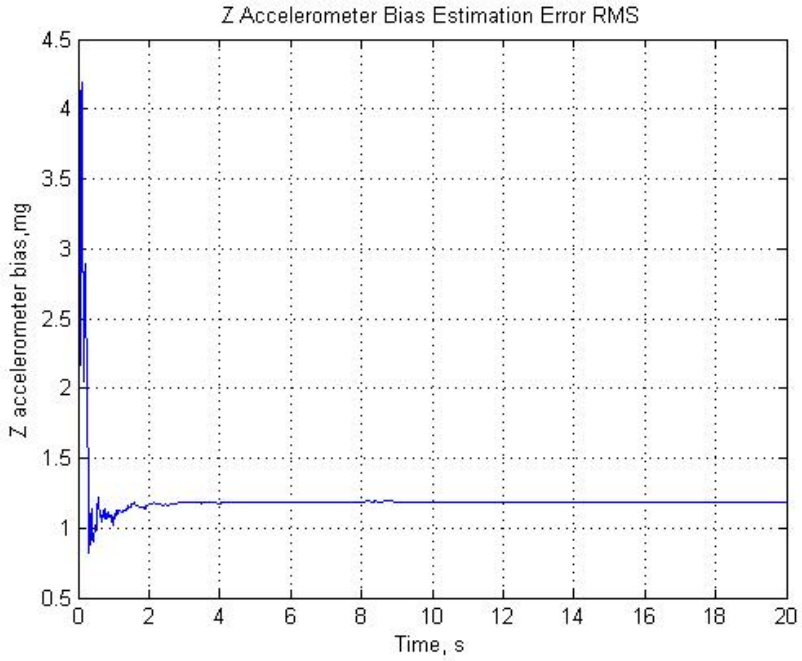

Figure 6.27 Z Accelerometer Bias Estimation Error (Root Mean Square Error)

6.2.2.2 Fine Alignment Experiment Set 2

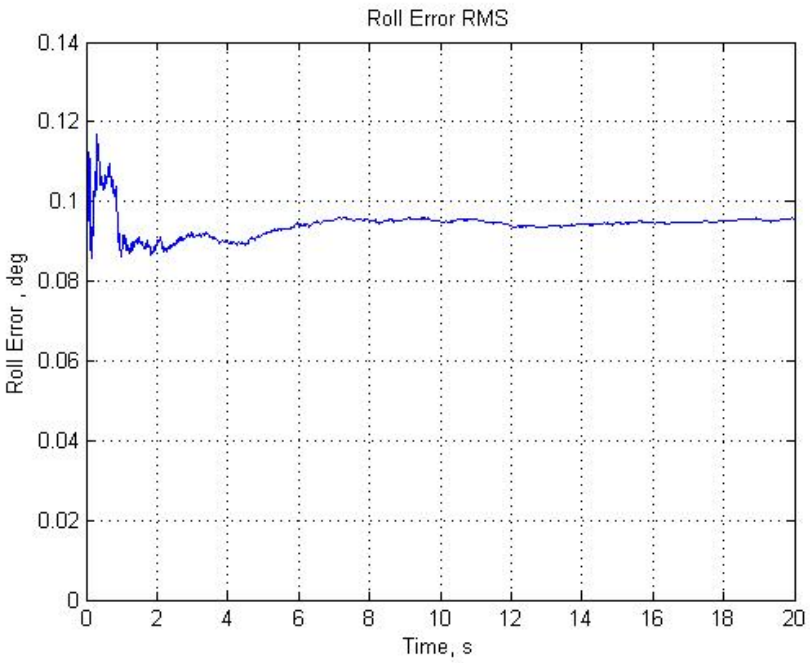

Figure 6.28 Roll Estimation Error (Root Mean Square Error)

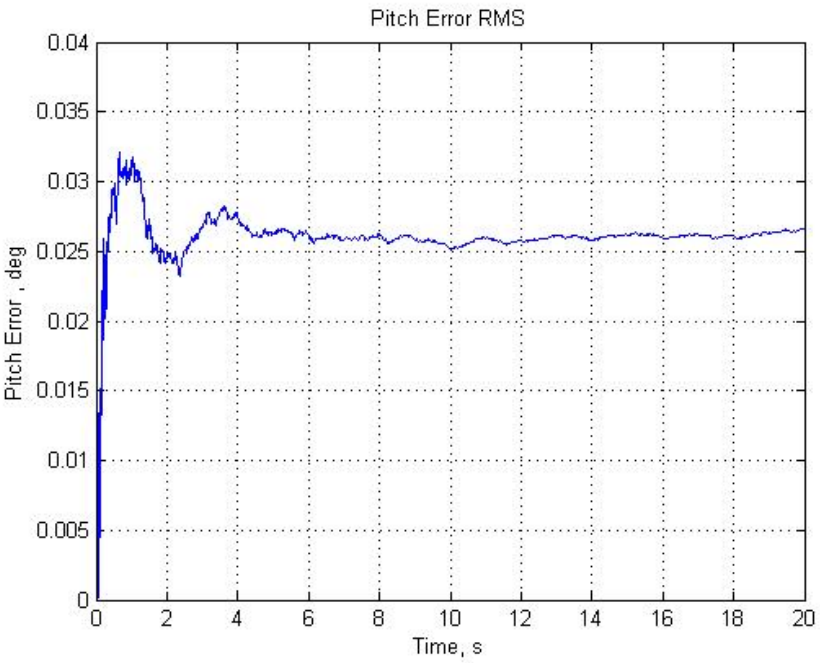

Figure 6.29 Pitch Estimation Error (Root Mean Square Error)

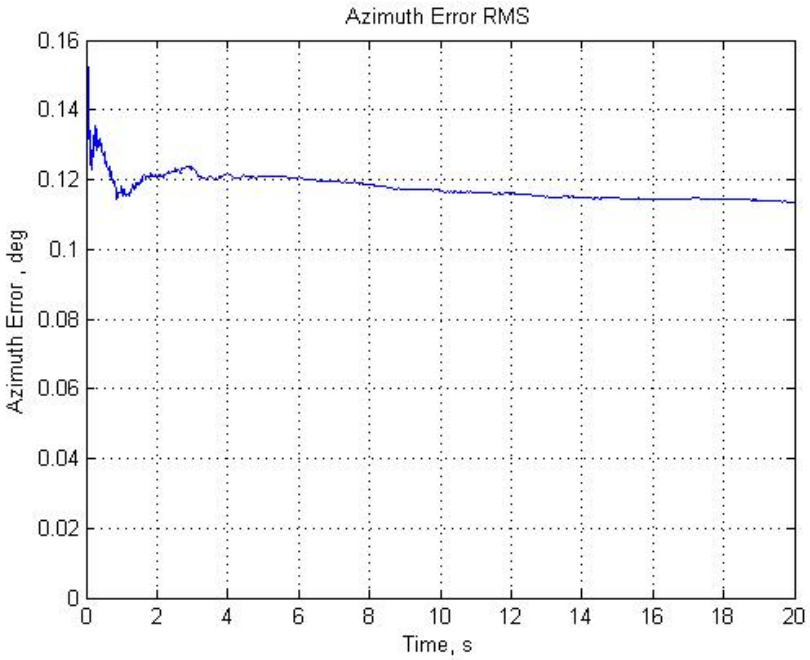

Figure 6.30 Azimuth Estimation Error (Root Mean Square Error)

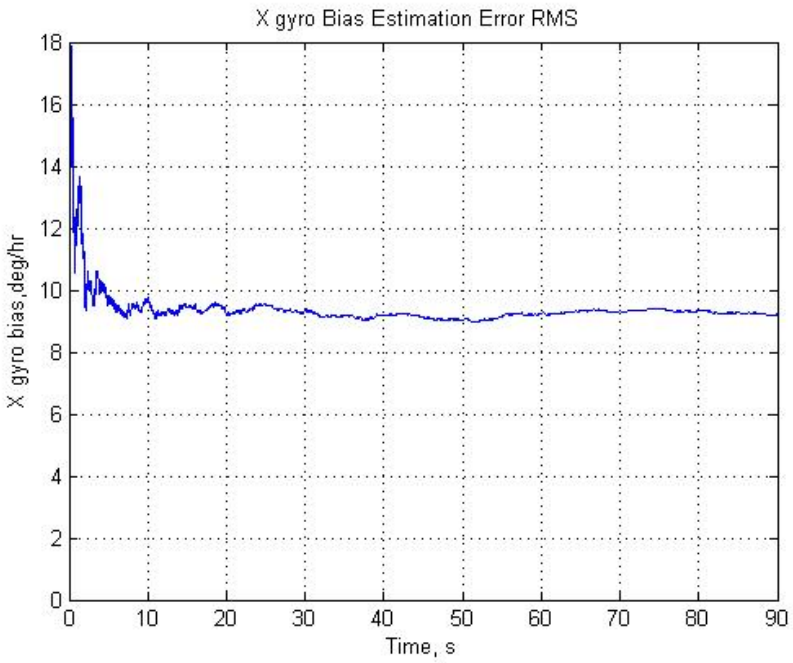

Figure 6.31 X Gyro Bias Estimation Error (Root Mean Square Error)

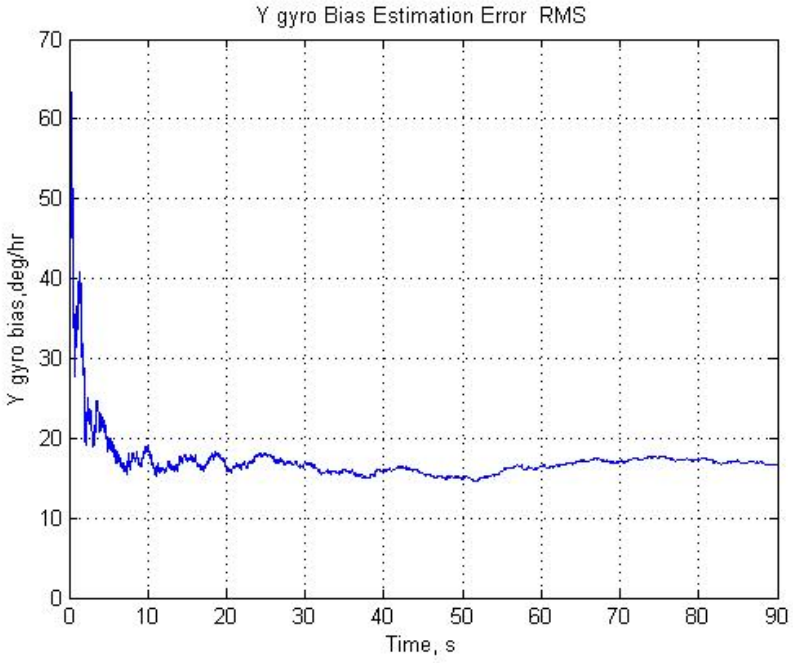

Figure 6.32 Y Gyro Bias Estimation Error (Root Mean Square Error)

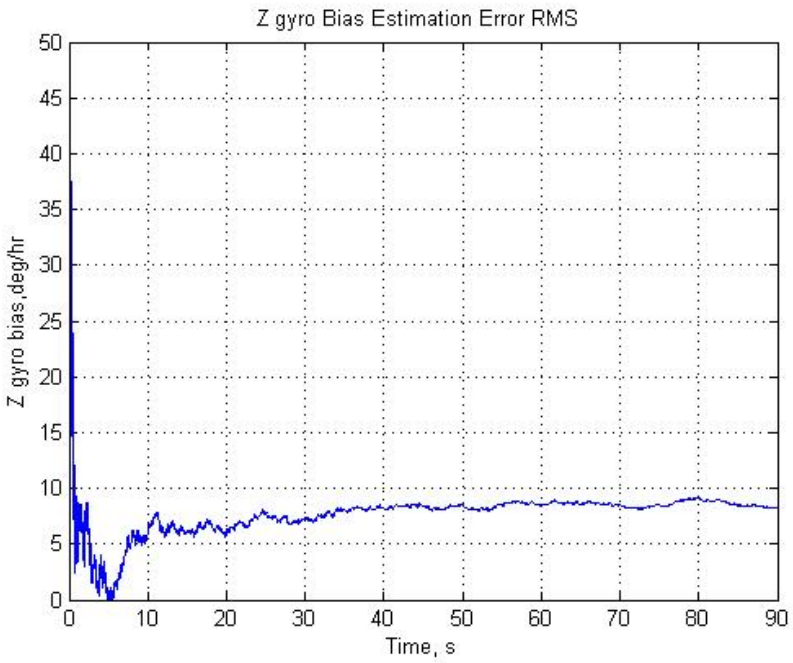

Figure 6.33 Z Gyro Bias Estimation Error (Root Mean Square Error)

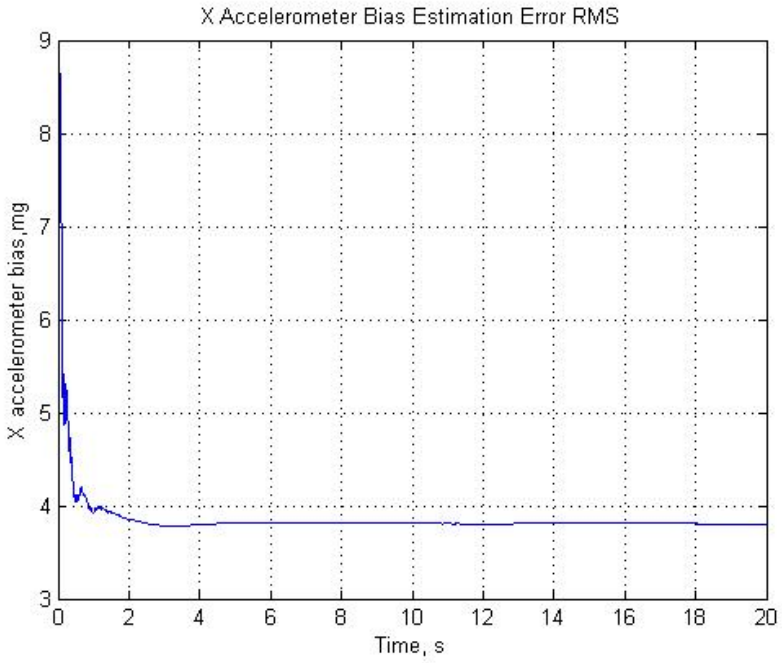

Figure 6.34 X Accelerometer Bias Estimation Error (Root Mean Square Error)

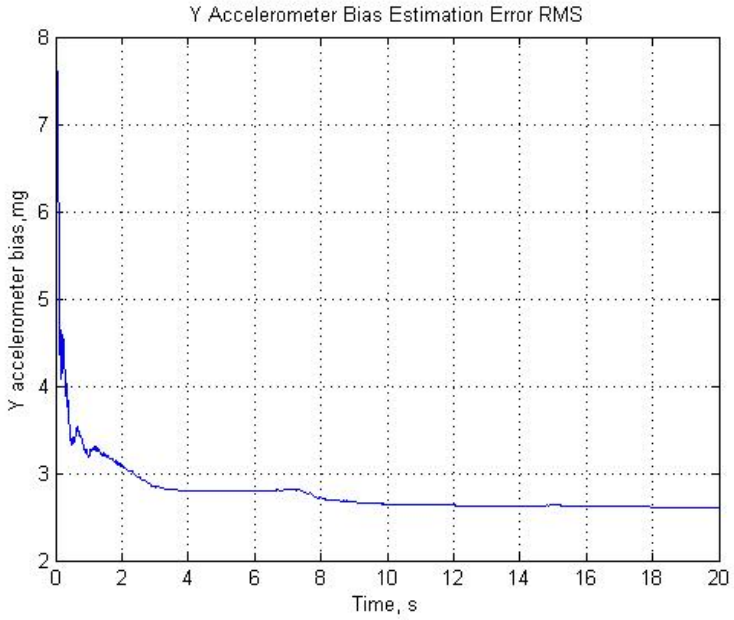

Figure 6.35 Y Accelerometer Bias Estimation Error (Root Mean Square Error)

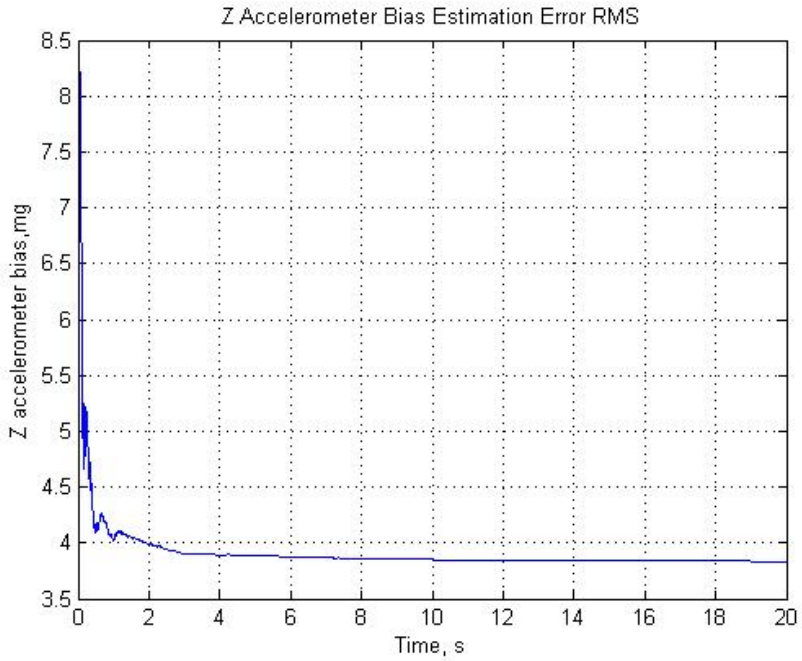

Figure 6.36 Z Accelerometer Bias Estimation Error (Root Mean Square Error)

CHAPTER 7

IN-MOTION ATTITUDE ESTIMATION

7.1 GPS Aided IMU+Magnetometer Navigation System

In the GPS/INS integrated systems, position and velocity errors are generally very low, but attitude errors are dependent on the system's maneuvers, because of the low observability degree [1, 11, 39]. With the addition of the magnetometer, observability of the system is increased, thus having low attitude errors.

To analyze the effectiveness of the developed method, a realistic case is taken into consideration. The spinning missiles are common in short range air defense systems, having high maneuverability and high kill effectiveness. The reference flight profile of the simulation is given as in Figures 7-1-7-7. [40]

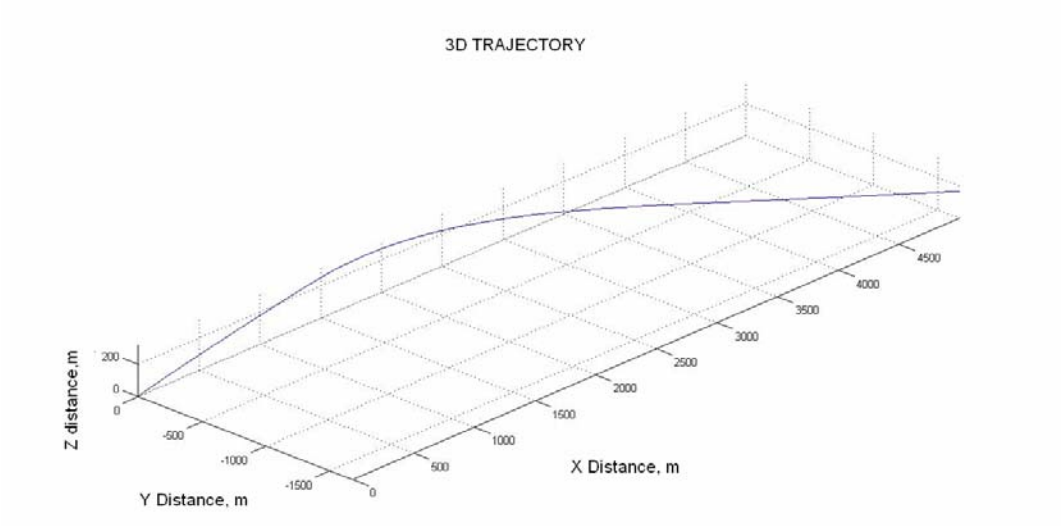

Figure 7.1 Trajectory of the Missile

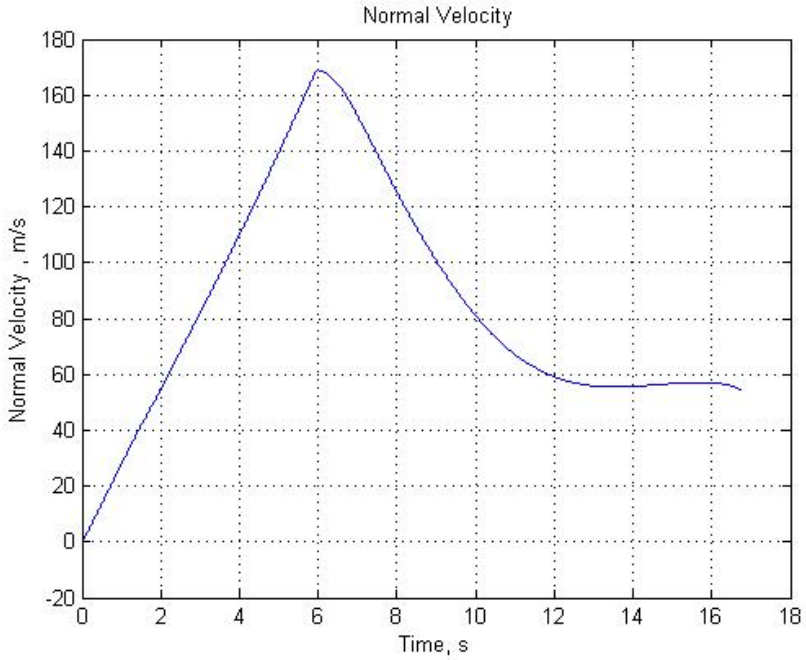

Figure 7.2 Normal Velocity Profile of the Missile

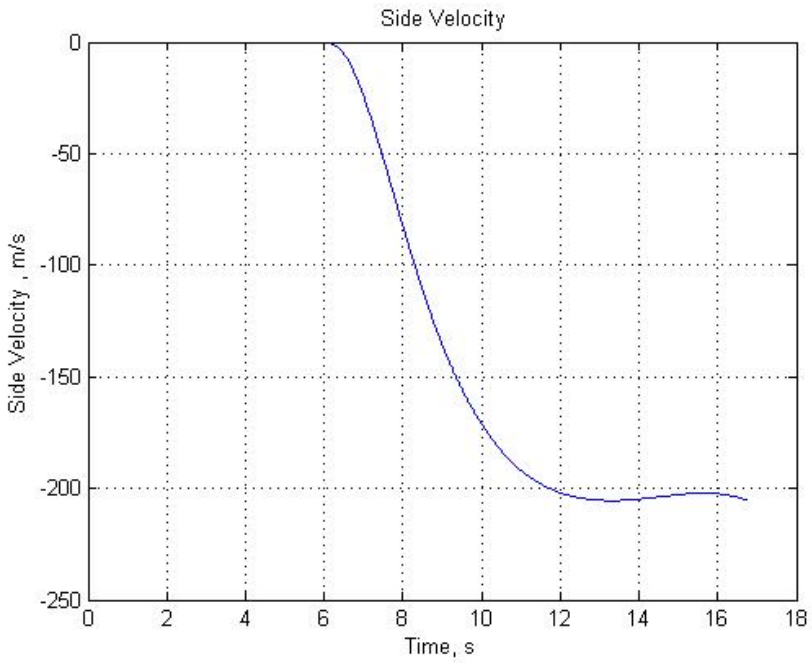

Figure 7.3 Side Velocity of the Missile

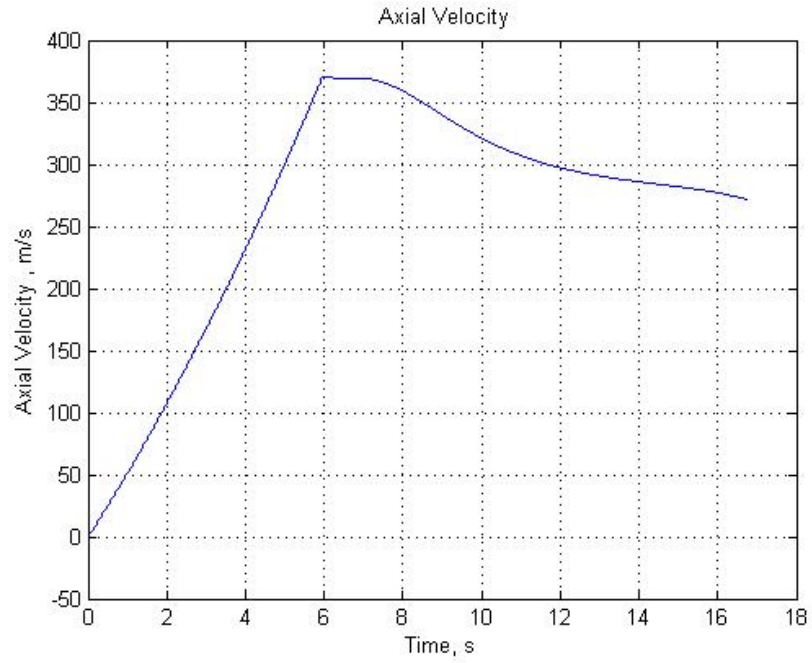

Figure 7.4 Axial Velocity of the Missile

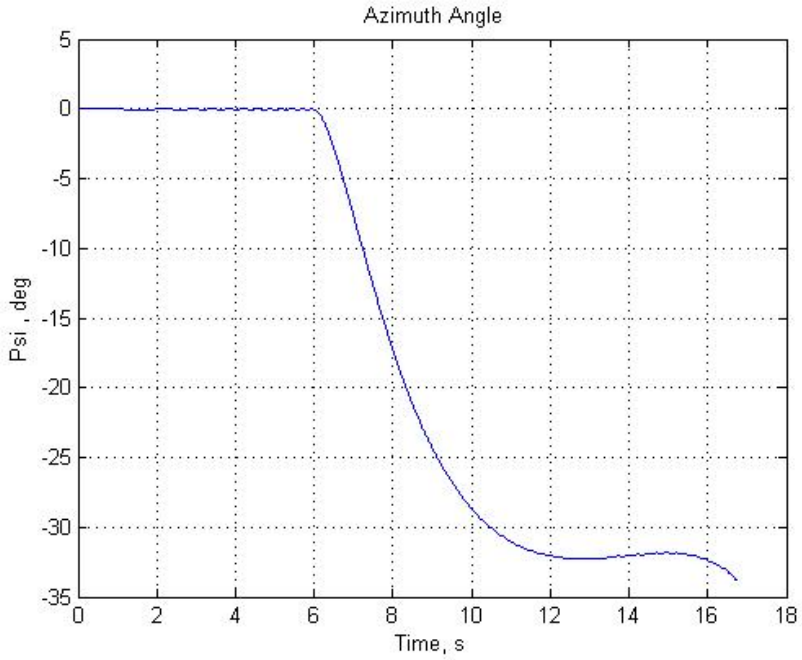

Figure 7.5 Azimuth profile of the Missile

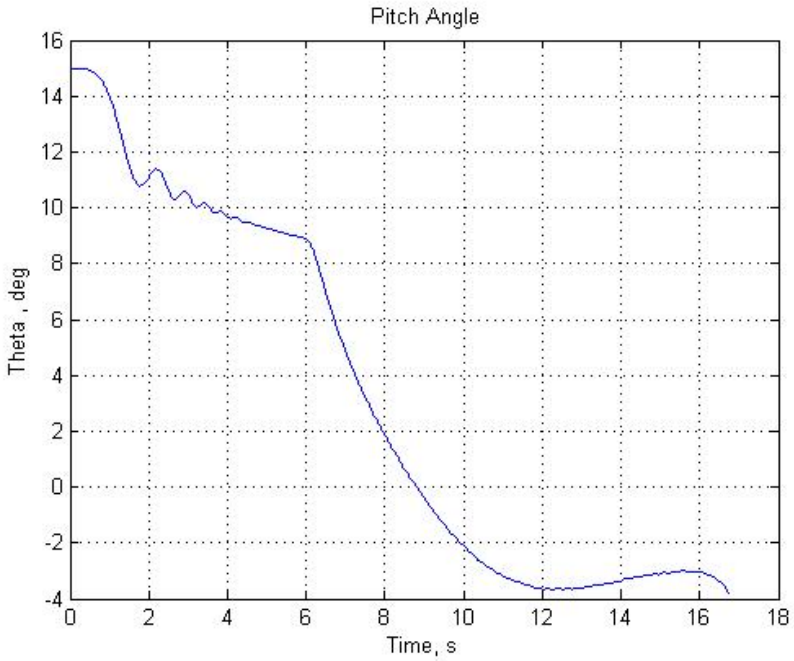

Figure 7.6 Pitch profile of the Missile

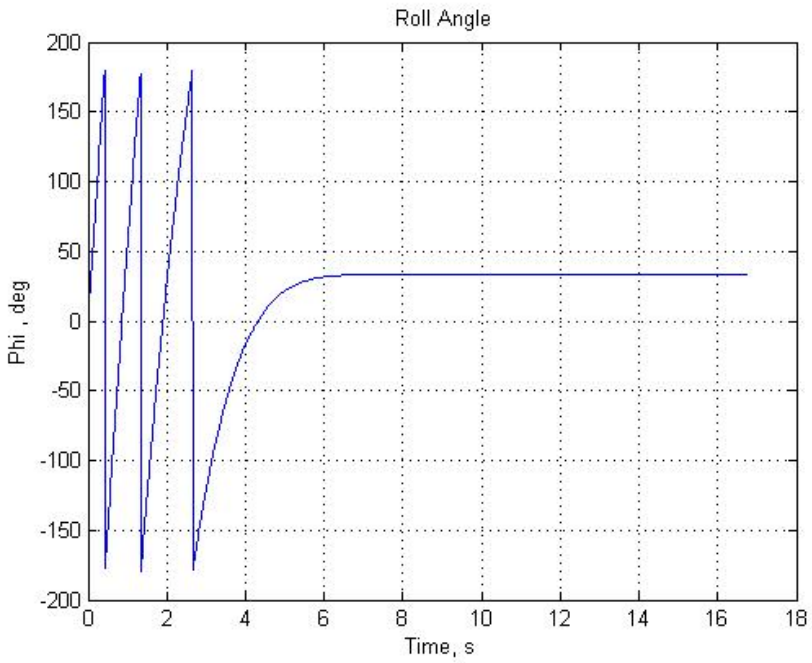

Figure 7.7 Roll profile of the missile

The simulation structure is the same as given in Chapter 6. The update rate of the inertial navigation system is 100 Hz, while the Kalman Filter is updated at 10 Hz.

The simulations are divided into three parts according to the sensor sets used;

- IMU aided by Magnetometer
- IMU aided by GPS
- IMU aided by GPS and Magnetometer

The states of the Kalman Filter are;

- 3 states of attitude error
- 3 states of velocity error

- 3 states of position error
- 3 states of gyro bias
- 3 states of accelerometer bias

Same state equations with fine alignment algorithm are used.

The process noises are;

- Accelerometer noises
- Gyro noises

The measurements for Magnetometer aiding;

- Magnetometer measurements

The measurement noises in Magnetometer aiding;

- Magnetometer noises

The measurements for GPS aiding;

- Velocity measurements
- Position measurements

The measurement noises in GPS aiding;

- Position uncertainty
- Velocity uncertainty

Accelerometer, gyro and magnetometer noises account for all unobservable sensor errors. Scale factor, cross couplings, g dependent bias etc. are assumed to be pre-calibrated. Initial values for noise covariance matrices are chosen according to the sensor's performance specifications.

Initial state covariance values;

- Attitude error (1σ) : 5 degrees
- Velocity error (1σ) : 0.1 m/s
- Position error (1σ) : 0.1 m
- Gyro Bias (1σ) : 100 deg/hr
- Accelerometer Bias (1σ) : 10 mg

Noise covariance values:

- Gyro noises: 1 deg/s
- Accelerometer noises : 5 mg
- Magnetometer noises: 10 mGauss
- Velocity uncertainty: 0.1 m/s
- Position uncertainty: 5 m

The random variables in the Monte Carlo Simulations are as follows,

- Gyro Bias Repeatability : 100 deg/hr (1 σ), Normal Distribution
- Gyro Noise: 1 deg/s (1 σ), Normal Distribution
- Gyro Scale Factor Error: 1000 ppm (1 σ), Normal Distribution
- Accelerometer Bias Repeatability 10 mg (1 σ), Normal Distribution
- Accelerometer Noise : 5 mg (1 σ), Normal Distribution
- Accelerometer Scale Factor Error: 1000 ppm (1 σ), Normal Distribution
- Magnetometer Noise: 5 mgauss (1 σ), Normal Distribution
- Attitude of the Sensor Block (North, East, Down) : Uniform Distribution
- Velocity uncertainty: 0.1 m/s, (1 σ), Normal Distribution
- Position uncertainty: 5 m, (1 σ), Normal Distribution

The gyro, accelerometer and magnetometer variances are chosen in accordance with the performance specification of the sensors, given in Appendix B. The position and velocity variances are the GPS uncertainties [1]

Note that, all variables except attitude of the sensor block have normal distribution. Attitude is chosen to have uniform distribution so that the effects of the attitude in the simulations are eliminated [37, 38].

As the magnetometer provides only attitude information, position errors quickly accumulate; where GPS aided navigation system has a stable position error behavior. (Figure 7-8- 7-10)

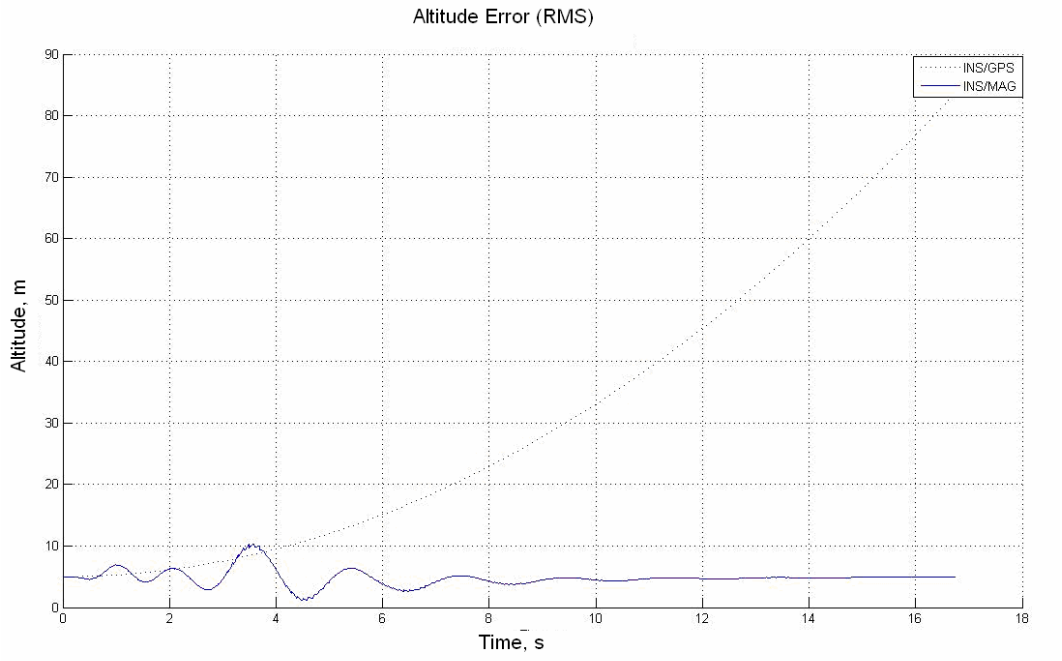

Figure 7.8 Altitude Estimation Error (Root Mean Square Error)

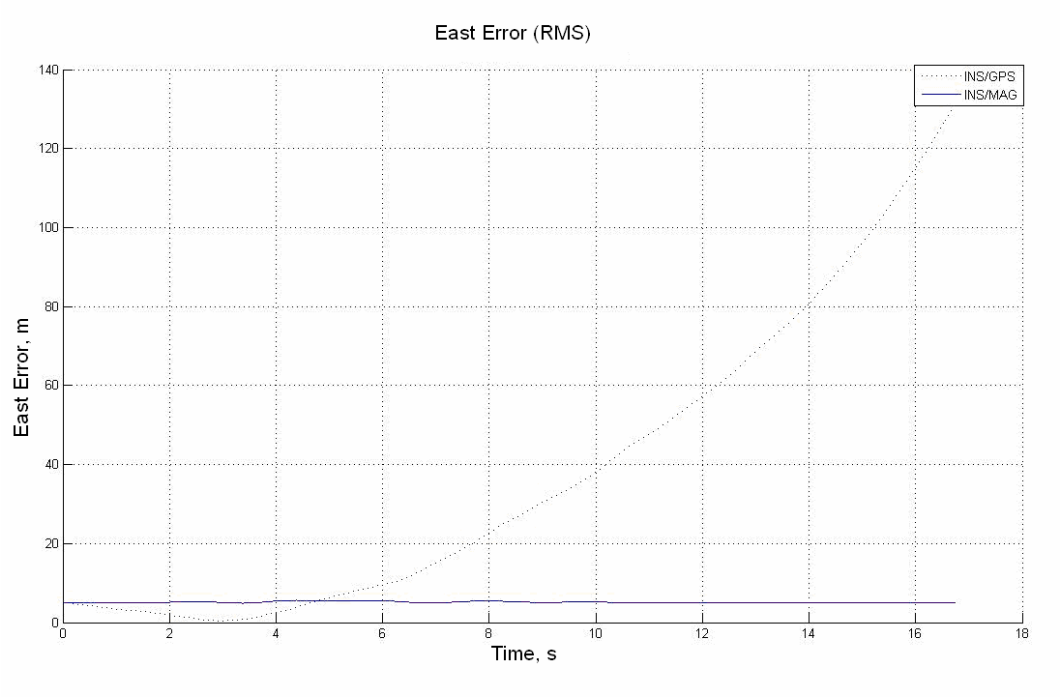

Figure 7.9 East Position Estimation Error (Root Mean Square Error)

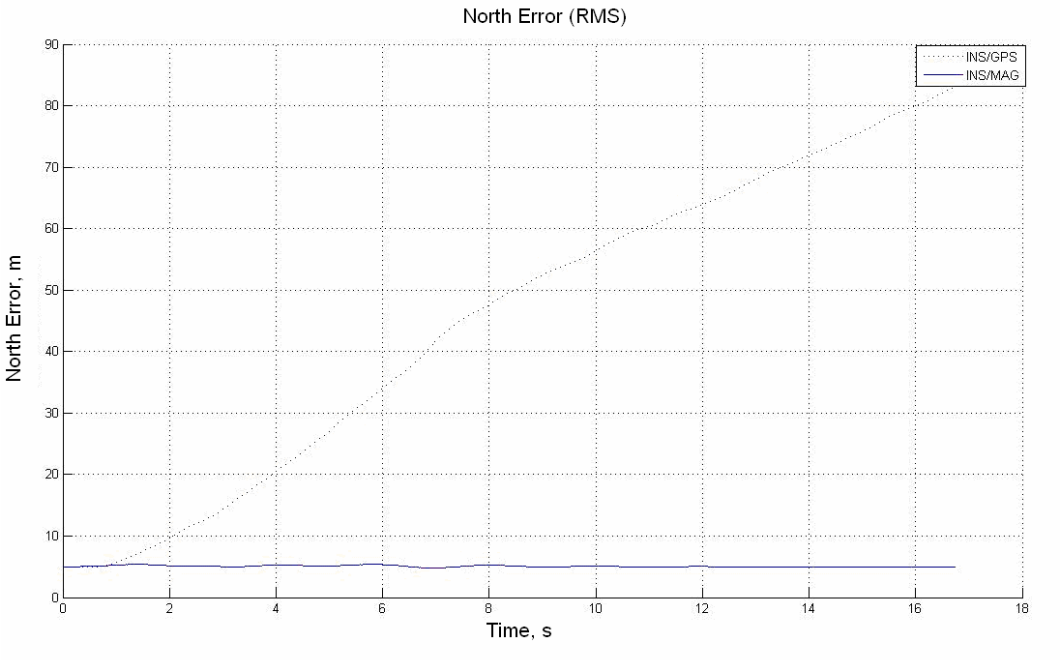

Figure 7.10 North Position Estimation Error (Root Mean Square Error)

In the attitude error behaviors, the magnetometer aided system is superior to GPS aided system. In the GPS aided system, reference attitude information is hidden inside the position and velocity measurements. The magnetometer provides directly attitude measurements, but GPS provides position and velocity measurements, thus the attitude information is indirectly observable. The best attitude solution is the combination of GPS and magnetometer systems, where the attitude solution converges in a quick manner; the attitude information comes form both GPS and magnetometer. With the combined system, the attitude is observed from all navigation (position, velocity and attitude) measurements

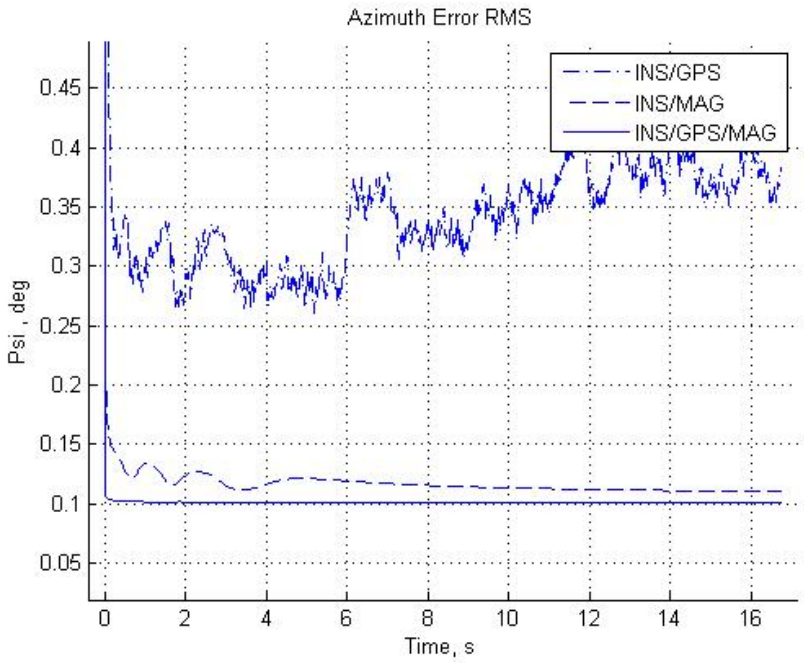

Figure 7.11 Azimuth Estimation Error (Root Mean Square Error)

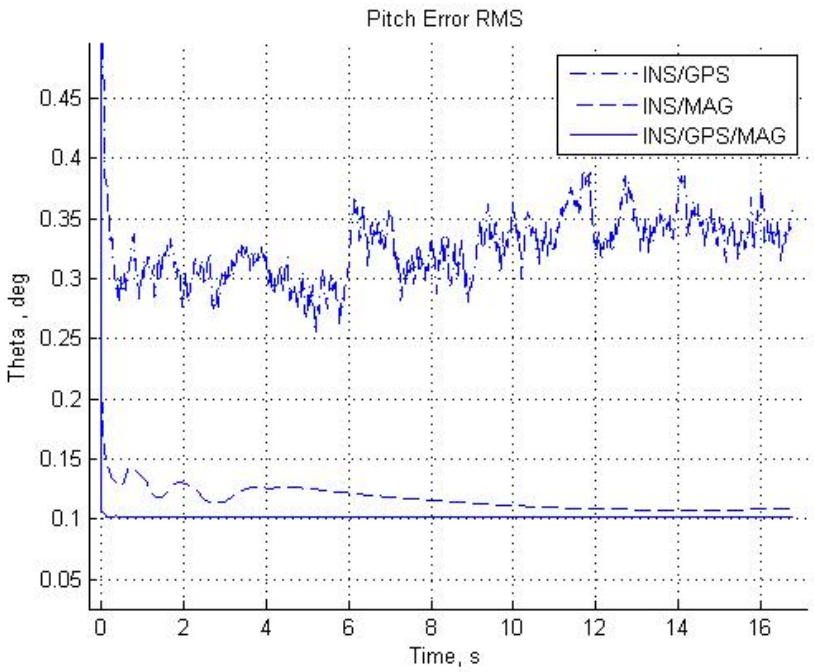

Figure 7.12 Pitch Estimation Error (Root Mean Square Error)

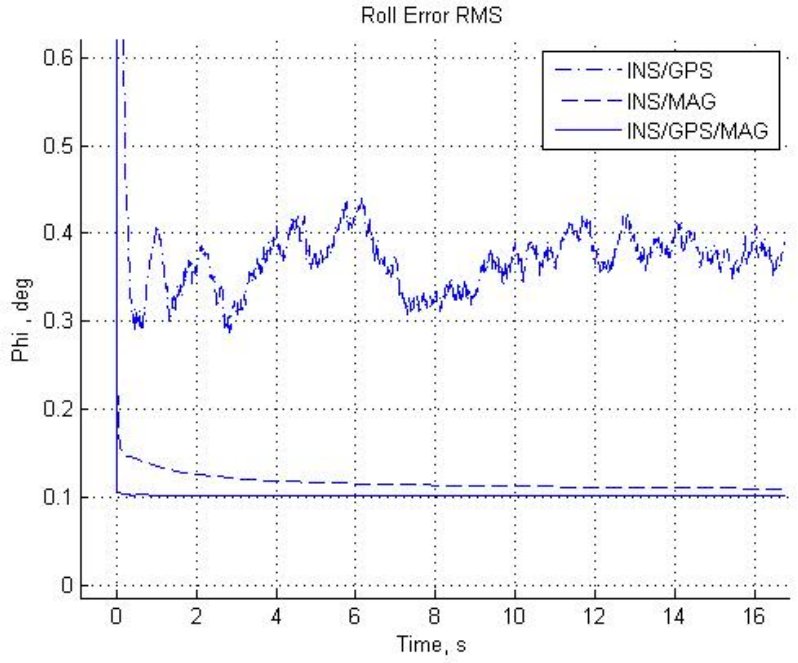

Figure 7.13 Roll Estimation Error (Root Mean Square Error)

As in the attitude estimation case, gyro biases are better estimated in magnetometer case, the best estimation is in the GPS/Magnetometer aiding system. GPS aiding has a relatively low accuracy and low convergence rate. The combined aiding system has a high accuracy in gyro bias estimation, providing better navigation solution when measurements are denied, i.e. jammed GPS signals or high magnetic anomaly occurs.

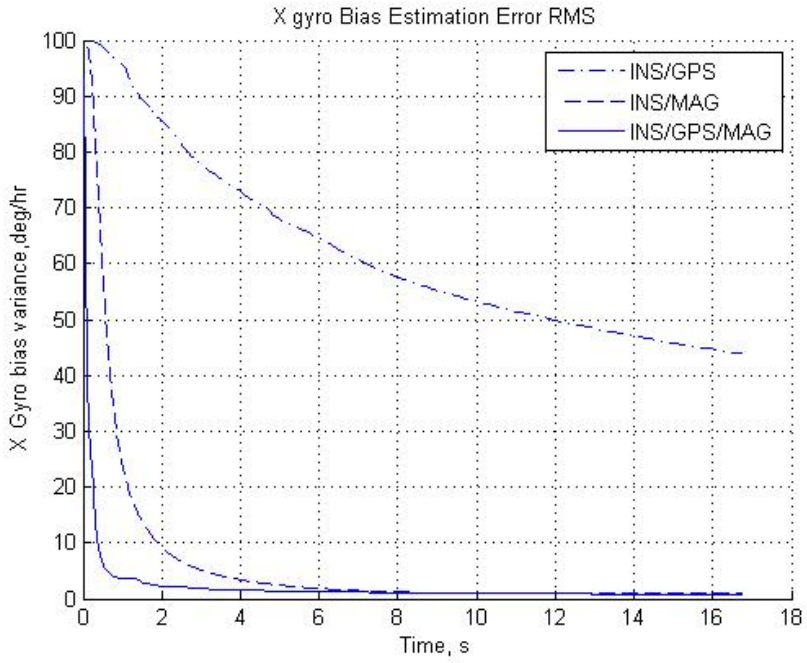

Figure 7.14 X Gyro Bias Estimation Error (Root Mean Square Error)

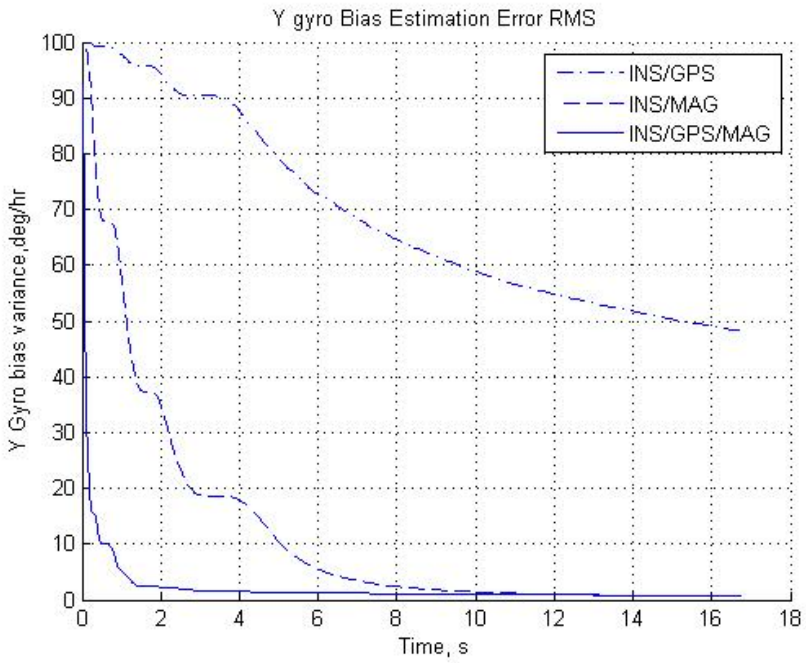

Figure 7.15 Y Gyro Bias Estimation Error (Root Mean Square Error)

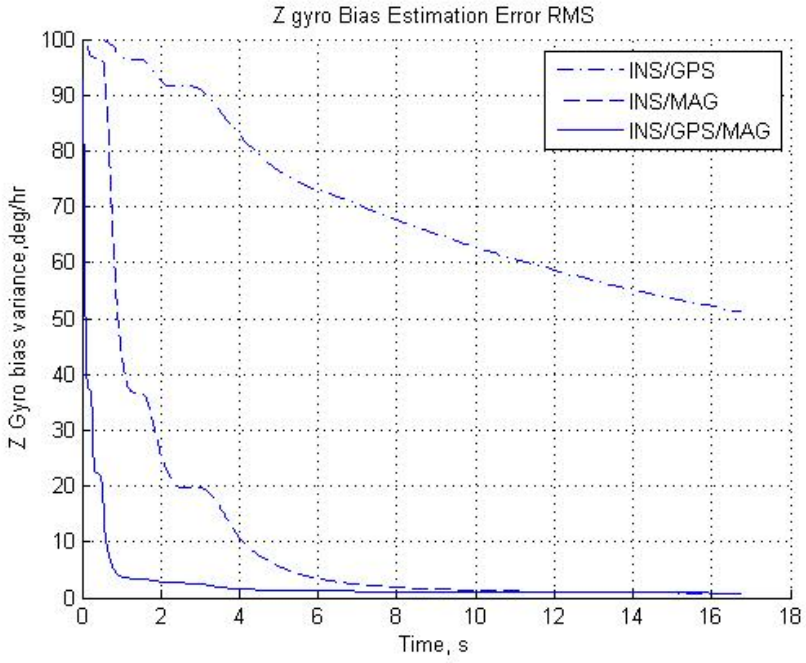

Figure 7.16 Z Gyro Bias Estimation Error (Root Mean Square Error)

The magnetometers are ineffective in accelerometer bias estimations, as there is no information about linear position/velocity/acceleration. GPS is a good reference to estimate the accelerometer observable errors.

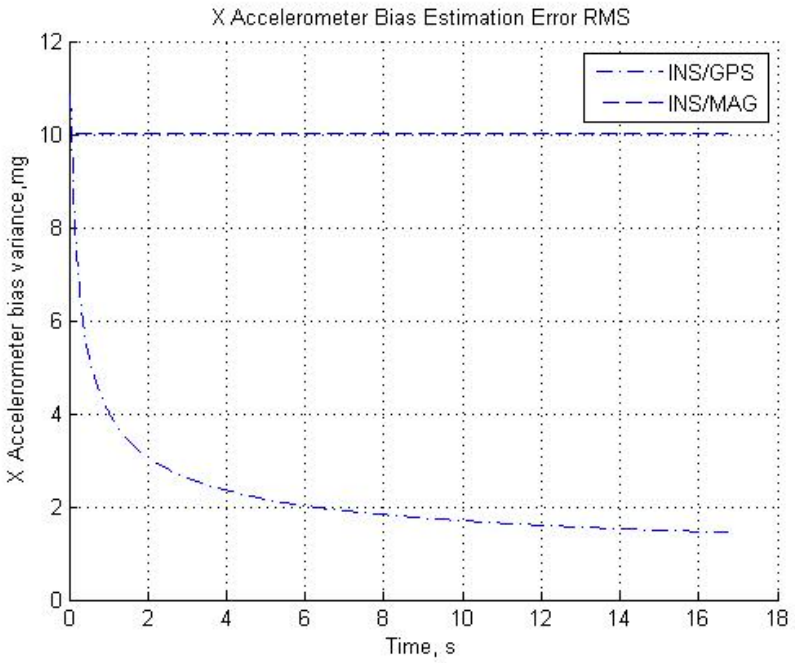

Figure 7.17 X Accelerometer Bias Estimation Error (Root Mean Square Error)

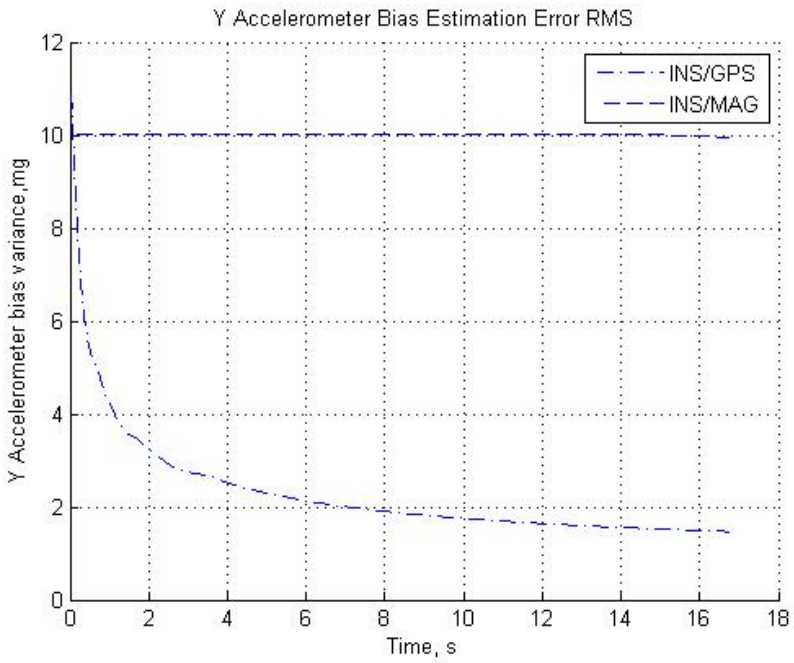

Figure 7.18 Y Accelerometer Bias Estimation Error (Root Mean Square Error)

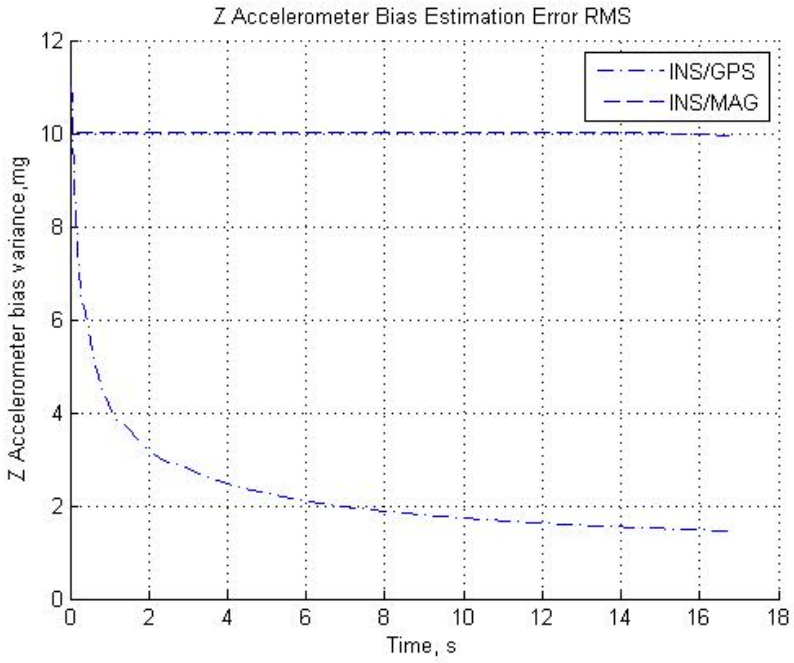

Figure 7.19 Z Accelerometer Bias Estimation Error (Root Mean Square Error)

7.2 Single Attitude Euler Determination

In a case where only one vector measurement can be used, only one Euler angle can be found provided that the other two Euler angles are provided. Details were given in chapter 5.

Kalman filter is theoretically an optimal stochastic estimator. Almost all the aided navigation systems use a Kalman Filter or its variant, but the filter also has a deficiency, computational load. Matrix decomposition techniques are generally used to deal with this problem. Also, Kalman Filter may diverge in a case where one of the sensors saturate, resulting in highly erroneous navigation solution and the linearity assumption in the inertial navigation error equations will not be true anymore.

The spinning missiles generally have high spin rates, which are in the order of 10 Hz (3600 deg/s). Most of the gyros in the military industry does not have such a measurement range, or have very low accuracy in that range. In the developed method, an IMU and magnetometer can provide good estimates of roll angle. The solution is certainly not accurate as the Kalman Filter solution, and the IMU errors can not be estimated. On the other hand, this deterministic solution is a low cost solution.

The effectiveness of this method is also shown by Monte Carlo Simulations. The same flight profile and same random variables are used with the Kalman Filter estimation case. The simulations are divided into three cases;

- Azimuth Estimation
- Pitch Estimation
- Roll Estimation

As it can be seen from Figure 7-20-7-23, the accuracy of the developed method is lower than the Kalman Filter case, but it is a computational and cost efficient solution. Besides, there is no guarantee that the single axis attitude solution is bounded because the other two Euler angles are not aided in a three rotational degree of freedom system. The accuracy of the unaided Euler angles directly affect the accuracy of this solution.

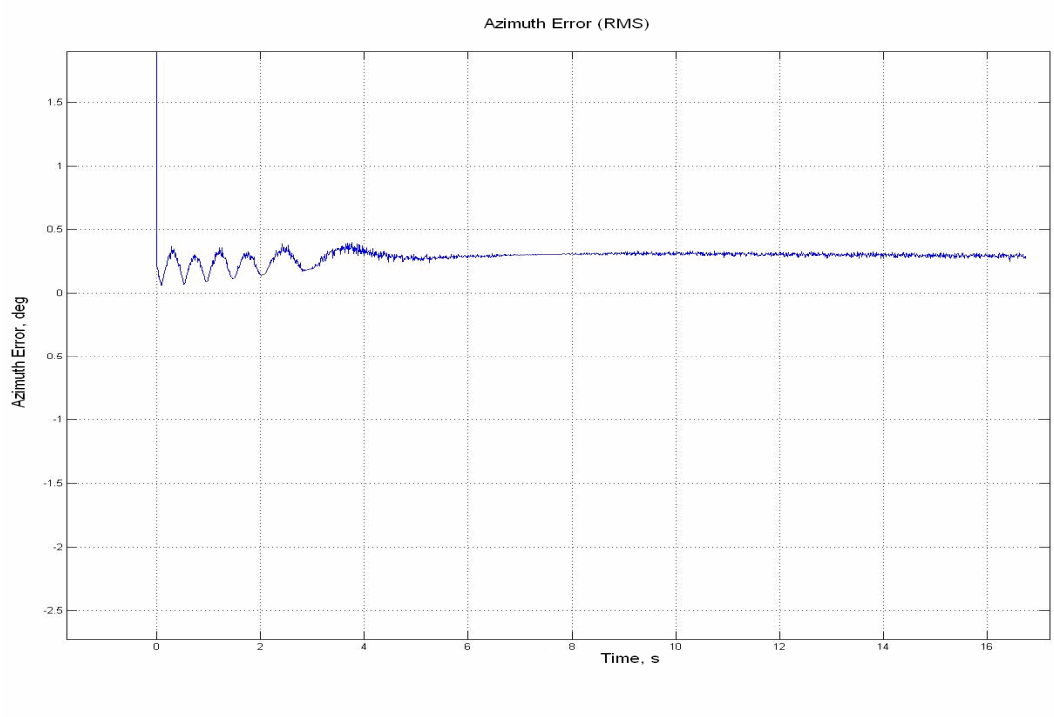

Figure 7.20 Azimuth Estimation Error (Root Mean Square Error)

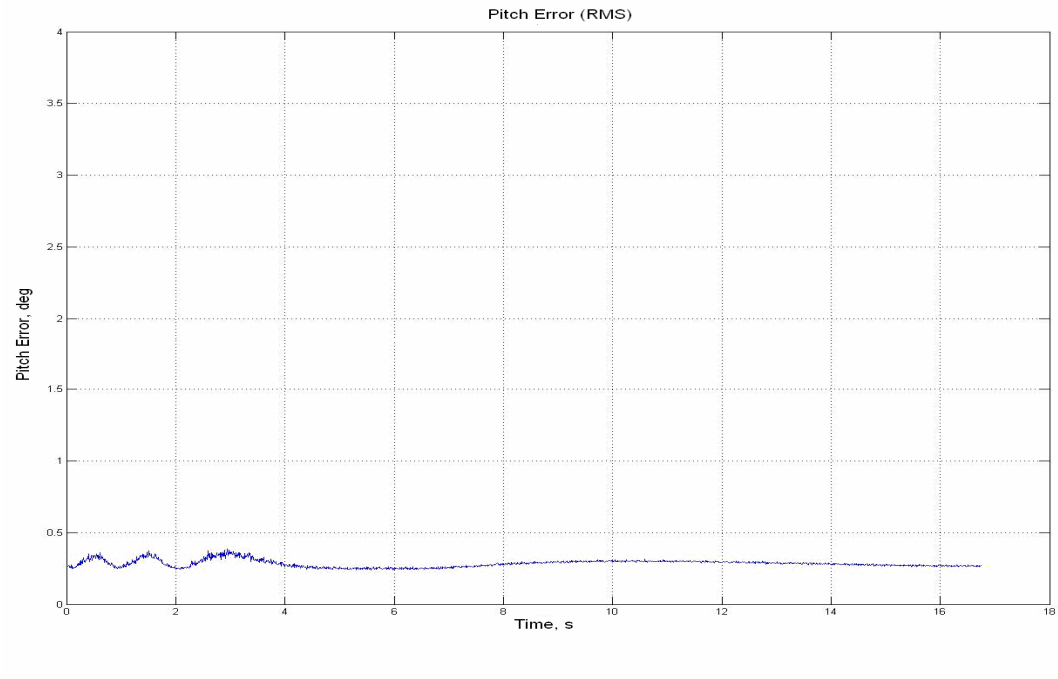

Figure 7.21 Pitch Estimation Error (Root Mean Square Error)

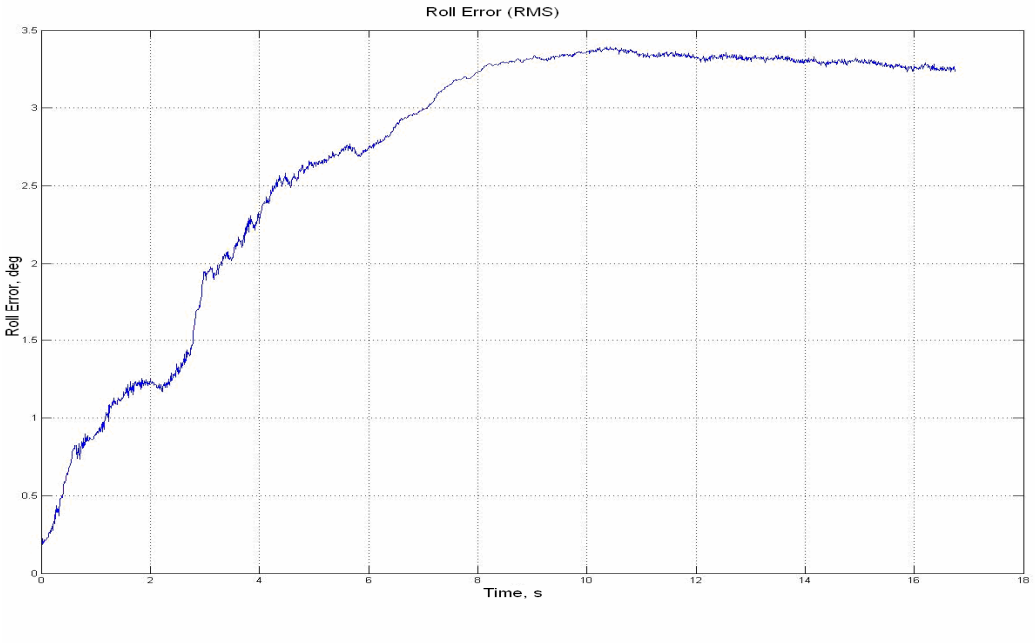

Figure 7.22 Roll Estimation Error (Root Mean Square Error)

CHAPTER 8

DISCUSSION and CONCLUSION

Magnetic field sensors are generally characterized by low cost and high signal to noise ratio. Moreover, effective bias compensation can easily be achieved via a simple set/reset circuit. Taking advantage of these features and based on real needs, this work has presented magnetometer algorithms as aiding means for INS. Magnetic measurements can either be directly used in Euler angle calculations or fused in a Kalman filter with gyro measurements to yield improved navigation results.

The Kalman filter solution improves DCM estimates, which leads to better position calculations. This approach is especially useful when either GPS is not implemented or its signals are unavailable. Even if GPS is utilized, it cannot provide the attitude accuracy which otherwise can be captured with the aid of a magnetometer. The only drawback of Kalman filtering is the computational power it may require depending on the number of states in the mathematical formulation.

Roll gyro saturation problem in spinning missiles may be solved with the proposed analytic roll angle calculation. Following the fact that gyros capable of measuring high roll rates are either poor in performance or unreasonably expensive, this deterministic solution provides an effective and cheap solution to this dilemma. Whichever is the preferred way; deterministic or stochastic, the

primary result of magnetometer algorithms is considerable reduction in gyro costs.

In the modeling and simulation studies, following tasks are performed

1. Error model of a generic inertial measurement unit is derived
2. Linear error mechanization equations of a inertial navigation system is derived with small attitude error assumptions
3. World Magnetic Field is embedded into simulation environment
4. Alternative magnetic field model is proposed.
5. Deterministic attitude determination equations with two vector sets are derived.
6. Magnetometer measurement equations are derived for Kalman Filter
7. Single axis deterministic attitude determination algorithm is derived.
8. Experimental studies are carried for ground alignment
9. Monte Carlo simulations are done for ground alignment and in motion estimations.

The developed navigation system has a self alignment capability, which is not the case in unaided MEMS IMU. The classical two phase alignment process (coarse and fine) is applied to the proposed system, resulting in a fast and accurate alignment solution. Even in a RLG navigation unit, the ground alignment take at least several minutes, where the magnetometer + IMU system aligns itself in a few seconds.

The flight performance of the proposed system is demonstrated in a spinning missile application. It is shown that magnetometer aiding is superior to GPS for attitude and gyro error estimations. When the magnetometer + IMU system is combined with GPS, not only the position and velocity errors become observable, but also the accuracy and the convergence rate of the attitude and gyro error estimations increases.

For a low computational cost solution, a single axis attitude determination algorithm is developed. In the simulations, it is shown that the solution is not good as Kalman Filter, but the computational load is very low relative to the stochastic estimation filters.

This thesis has shown the effectiveness of magnetometer algorithms in navigation calculations. However, the crucial issue that needs to be raised is about the correctness of the measurements and reliability of the reference field model, and the consistency between. Theoretically, these two are the representations of the same vector in different frames. In practice; however, none of them will be available without errors and/or uncertainties, which means that they will not be equal when transformed from one frame to another. Consequently, care must be taken in acquisition and interpretation of magnetic data. One imposed condition is that in-vehicle magnetic disturbances must never affect sensor outputs. This can be accomplished by convenient sensor placement and selection of non-magnetic material. Secondly, the algorithms require that the outer field be known a priori as a function of location. Over short ranges, this does not constitute a problem since the directional and time derivatives of the Earth's magnetic strength are negligible; as a result, the reference magnetic vector can be approximated as constant. Over long ranges; however, some other means of estimating the reference vector becomes necessary. Mathematical models such as WMM2005 might be used here; but, one must be cautious against their applicability. There is always possibility of being confronted by some outer, local magnetic disturbances especially at low altitudes. These approximations are most accurate at sufficiently high altitudes.

As a future work, real time in motion experiments can be done to demonstrate the effectiveness of the developed algorithms. Thus, the effect of the magnetic anomalies in the algorithms can be seen. Also, the alternative magnetic field modeling can be applied to correct local WMM2005 errors.

REFERENCES

1. Titterton, D. H., Weston, J. L., *Strapdown Inertial Navigation Technology*, American Institute of Aeronautics and Astronautics & Institution of Electrical Engineers, 2004

2. Britting, Kenneth R. Inertial Navigation Systems Analysis. Wiley-Interscience, 1971.

3. Salychev, O.S., Applied Inertial Navigation: Problems and Solutions, BMSTU Press Moscow, Russia, 2004.

4. Psiaki, M. L., Martel, F., and Pal, P. K., "Three-Axis Attitude Determination via Kalman Filtering of Magnetometer Data," Journal of Guidance, Control, and Dynamics, Vol. 13, No. 3, May-June 1990, pp. 506–514.

5. Lefferts, E. J., Markley, F. L., and Shuster, M. D., "Kalman Filtering for Spacecraft Attitude Estimation," Journal of Guidance, Control, and Dynamics, Vol. 5, No. 5, Sept.-Oct. 1982, pp. 417–429.

6. Kok-Lam,.L., Crassidis, J.L.,Harman, R.R., " Real Time Attitude Independent Gyro Calibration from 3 axis Magnetometer Measurements, AIAA-AAS Astrodynamics Specialist Conference and Exhibit, AIAA-2004-4855.

7. National Geomagnetic Information Center, website URL http://geomag.usgs.gov/.

8. Rogers, M.R., Applied Mathematics in Integrated Navigation Systems, AIAA, Inc., 2000.

9. Rogers R. M., Weapon IMU Transfer Alignment Using Aircraft Position from Actual Flight Tests, IEEE PLANS, pp328-335, 1996.

10. Yüksel,Y., “Design and Analysis of Transfer Alignment Algorithms”, METU Thesis,2005.

11. Savage, P., Strapdown Analytics: Part1-2, Strapdown Associates, Inc., Maple Plain, Minnesota, 2000.

12. Barbour N., Schmidt G. “Inertial sensor technology trends”, Proc. of 1998 Workshop on Autonomous Underwater Vehicles, August 1998, pp. 55-62.

13. Bose, S.C., GPS-INS Integrated Navigation Systems: Lecture Notes, Technalytics Inc., 2006.

14. Siouris, G.M., Aerospace Avionics Systems A Modern Synthesis, Academic Press Inc., 1993.

15. Scherzinger, B.M., “Inertial Navigator Error Models for Large Heading Uncertainty”, IEEE Position Location and Navigation Symposium, pp.477-484.

16. Chatfield, A.B. , Fundamentals of High Accuracy Inertial Navigation, Published by American Institute of Aeronautics and Astronautics, 1997.

17. Broxmeyer, C., Inertial Navigation Systems, McGraw-Hill Company Inc., USA, 1964.

18. Farrell, J.L., Integrated Aircraft Navigation, Academic Press Inc., London, England, 1976.

19. Bortz J.E., “A new mathematical formulation for strapdown inertial formulation”, IEEE Transactions on Aerospace and Electronic Systems, vol.7, no. 1, Jan. 1971, pp. 61-66.

20. Savage P. G., “Strapdown System Algorithms, Advances in Strapdown Inertial Systems”, NATO AGARD Lecture Series, No:133, 1984.

21. Ignagni M.B., “Optimal strapdown attitude integration algorithms”, Journal of Guidance, Control, and Dynamics, vol. 13, no. 2, March-April 1990, pp.363-369.

22. Savage P. G., Strapdown System Performance Analysis, Advances in Navigation and Integration Technology , NATO RTO Sensors and Electronics Technology Lecture Series, No:64, 2003.

23. Bar-Itzhack, Berman N., “Control Theoretic Approach to Inertial Navigation Systems”, Journal of Guidance and Control, Vol.11, No. 3, 1988.

24. Caruso, M.J., “A New Perspective On Magnetic Field Sensing”, Sensor Magazine Online, December 1998.

25. Caruso, M.J., “Application of Magnetic Sensors for Low Cost Compass Systems”, Honeywell A.N., 2004.

26. Brown G.B., Hwang P.Y.C., Introduction to Random Signals and Applied Kalman Filtering, 1992, John Wiley & Sons Inc.

27. Gelb A., Applied Optimal Estimation, 1974, MIT Press.

28. Shin, E. “Estimation Techniques for Low-Cost Inertial Navigation”, PhD. Thesis, University of Calgary, Department of Geomatics Engineering, May 2005.

29. Biezad, J.D., Satellite Navigation Systems Lecture Notes, Calpoly , 2004.

30. Maybeck, P.S., Stochastic Models, Estimation, and Control, Volume 1-2, Academic Press Inc., 1979.

31. Wahba, G., and et. al. Problem 65-1 (Solution). SIAM, Review, 8:384-386, 1966.

32. Schimelevich, L., Naor, R., “New Approach to Coarse Alignment”, IEEE Position Location and Navigation Symposium, 1996, pp. 324-327.

33. A Gyro free Quaternion Based Attitude Determination System Suitable for Implementation Using Low Cost Sensor”, IEEE 2000 Position Location and Navigation Symposium, pp185-192, 2000.

34. Fleck,V., Sommer,E., Brökelmann,M., Study of Real-time Filtering for an Inertial Measurement Unit(IMU) with Magnetometer in a 155mm Projectile“,IEEE 2006 Position Location and Navigation Symposium, pp803-807, 1998.

35. Aspects of pure and satellite aided Inertial Navigation for Gun Launched Munitions IEEE 2004 Position Location and Navigation Symposium, pp327-336, 2004.
36. Fang, J.C., Wan, D.J., "A Fast Initial Alignment Method for Strapdown Inertial Navigation System on Stationary Base", IEEE Transactions on Aerospace and Electronic Systems, Vol. 32, No. 4, 1996, pp. 1501-1505.

37. Park, H.W. , Lee, J.G. , Park, C.G. , "Error Analysis of Strapdown Inertial Navigation System Aligned by Gyrocompassing," Proceedings of the 1995 IFAC Intelligent Automation Control in Aerospace, Beijing, China, August 1995, pp. 191-195.

38. Eduardo, N. Hugh, D.W., "Initial Calibration and Alignment of an Inertial Navigation," IEEE Position Location and Navigation Symposium, 1997, pp. 175-180.

39. Klotz H. A., Derbak C. B., GPS-Aided Navigation and Unaided Navigation on the Joint Direct Attack Munition, IEEE 1998 Position Location and Navigation Symposium, pp412-419, 1998.

40. Gorecki, R.M., A Baseline 6 Degree of Freedom Generic Missile Simulation, Defense System and Technology, DSTO-TR-0931, 2003.

41. Seymen ,N.B., "Robust Set Valued Estimation and It's Application to In-Flight Alignment of SINS", METU Thesis,2005.

APPENDIX A

WORLD MAGNETIC MODEL 2005

A.1 World Magnetic Model

The Earth's magnetic field (**B**) is a vector quantity varying in space (***r***) and time (*t*). The field, as measured by a magnetic sensor on or above the Earth's surface, is actually a composite of several magnetic fields, generated by a variety of sources. These fields are superimposed on each other and through inductive processes interact with each other. The most important of these geomagnetic sources are:

1. The main field (Figure 1), generated in Earth's conducting, fluid outer core (**B**m);
2. The crustal field from Earth's crust/upper mantle (**B**c);
3. The combined disturbance field from electrical currents flowing in the upper atmosphere and magnetosphere, which also induce electrical currents in the sea and the ground (**B**d)

Thus, the observed magnetic field is a sum of these contributions

$$B(r,t) = B_m(r,t) + B_c(r,t) + B_d(r,t) \qquad \text{(A.1)}$$

Bm is the dominating part of the field, accounting for over 95% of the field strength at the Earth's surface. *Secular variation* is the slow change in time of **B**m. **B**c, the field arising from magnetized crustal rocks, varies spatially, but is considered constant in time for the time-scales considered here. **B**c is usually much smaller in magnitude than **B**m. The crustal field is constant over the time-scales considered here. The field arising from currents flowing in the ionosphere and magnetosphere and their resultant induced currents in the Earth's mantle and crust, **B**d, varies both with location and time. The WMM represents only the main geomagnetic field, **B**m. To create an accurate main field model, it is necessary to have data with good global coverage and as low a noise level as possible. The Danish Ørsted and German CHAMP satellite data sets satisfy these requirements. Both satellites provide high quality vector and scalar data at all latitudes and longitudes, but not during all time periods needed for modeling. These satellite data were therefore augmented with ground observatory hourly mean data, which were available almost continuously over the period of interest, although with poorer spatial coverage. The observatory data therefore provide valuable constraints on the time variations of the geomagnetic field. Used together, satellite and observatory data provide an exceptional quality data set for modeling the behavior of the main magnetic field in space and time. **B**c has spatial variations on the order of meters to thousands of kilometers and cannot be fully modeled with low degree spherical harmonic models. Therefore, the WMM does not include contributions from the crust except for those of very long wavelength. **B**c is usually smaller at sea than on land, and decreases with increasing altitude. The rock magnetization resulting in **B**c may be either induced (by the main magnetic field) or remnant or a combination of both. The field arising from currents flowing in the ionosphere and magnetosphere and their associated induced currents in the Earth, **B**d, varies both with location and time. The regular variations are both diurnal and annual and they are essentially generated by the daylit atmosphere at altitudes of 100-130 km, ionized by the Sun's radiation, being moved in the Earth's main field by winds and tides, thus producing the necessary conditions (motion of a conductor in a magnetic field) for a dynamo to operate. Further daily

and annual variations are caused by the rotation of the Earth in the external magnetosphere field, which is organized in a sun-synchronous reference frame. The irregular variations are due to magnetic storms and sub storms. Magnetic storms generally have three phases: an initial phase, often with a sudden commencement and increased horizontal field at mid-latitudes, a main phase, and a recovery phase. The main phase involves an intensification of the ring current from the plasma sheet.

During the recovery phase the ring current returns to normal over a number of days and associated sub-storms subside. Magnetic storm and sub-storm effects are generally more severe at high geomagnetic latitudes where the ionized region of the upper atmosphere (the ionosphere) is coupled to the magnetosphere by field-aligned currents and is therefore strongly influenced by the interplanetary magnetic field and current systems in the magneto tail. Both the regular and irregular disturbance field variations are modulated by season and the solar magnetic activity cycle. The primary disturbance field is often known as the external field, as its main sources, the ionosphere and magnetosphere, are external to the surface of the Earth where geomagnetic measurements were traditionally made. However, this term can be confusing and is avoided when using satellite data, as the ionosphere is below the altitude of these data and is therefore effectively internal to this observation surface.

A.2 Model Parameterization

The geomagnetic field measured at the Earth's surface or at satellite altitude is the sum of the fields generated by sources internal or external to the solid Earth. Away from its sources, the internal magnetic field $\boldsymbol{B}$ is a potential field and therefore can be written as the negative gradient of a scalar potential

$$B(\varphi', \lambda, r, t) = -\nabla V(\varphi', \lambda, r, t) \qquad \text{(A.1)}$$

This potential can be expanded in terms of spherical harmonics:

$$V(\varphi',\lambda,r,t) = a\left\{\sum_{n=1}^{N}\sum_{m=1}^{N}(g_n^m(t)\cos(m\lambda)+h_n^m(t)\sin(m\lambda))(\frac{a}{r})^{n+1}\breve{P}_n^m(\sin\varphi')\right\} \quad \text{(A.2)}$$

where a (6371.2 km) is the standard Earth's magnetic reference radius (φ',λ,r) are the latitude, longitude and radius in a spherical, geocentric reference frame, $(g_n^m(t),h_n^m(t))$ are the time-dependent Gauss coefficients of degree n and order m describing internal sources. $\breve{P}_n^m(\sin\varphi')$ are the Schmidt semi-normalized Associated Legendre Functions, defined as

$$\breve{P}_n^m(\sin\varphi') = \sqrt{2\frac{(n-m)!}{(n+m)!}}P_n^m(\sin\varphi') \text{ if m > 0}$$
$$\breve{P}_n^m(\sin\varphi') = P_n^m(\sin\varphi') \text{ if m=0} \quad \text{(A.3)}$$

WMM 2005 used 36 = N as the truncation level of the internal expansion. The internal Gauss coefficients from degree 1 to 8 are assumed to have a quadratic dependence on time,

$$g_n^m(t) = g_n^m + \dot{g}_n^m(t-t_0) + \frac{1}{2}\ddot{g}_n^m(t-t_0)^2$$
$$h_n^m(t) = h_n^m + \dot{h}_n^m(t-t_0) + \frac{1}{2}\ddot{h}_n^m(t-t_0)^2 \quad \text{(A.4)}$$

where, on the left side, $g_n^m(t)$ and $h_n^m(t)$ are time varying functions, while $g_n^m,\dot{g}_n^m,\ddot{g}_n^m,h_n^m,\dot{h}_n^m,\ddot{h}_n^m$ denote constants. The time is given in decimal year and 0 t is the reference date of the model, chosen to be at the approximate mid-point of the time span of satellite and observatory hourly mean values (2002.0). From degree 9 up to 12 a linear dependence on time of the internal Gauss

coefficients is assumed, and, for higher degrees, the internal Gauss coefficients are assumed to be constant with time. These truncation levels are chosen as the degrees up to which coefficients can be determined robustly without recourse to damping.

This model given by WMM 2005 is valid only for sources internal to the Earth, like the main field and the crustal field. For the external field, caused by currents in the ionosphere and magnetosphere, a spherical harmonic representation can be used. However, the external fields are organized in a sun synchronous reference frame. WMM 2005 parent model includes a constant degree-2 parameterization of magnetospheric fields in a sunsynchronous reference frame. For an earth-fixed, rotating observer, these external fields are perceived to have daily and seasonal variations. Our parent model accounts for these periodic variations, as well as for their electromagnetic induction in the Earth.

Following evidence of a penetration of the Interplanetary Magnetic Field (IMF), an IMF By correlated component in a sun-synchronous reference frame was included in the modeling. This component reaches about half of the IMF By at the Earth's surface, with typical strengths of 1-2 nT.

Tidal movement of conducting seawater through the Earth's magnetic field induces electric fields, currents, and secondary magnetic fields, which reach about 7 nT at the ocean surface and 3 nT at satellite altitude. These fields are clearly visible in satellite data and closely coincide with independent predictions from tidal ocean flow models. The satellite measurements were corrected for the eight major tidal constituents.

Finally, when the data set contains hourly mean observatory data, offsets at each observatory have to be introduced to take into account the local field, mainly generated in the crust, which cannot be described by the model. Then, at an observatory, the magnetic field $\boldsymbol{B}$ is:

$$B(\varphi', \lambda, r, t) = -\nabla V(\varphi', \lambda, r, t) + O(\varphi', \lambda, r) \qquad \text{(A.5)}$$

where the offset vector $O(\varphi', \lambda, r)$, also referred to as crustal bias, is constant in time.

The above parameterization is used to fit data sets selected from satellite measurements and observatory hourly mean values. The equations for the internal part of the field are:

$$X'(\varphi', \lambda, r) = \frac{1}{r}\frac{\partial V}{\partial \varphi'} = -\sum_{n=1}^{N}\left(\frac{a}{r}\right)^{n+2}\sum_{m=0}^{n}(g_n^m(t)\cos(m\lambda) + h_n^m(t)\sin(m\lambda))\frac{d\breve{P}_n^m(\sin\varphi')}{d\varphi'} \tag{A.6}$$

$$Y'(\varphi', \lambda, r) = \frac{1}{r\cos\varphi'}\frac{\partial V}{\partial \lambda} = \frac{1}{\cos\varphi'}\sum_{n=1}^{N}\left(\frac{a}{r}\right)^{n+2}\sum_{m=0}^{n} m(g_n^m(t)\cos(m\lambda) + h_n^m(t)\sin(m\lambda))\breve{P}_n^m(\sin\varphi') \tag{A.7}$$

$$Z'(\varphi', \lambda, r) = \frac{\partial V}{\partial r} = -\sum_{n=1}^{N}(n+1)\left(\frac{a}{r}\right)^{n+2}\sum_{m=0}^{n} m(g_n^m(t)\cos(m\lambda) + h_n^m(t)\sin(m\lambda))\breve{P}_n^m(\sin\varphi') \tag{A.8}$$

A.3 Model Determination

The above equations, with the magnetic field vector observations on the left-hand side, form the equations of condition. Thus, if there are *d* data, there are *d* linear equations with the *p* parameters of the parent model:

$$y = Am \tag{A.9}$$

where is **y** the column vector (d x 1) of observations, **A** is the matrix (d x p) of coefficients to the unknowns which are functions of position, and **m** is the column vector (p x 1) of unknowns, the Gauss coefficients of the model. As there are many more observations than unknowns, i.e. as $d > p$, the system is over-determined and therefore does not have an exact solution. Suppose **m**~ is an estimate of **m**. Then

$$\tilde{y} = A\tilde{m} \tag{A.10}$$

where $\tilde{y}$ are estimates of the observations. The residuals are $(y - \tilde{y})$ and the least-squares method requires that $\tilde{m}$ is chosen so as to minimize the weighted sum of the squares of the residuals, S,

i.e.: minimize $S = (y - \tilde{y})^T W (y - \tilde{y}) = (y - A\tilde{m})^T W (y - A\tilde{m})$ with respect to $\tilde{m}$

W is the weight matrix (d x d) of the data. For satellite data there are off-diagonal terms in this matrix to account for the anisotropic errors arising from the star camera. The minimum is reached when $\frac{\partial S}{\partial \tilde{m}} = 0$, now;

$$\begin{aligned}
&\frac{\partial S}{\partial \tilde{m}} = \lim_{\partial\tilde{m}\to 0} \frac{S(\tilde{m}+\partial\tilde{m}) - S(\tilde{m})}{\partial\tilde{m}} \\
&\frac{\partial S}{\partial \tilde{m}} = \lim_{\partial\tilde{m}\to 0} \frac{(y - A(\tilde{m}+\partial\tilde{m}))^T W (y - A(\tilde{m}+\partial\tilde{m})) - (y - A\tilde{m})^T W (y - A\tilde{m})}{\partial\tilde{m}} \\
&\frac{\partial S}{\partial \tilde{m}} = \lim_{\partial\tilde{m}\to 0} \frac{(z - A(\partial\tilde{m}))^T W (z - A(\partial\tilde{m})) - z^T W z}{\partial\tilde{m}}, z = y - A\tilde{m} \\
&\frac{\partial S}{\partial \tilde{m}} = \lim_{\partial\tilde{m}\to 0} \frac{-2\partial\tilde{m}^T A^T W z + O(\partial\tilde{m}^2)}{\partial\tilde{m}} \\
&\frac{\partial S}{\partial \tilde{m}} = 0
\end{aligned} \tag{A.11}$$

These are the normal equations and the estimated unknowns $\tilde{\mathbf{m}}$ are found from

$$\tilde{m} = (A^T W A)^{-1} A^T W y \tag{A.12}$$

A.4 Coordinate Transformation

Satellite data are already located in a geocentric coordinate system but surface data are almost invariably located in a geodetic coordinate system, i.e. relative to the mean sea surface of the Earth, which can be approximated by an ellipsoid. The locations of surface data, and the data themselves, must be transformed from geodetic to geocentric coordinates prior to spherical harmonic modeling.

When computing the model, the locations (h, φ, λ), where h is the geodetic altitude and ö is the geodetic latitude, are transformed into (r, φ', λ) using

$$\tan(\varphi') = \frac{(A^2 \cos^2 \varphi + B^2 \sin^2 \varphi)^{0.5} h + B^2}{(A^2 \cos^2 \varphi + B^2 \sin^2 \varphi)^{0.5} h + A^2} \tan(\varphi) \tag{A.13}$$

$$r^2 = h^2 + 2h(A^2 \cos^2 \varphi + B^2 \sin^2 \varphi)^{0.5} + \frac{(A^4 \cos^2 \varphi + B^4 \sin^2 \varphi)}{(A^2 \cos^2 \varphi + B^2 \sin^2 \varphi)} \tag{A.14}$$

where A=6378.137 km is the semi-major axis (equatorial radius) of the ellipsoid and B=6356.7523142 km is the semi-minor axis as defined by the World Geodetic System 1984(WGS84).

The observations of the northerly, easterly and vertically down intensities X, Y, and Z, relative to an ellipsoid, are transformed into the northerly, easterly and vertically down intensities relative to a sphere, X', Y', and Z':

$$\begin{aligned} X' &= X \cos\psi + Z \sin\psi \\ Y' &= Y \\ Z' &= -X \sin\psi + Z \cos\psi \end{aligned} \tag{A.15}$$

where ψ is the difference between geocentric and geodetic latitude in the sense $\psi = \varphi' - \varphi$

Another coordinate system used in global magnetic field modeling is the geomagnetic coordinate system. This is used in the derivation of WMM2005 to identify data locations within a certain latitude band of the geomagnetic equator for which vector data values are required. This coordinate system is based on the internal centered dipolar field and is defined by the first three main-field coefficients of an existing global spherical harmonic model. Its reference axis is aligned along the dipole axis, which is tilted from the rotational axis of the Earth by about 11° and cuts the surface of the Earth at the geomagnetic poles. The geomagnetic equator is the great circle 90° from the geomagnetic poles and geomagnetic latitude varies from 0° at the geomagnetic equator to ±90° at the geomagnetic poles.

A.5 Secular Variation Prediction

Predictions of future changes in the magnetic field were derived from the long-term observatory annual mean data as well as polynomial extrapolation of the parent model based on satellite data and observatory hourly mean values. Annual mean data were utilized by determining and applying linear predictor filters to series of first differences to result in estimates of secular variation up to 2010.0. Linear prediction is successful at extrapolating signals which are smooth and oscillatory, though not necessarily periodic, and tests have shown that when predicting more than about 3 years ahead, this method is better than linear regression applied to recent first differences (equivalent to quadratic polynomial fitted to annual means). For incorporation into the final secular-variation model we used averages of the predictions for 2005.0-2010.0 at 159 observatories with sufficiently long time series. They were assigned uncertainties that reflected the past success of prediction for the data series in question. Data from 29

observatories, which had time series too short for the application of linear prediction filters, were also used by computing average secular-variation estimates and assuming that these did not change with time.

A.6 Derivation of World Magnetic Model

The final main-field coefficients for 2005.0 were derived by polynomial extrapolation of the main-field Gauss coefficients from the parent model to this date.

Before the final secular-variation coefficients could be derived, the secular-variation estimates from the parent model (valid for 1999.0-2004.5) were combined with the long-term predictions at the observatories described in Section 4.4. This was done by using the parent model to estimate annual rates of change in the north, east and vertically down directions, in a geocentric coordinate system, at the centers of 1654 equal-area tessera. Each tessera was equivalent in size to a 5° latitude by 5° longitude box at the equator. This synthetic dataset was combined with the predicted mean *X, Y* and *Z* rates of change for 2005.0-2010.0 at the 188 observatories, rotated into a geocentric coordinate system. Equations (8)-(10) of Section 4.1, with the time varying Gauss coefficients $g_n^m(t), h_n^m(t)$ replaced by their derivatives g_n^m and h_n^m were then used to determine the final secular-variation coefficients.

A.7 Resulting Model

This section lists the final model coefficients, the corresponding magnetic pole and eccentric dipole locations, provides the equations for computing the magnetic field components at a given location, and discusses the accuracy and limitations of the model.

A.8 Model Coefficients

The model coefficients also referred to as Gauss coefficients; provide an accurate and convenient representation of the Earth's main magnetic field. Their values are listed in Table A.1. These coefficients can be used to compute values for the field elements and their annual rates of change at any location near the surface of the Earth and at any date between 2005.0 and 2010.0.

Table A.1

n	m	g_n^m	h_n^m	$\dot{g}_n^m$	$\dot{h}_n^m$
1	0	-29556.8		8.0	
1	1	-1671.7	5079.8	10.6	-20.9
2	0	-2340.6		-15.1	
2	1	3046.9	-2594.7	-7.8	-23.2
2	2	1657.0	-516.7	-0.8	-14.6
3	0	1335.4		0.4	
3	1	-2305.1	-199.9	-2.6	5.0
3	2	1246.7	269.3	-1.2	-7.0
3	3	674.0	-524.2	-6.5	-0.6
4	0	919.8		-2.5	
4	1	798.1	281.5	2.8	2.2
4	2	211.3	-226.0	-7.0	1.6
4	3	-379.4	145.8	6.2	5.8
4	4	100.0	-304.7	-3.8	0.1
5	0	-227.4		-2.8	
5	1	354.6	42.4	0.7	0.0
5	2	208.7	179.8	-3.2	1.7
5	3	-136.5	-123.0	-1.1	2.1
5	4	-168.3	-19.5	0.1	4.8
5	5	-14.1	103.6	-0.8	-1.1
6	0	73.2		-0.7	
6	1	69.7	-20.3	0.4	-0.6
6	2	76.7	54.7	-0.3	-1.9
6	3	-151.2	63.6	2.3	-0.4
6	4	-14.9	-63.4	-2.1	-0.5
6	5	14.6	-0.1	-0.6	-0.3
6	6	-86.3	50.4	1.4	0.7
7	0	80.1		0.2	
7	1	-74.5	-61.5	-0.1	0.6
7	2	-1.4	-22.4	-0.3	0.4
7	3	38.5	7.2	1.1	0.2
7	4	12.4	25.4	0.6	0.3
7	5	9.5	11.0	0.5	-0.8
7	6	5.7	-26.4	-0.4	-0.2
7	7	1.8	-5.1	0.6	0.1
8	0	24.9		0.1	
8	1	7.7	11.2	0.3	-0.2
8	2	-11.6	-21.0	-0.4	0.1
8	3	-6.9	9.6	0.3	0.3
8	4	-18.2	-19.8	-0.3	0.4

8	5	10.0	16.1	0.2	0.1
8	6	9.2	7.7	0.4	-0.2
8	7	-11.6	-12.9	-0.7	0.4
8	8	-5.2	-0.2	0.4	0.4
9	0	5.6		0.0	
9	1	9.9	-20.1	0.0	0.0
9	2	3.5	12.9	0.0	0.0
9	3	-7.0	12.6	0.0	0.0
9	4	5.1	-6.7	0.0	0.0
9	5	-10.8	-8.1	0.0	0.0
9	6	-1.3	8.0	0.0	0.0
9	7	8.8	2.9	0.0	0.0
9	8	-6.7	-7.9	0.0	0.0
9	9	-9.1	6.0	0.0	0.0
10	0	-2.3		0.0	0.0
10	1	-6.3	2.4	0.0	0.0
10	2	1.6	0.2	0.0	0.0
10	3	-2.6	4.4	0.0	0.0
10	4	0.0	4.8	0.0	0.0
10	5	3.1	-6.5	0.0	0.0
10	6	0.4	-1.1	0.0	0.0
10	7	2.1	-3.4	0.0	0.0
10	8	3.9	-0.8	0.0	0.0
10	9	-0.1	-2.3	0.0	0.0
10	10	-2.3	-7.9	0.0	0.0
11	0	2.8		0.0	0.0
11	1	-1.6	0.3	0.0	0.0
11	2	-1.7	1.2	0.0	0.0
11	3	1.7	-0.8	0.0	0.0
11	4	-0.1	-2.5	0.0	0.0
11	5	0.1	0.9	0.0	0.0
11	6	-0.7	-0.6	0.0	0.0
11	7	0.7	-2.7	0.0	0.0
11	8	1.8	-0.9	0.0	0.0
11	9	0.0	-1.3	0.0	0.0
11	10	1.1	-2.0	0.0	0.0
11	11	4.1	-1.2	0.0	0.0
12	0	-2.4		0.0	0.0
12	1	-0.4	-0.4	0.0	0.0
12	2	0.2	0.3	0.0	0.0
12	3	0.8	2.4	0.0	0.0
12	4	-0.3	-2.6	0.0	0.0
12	5	1.1	0.6	0.0	0.0
12	6	-0.5	0.3	0.0	0.0
12	7	0.4	0.0	0.0	0.0

A.9 Equations for computing magnetic field elements

A step by step procedure is given for computing the magnetic field elements at a given location and time (h,φ,λ,t), h is the geodetic altitude, φ and λ are the geodetic latitude and longitude, and t is the time given in decimal year.

In the first step, the ellipsoidal geodetic coordinates (h,φ,λ) are transformed into spherical geocentric coordinates using

$$\tan(\varphi') = \frac{(A^2\cos^2\varphi + B^2\sin^2\varphi)^{0.5}h + B^2}{(A^2\cos^2\varphi + B^2\sin^2\varphi)^{0.5}h + A^2}\tan(\varphi) \tag{A.16}$$

$$r^2 = h^2 + 2h(A^2\cos^2\varphi + B^2\sin^2\varphi)^{0.5} + \frac{(A^4\cos^2\varphi + B^4\sin^2\varphi)}{(A^2\cos^2\varphi + B^2\sin^2\varphi)} \tag{A.17}$$

where A=6378.137 km is the semi-major axis (equatorial radius) of the ellipsoid and B=6356.7523142 km is the semi-minor axis referenced to the WGS84 ellipsoid.

In the second step, the Gauss coefficients $(g_n^m(t), h_n^m(t))$ of degree n and order m are determined for the desired time. This is achieved by adjusting the coefficients (g_n^m, h_n^m) of the field at $t_0 = 2005.0$ for the linear secular variation $(\dot{g}_n^m, \dot{h}_n^m)$ as

$$\begin{aligned} g_n^m(t) &= g_n^m + \dot{g}_n^m(t - t_0) \\ h_n^m(t) &= h_n^m + \dot{h}_n^m(t - t_0) \end{aligned} \tag{A.18}$$

where the time is given in decimal year and $t_0 = 2005.0$ is the reference date of the model

In the third step, the field vector components X', Y' and Z' in geocentric coordinates are computed as

$$X'(\varphi',\lambda,r)=\frac{1}{r}\frac{\partial V}{\partial \varphi'}$$
$$=-\sum_{n=1}^{N}\left(\frac{a}{r}\right)^{n+2}\sum_{m=0}^{n}(g_n^m(t)\cos(m\lambda)+h_n^m(t)\sin(m\lambda))\frac{d\breve{P}_n^m(\sin\varphi')}{d\varphi'} \tag{A.19}$$

$$Y'(\varphi',\lambda,r)=\frac{1}{r\cos\varphi'}\frac{\partial V}{\partial \lambda}$$
$$=\frac{1}{\cos\varphi'}\sum_{n=1}^{N}\left(\frac{a}{r}\right)^{n+2}\sum_{m=0}^{n}(g_n^m(t)\cos(m\lambda)+h_n^m(t)\sin(m\lambda))\breve{P}_n^m(\sin\varphi') \tag{A.20}$$

$$Z'(\varphi',\lambda,r)=\frac{\partial V}{\partial r}$$
$$=\sum_{n=1}^{N}\left(\frac{a}{r}\right)^{n+2}\sum_{m=0}^{n}(g_n^m(t)\cos(m\lambda)+h_n^m(t)\sin(m\lambda))\breve{P}_n^m(\sin\varphi') \tag{A.21}$$

At this point, one can also compute the secular variation of the field components as

$$X'(\varphi',\lambda,r)=\frac{1}{r}\frac{\partial V}{\partial \varphi'}$$
$$=-\sum_{n=1}^{N}\left(\frac{a}{r}\right)^{n+2}\sum_{m=0}^{n}(g_n^m(t)\cos(m\lambda)+h_n^m(t)\sin(m\lambda))\frac{d\breve{P}_n^m(\sin\varphi')}{d\varphi'} \tag{A.22}$$

$$Y'(\varphi',\lambda,r)=\frac{1}{r\cos\varphi'}\frac{\partial V}{\partial \lambda}$$
$$=\frac{1}{\cos\varphi'}\sum_{n=1}^{N}\left(\frac{a}{r}\right)^{n+2}\sum_{m=0}^{n}m(g_n^m(t)\cos(m\lambda)+h_n^m(t)\sin(m\lambda))\breve{P}_n^m(\sin\varphi') \tag{A.23}$$

$$Z'(\varphi',\lambda,r)=\frac{\partial V}{\partial r}$$
$$=-\sum_{n=1}^{N}(n+1)\left(\frac{a}{r}\right)^{n+2}\sum_{m=0}^{n}m(g_n^m(t)\cos(m\lambda)+h_n^m(t)\sin(m\lambda))\breve{P}_n^m(\sin\varphi') \tag{A.24}$$

In the fourth step, the geocentric vector components X', Y' and Z' are transformed back into the geodetic reference frame, using

$$
\begin{aligned}
X &= X'\cos\psi + Z'\sin\psi \\
Y &= Y' \\
Z &= -X'\sin\psi + Z'\cos\psi
\end{aligned}
\tag{A.25}
$$

where $\psi = \varphi' - \varphi$ is the difference between geocentric and geodetic latitude and φ' was computed in step 1. Similarly, the time derivatives of the vector components are transformed using

$$
\begin{aligned}
\dot{X} &= \dot{X}'\cos\psi + \dot{Z}'\sin\psi \\
\dot{Y} &= \dot{Y}' \\
\dot{Z} &= -\dot{X}'\sin\psi + \dot{Z}'\cos\psi
\end{aligned}
\tag{A.26}
$$

In the last step, the magnetic elements *H, F, D*, *I*, and the grid variation, *GV*, are computed from the vector components as

$$
\begin{aligned}
&H = \sqrt{X^2 + Y^2}, F = \sqrt{H^2 + Z^2}, D = \arctan(Y, X), I = \arctan(Z, H) \\
&GV = D - \lambda, \; for \varphi > 55^o \\
&GV = D + \lambda, \; for \varphi < -55^o
\end{aligned}
\tag{A.27}
$$

For H=0 the declination is undefined.

The secular variation of these elements is computed using

$$
\begin{aligned}
\dot{H} &= \frac{X.\dot{X} + Y.\dot{Y}}{H} \\
\dot{F} &= \frac{X.\dot{X} + Y.\dot{Y} + Z.\dot{Z}}{F} \\
\dot{D} &= \frac{180}{\pi}\frac{X.\dot{Y} - Y.\dot{X}}{H^2} \\
\dot{I} &= \frac{180}{\pi}\frac{H.\dot{Z} - Z.\dot{H}}{F^2} \\
G\dot{V} &= \dot{D}
\end{aligned}
\tag{A.28}
$$

where $\dot{D}$, $\dot{I}$ and $G\dot{V}$ are given in degrees/year. Here, the factor $\frac{180}{\pi}$ converts from radians to degree. This conversion factor is not present in equation (A.29), assuming that the arctan function provides the result in degrees.

A.10 Model Limitations

It is important to recognize that the WMM geomagnetic model and the charts produced from this model characterize only that portion of the Earth's magnetic field that is generated by dynamo action in the Earth's fluid outer core (**B**m). The portions of the geomagnetic field generated by the Earth's crust and upper mantle (**B**c), and by the ionosphere and magnetosphere (**B**d), are not represented in the WMM. Consequently, a magnetic sensor such as a compass or magnetometer may observe spatial and temporal magnetic anomalies when referenced to the WMM. In particular, certain local, regional, and temporal magnetic declination anomalies can exceed 10 degrees. Anomalies of this magnitude are not common but they do exist. Declination anomalies of the order of 3 or 4 degrees are not uncommon but are of small spatial extent and are relatively isolated. On land, spatial anomalies are produced by mountain ranges, ore deposits, ground struck by lightning, geological faults, and cultural features such as trains, planes, tanks, railroad tracks, power lines, etc. The corresponding deviations are usually smaller at sea, and decrease with increasing altitude of an aircraft or spacecraft. In ocean areas, these anomalies occur most frequently along continental margins, near seamounts, and near ocean ridges, trenches, and fault zones, particularly those of volcanic origin. Ships and submarines are also sources of magnetic anomalies in the ocean. The crustal contributions could be included in an extended model, expanded to high degrees, as is common for modern gravity field models. Since the crustal field is almost constant in time, it can be inferred from all available marine, aeromagnetic, and high resolution CHAMP and future SWARM satellite data, measured at all times. However, this extended model would differ significantly in format from the current WMM, requiring changes in supporting software.

APPENDIX B

LOW COST MEMS IMU + MAGNETOMETER PERFORMANCE SPECIFICATIONS

Table B.1

PERFORMANCE	(1 σ)
Gyros (Inertial Science RRS75)	
Measurement Range	> ± 500 deg/sec
Dynamic Bandwidth	50 Hz
Scale Factor Repeatability	< 1000 ppm
Nonlinearity	< 1000 ppm
Bias Repeatability	< 100 deg/hr
Axis Misalignment	≤ 3 mrad
Random Walk	≤ 1 deg/√hr
Start-up Time	≤ 100 ms
g Sensitivity	< 100 deg/hr/g
Accelerometers (Colibrys Ms8000C)	
Measurement Range	±30g
Dynamic Bandwidth	50 Hz
Scale Factor Repeatability	< 1000 ppm

Nonlinearity	< 1000 ppm
Bias Repeatability	< 10 mg
Axis Misalignment	≤ 3 mrad
Random Walk	0.5 m/s/√hr
Start-up Time	≤ 100 ms
Magnetometers(Honeywell HMR2300)	
Measurement Range	±2 Gauss
Dynamic Bandwidth	50 Hz
Scale Factor Repeatability	< 750 ppm
Nonlinearity	< 500 ppm
Bias Repeatability	< %0.05 of full scale
Axis Misalignment	≤ 5 mrad
Noise Level	0.1 mGauss
Start-up Time	≤ 100 ms

APPENDIX C

DERIVATION OF INERTIAL NAVIGATION MECHANIZATION EQUATIONS

In this system, it is required to calculate the vehicle speed with respect to earth, the ground speed, in inertial axes, denoted by v_e^i. First of all, it is essential to express the fundamental navigation equations[17,18]

$$\left.\frac{d^2r}{dt^2}\right|_i = f \tag{C.1}$$

And

$$\left.\frac{d^2r}{dt^2}\right|_i = a + g \tag{C.2}$$

where

f: the acceleration of the rigid body with respect to the inertial axis set

a: accelerations measured by accelerometers

g: gravitational acceleration

r: position vector

Note that an accelerometer can not directly measure gravitational acceleration

To obtain velocity with respect to earth, Coriolis equation is introduced;

$$\left.\frac{dr}{dt}\right|_i = \left.\frac{dr}{dt}\right|_e + \omega_{ie} \times r \tag{C.3}$$

Differentiating this equation and introducing $\left.\frac{dr}{dt}\right|_e = v_e$;

$$\left.\frac{d^2r}{dt^2}\right|_i = \left.\frac{dv_e}{dt}\right|_i + \left.\frac{d(\omega_{ie} \times r)}{dt}\right|_i \tag{C.4}$$

$$\left.\frac{d^2r}{dt^2}\right|_i = \left.\frac{dv_e}{dt}\right|_i + \omega_{ie} \times v_e + \omega_{ie} \times (\omega_{ie} \times r) \tag{C.5}$$

where $\frac{d\omega_{ie}}{dt} = 0$ is assumed, i.e. the rate of rotation of Earth is assumed to be constant

Rearranging these equations yield;

$$\left.\frac{dv_e}{dt}\right|_i = a^n - \omega_{ie} \times v_e - \omega_{ie} \times (\omega_{ie} \times r) + g \tag{C.6}$$

Where;

a^n : Acceleration to which the inertial measurement unit is subjected

$\omega_{ie} x v_e$: Transport rate

$\omega_{ie} x(\omega_{ie} xr)$: Centrifugal acceleration experienced by the system as a result of the rotational rate of Earth. This term is not separately distinguishable from the gravitational acceleration which arises through mass attraction. The sum of the accelerations caused by the mass attraction force and the centrifugal acceleration constitutes what is known as the local gravity vector (plumb bob gravity);

$$g_p = g - \omega_{ie} x(\omega_{ie} xr) \tag{C.7}$$

A local geographic (or navigation) axis set is needed in order to navigate over large distances around the Earth. In a local geographic frame, the position is expressed in terms of latitude, longitude and altitude. The velocity is expressed in NED components.

The ground speed in navigation frame is denoted as v_e^n. Writing its rate of change with respect to navigation frame in terms of inertial frame;

$$\left.\frac{dv_e}{dt}\right|_n = \left.\frac{dv_e}{dt}\right|_i - (\omega_{ie} + \omega_{en}) \times v_e \tag{C.8}$$

Substituting $\left.\frac{dv_e}{dt}\right|_i$;

$$\left.\frac{dv_e}{dt}\right|_n = a^n - (2.\omega_{ie} + \omega_{en}) \times v_e + g_p \tag{C.9}$$

which can also be expressed as;

$$\dot{v}_e^n = C_b^n.a^b - (2.\omega_{ie} + \omega_{en}) \times v_e^n + g_p \quad \text{(C.10)}$$

C_b^n : The direction cosine matrix (DCM) that is used to transform body coordinate frame into navigation coordinate frame. DCM propagates in accordance with the following equation;

$$\dot{C}_b^n = C_b^n(\tilde{\omega}_{nb}^b)$$

ω_{nb}^b :The angular rate of the body with respect to the navigation frame

$\tilde{\omega}_{nb}^b$: Skew symmetric matrix representation of ω_{nb}^b

ω_{nb}^b can be expressed as the measured body rates (ω_{ib}^b) and estimates of the components of the navigation frame rate ($\omega_{in} = \omega_{ie} + \omega_{en}$) ;

$$\omega_{nb}^b = \omega_{ib}^b - C_b^n.(\omega_{ie}^n + \omega_{en}^n) \quad \text{(C.11)}$$

Note that the navigation frame is required to rotate continuously as the system moves over the surface of the Earth in order to keep x axis parallel to the ground. The turn rate of the navigation frame can be expressed as;

$$\omega_{en}^n = [V_E/(R_e + h) \quad -V_N/(R_n + h) \quad -V_E.\tan(L)/(R_e + h)] \quad \text{(C.12)}$$

This is also known as transport rate.

The DCM that relates earth and navigation frames can be expressed as [19, 20, 21];

$$\dot{C}_n^e = C_n^e(\tilde{\omega}_{en}^n) \quad \text{(C.13)}$$

The rate of change in latitude, longitude and altitude is also expressed as

$$\dot{L} = \frac{V_N}{R_N + h} \tag{C.14}$$

$$\dot{l} = \frac{V_E \sec(L)}{R_N + h} \tag{C.15}$$

$$\dot{h} = -V_D \tag{C.16}$$

APPENDIX D

DERIVATION OF INERTIAL NAVIGATION ERROR MECHANIZATION EQUATIONS

In this section, error behavior of a six degree of freedom inertial navigation system is analyzed. Error equations in navigation frame are examined [1, 22 and 23].

D.1 Attitude Errors

The attitude difference between the navigation and computer (erroneous navigation) frame can be expressed as;

$$\hat{C}_b^n = \delta C_b^n . C_b^n \tag{D.1}$$

where

$\hat{C}_b^n$: True navigation frame

C_b^n : Erroneous navigation (computer) frame

δC_b^n : Misalignment matrix that relates true and erroneous navigation frame

Remember that the attitude kinematics is given as;

$$\dot{C}_b^n = C_b^n.(\tilde{\omega}_{ib}^b) - (\tilde{\omega}_{in}^n).C_b^n \tag{D.2}$$

Differentiating this equation;

$$\delta\dot{C}_b^n = \delta C_b^n.(\tilde{\omega}_{ib}^b) + C_b^n.(\delta\tilde{\omega}_{ib}^b) - (\delta\tilde{\omega}_{in}^n).C_b^n - (\tilde{\omega}_{in}^n).\delta C_b^n \tag{D.3}$$

where δC_b^n can be expressed as a misalignment vector with small angles assumption;

$$\delta C_b^n = -(\tilde{\gamma}^n).C_b^n \tag{D.4}$$

$\tilde{\gamma}^n$: Misalignment vector

Taking this equation's derivative with respect to time;

$$\delta\dot{C}_b^n = -(\dot{\tilde{\gamma}}^n).C_b^n - (\tilde{\gamma}^n).\dot{C}_b^n \tag{D.5}$$

Substitute for $\dot{C}_b^n$

$$\delta\dot{C}_b^n = -(\dot{\tilde{\gamma}}^n).C_b^n - (\tilde{\gamma}^n).(C_b^n.(\tilde{\omega}_{ib}^b) - (\tilde{\omega}_{in}^n).C_b^n) \tag{D.6}$$

Equating both equations;

$$\begin{aligned} &C_b^n.(\tilde{\omega}_{ib}^b) + C_b^n.(\delta\tilde{\omega}_{ib}^b) - (\delta\tilde{\omega}_{in}^n).C_b^n - (\tilde{\omega}_{in}^n).\delta C_b^n = \\ &-(\dot{\tilde{\gamma}}^n).C_b^n - (\tilde{\gamma}^n).(C_b^n.(\tilde{\omega}_{ib}^b) - (\tilde{\omega}_{in}^n).C_b^n) \end{aligned} \tag{D.7}$$

And solving for misalignment vector derivative

$$\begin{aligned} &(\dot{\tilde{\gamma}}^n).C_b^n = -C_b^n.(\delta\tilde{\omega}_{ib}^b) + (\tilde{\gamma}^n).(\tilde{\omega}_{in}^n).C_b^n \\ &-(\tilde{\omega}_{in}^n).(\tilde{\gamma}^n).C_b^n + (\delta\tilde{\omega}_{in}^n).C_b^n \end{aligned} \tag{D.8}$$

Multiplying on the right by the inverse of C_b^n;

$$(\dot{\tilde{\gamma}}^n) = -C_b^n.(\delta\tilde{\omega}_{ib}^b)(C_b^n)^T + (\tilde{\gamma}^n).(\tilde{\omega}_{in}^n) - (\tilde{\omega}_{in}^n).(\tilde{\gamma}^n) + (\delta\tilde{\omega}_{in}^n) \tag{D.9}$$

$$\dot{\gamma}^n = -C_b^n.\delta\omega_{ib}^b - \omega_{in}^n \times \gamma^n + \delta\omega_{in}^n \tag{D.10}$$

Note that ω_{en}^n and ω_{ie}^n are defined as;

$$\omega_{en}^n = [\frac{V_E}{R_E + h} \quad \frac{V_N}{R_N + h} \quad \frac{-V_N.\tan(L)}{R_E + h}]^T \tag{D.11}$$

and

$$\omega_{ie}^n = [\Omega\cos(L) \quad 0 \quad -\Omega\sin(L)]^T \tag{D.12}$$

$\delta\omega_{in}^n$ is defined mathematically as;

$$\omega_{in}^n = \omega_{ie}^n + \omega_{en}^n \tag{D.13}$$

$$\delta\omega_{in}^n = \delta\omega_{ie}^n + \delta\omega_{en}^n \tag{D.14}$$

where

$$\delta\omega_{ie}^n = \delta C_n^e.\omega_{ie}^e \tag{D.15}$$

Note that ω_{ie}^e is constant in time.

Introducing the error in position, ε^n

$$\delta\omega_{ie}^n = -\varepsilon^n x C_n^e . \omega_{ie}^e \tag{D.16}$$

ε^n : Position Error vector

Rearranging the equation yields;

$$\delta\omega_{ie}^n = -\varepsilon^n x \omega_{ie}^n = \omega_{ie}^n x \varepsilon^n \tag{D.17}$$

In an alternative form, $\delta\omega_{en}^n$ and $\delta\omega_{ie}^n$ can be expressed by differentiating;

$$\delta\omega_{en}^n = \begin{bmatrix} \dfrac{\delta V_E}{R_E + h} - \dfrac{V_E \delta h}{R_E + h} \\ \dfrac{\delta V_N}{R_N + h} - \dfrac{V_N \delta h}{(R_N + h)^2} \\ \dfrac{-\delta V_N . \tan(L)}{R_E + h} + \dfrac{V_N . \tan(L) \delta h}{(R_E + h)^2} - \dfrac{-V_N .}{(R_E + h)(\cos(L))^2} \end{bmatrix} \tag{D.18}$$

$$\delta\omega_{ie}^n = [-\Omega \sin(L) \delta L \quad 0 \quad -\Omega \cos(L) \delta L]^T \tag{D.19}$$

D.2 Velocity Errors

Remember that differential equation for velocity is given as;

$$\dot{v}_e^n = C_b^n . a^b - (2.\omega_{ie} + \omega_{en}) \times v_e^n + g_p \tag{D.20}$$

Differentiating this equation;

$$\delta\dot{v}_e^n = \delta C_b^n.a^b + C_b^n.\delta a^b$$
$$-(2.\delta\omega_{ie} + \delta\omega_{en})\times v_e^n - (2.\omega_{ie} + \omega_{en})\times \delta v_e^n + \delta g_p \quad \text{(D.21)}$$

Introducing δC_b^n to this equation, neglecting second order effects and rearranging yields in the velocity error propagation equation;

$$\delta\dot{v}_e^n = (C_b^n.a^b)\times\gamma^n + C_b^n.\delta a^b - v_e^n\times(2.\omega_{ie}^n\times\varepsilon^n + \delta\omega_{en}^n)$$
$$-(2.\omega_{ie}^n + \omega_{en}^n)\times\delta v_e^n + \delta g_p \quad \text{(D.22)}$$

D.3 Position Errors

Position Equation is given as;

$$\dot{C}_n^e = C_n^e(\tilde{\omega}_{en}^n) \quad \text{(D.23)}$$

Differentiating this equation

$$\delta\dot{C}_n^e = \delta C_n^e(\tilde{\omega}_{en}^n) + C_n^e(\delta\tilde{\omega}_{en}^n) \quad \text{(D.24)}$$

Defining;

$$\delta C_n^e = C_n^e(\tilde{\varepsilon}^n) \quad \text{(D.25)}$$

$\tilde{\varepsilon}^n$: Position error vector

Taking derivative with respect to time;

$$\delta \dot{C}_n^e = \dot{C}_n^e(\tilde{\varepsilon}^n) + C_n^e(\dot{\tilde{\varepsilon}}^n) \tag{D.26}$$

Rearranging;

$$\delta \dot{C}_n^e = C_n^e(\tilde{\omega}_{en}^n)(\tilde{\varepsilon}^n) + C_n^e(\dot{\tilde{\varepsilon}}^n) \tag{D.27}$$

Equating these equations

$$C_n^e(\tilde{\omega}_{en}^n)(\tilde{\varepsilon}^n) + C_n^e(\dot{\tilde{\varepsilon}}^n) = \delta C_n^e(\tilde{\omega}_{en}^n) + C_n^e(\delta\tilde{\omega}_{en}^n) \tag{D.28}$$

Solving for ε^n

$$C_n^e(\dot{\tilde{\varepsilon}}^n) = \delta C_n^e(\tilde{\omega}_{en}^n) + C_n^e(\delta\tilde{\omega}_{en}^n) - C_n^e(\tilde{\omega}_{en}^n)(\tilde{\varepsilon}^n) \tag{D.29}$$

Multiply on the left by the inverse of C_n^e

$$(\dot{\tilde{\varepsilon}}^n) = (\tilde{\varepsilon}^n)(\tilde{\omega}_{en}^n) + (\delta\tilde{\omega}_{en}^n) - (\tilde{\omega}_{en}^n)(\tilde{\varepsilon}^n) \tag{D.30}$$

Rearranging;

$$\dot{\varepsilon}^n = -\omega_{en}^n x \varepsilon^n + \delta\omega_{en}^n \tag{D.31}$$

Altitude error is given by differentiating

$$\dot{h} = V_D \tag{D.32}$$

$$\delta\dot{h} = \delta V_D \tag{D.33}$$

As an alternative form, longitude and latitude errors can be found from their differential equations;

$$\delta\dot{L} = \delta V_N /(R_n + h) - V_N .\delta h /(R_n + h) \tag{D.34}$$

$$\begin{aligned}\delta\dot{l} = {} & \delta V_E .\sec(L)/(R_e + h) + \delta V_E .\sec(L).\tan(L).\delta L /(R_e + h) \\ & -\delta V_E .\sec(L).\delta h /(R_e + h)\end{aligned} \tag{D.35}$$

APPENDIX E

STATE SPACE REPRESENTATION OF THE NAVIGATION EQUATIONS

Error propagation equations of navigation states can be represented in state space formulation for Kalman filter implementation;

$$\dot{x} = F.x + G.w \tag{E.1}$$

$$z = H.x + v \tag{E.2}$$

Where x, w and v can be defined as follows;

$$x = \begin{pmatrix} \gamma^N \\ \delta V^N \\ \delta L \\ \delta l \\ \delta h \\ B_a^B \\ B_g^B \end{pmatrix} \tag{E.3}$$

$$w = \begin{pmatrix} N_a \\ N_g \end{pmatrix} \tag{E.4}$$

For magnetometer aiding;

$$v = \left(N_{Mgn} \right) \tag{E.5}$$

For GPS aiding;

$$v = \begin{pmatrix} N_{pos} \\ N_{vel} \end{pmatrix} \tag{E.6}$$

γ^N : Attitude error vector

δV^N : Velocity error vector

δL : Latitude error

δl : Longitude error

δh : Altitude error

B_a^B : Accelerometer bias vector

B_g^B : Gyro bias vector

N_a : Accelerometer noise vector

N_g : Gyro noise vector

N_{Mgn} : Magnetometer noise vector

N_{pos} : GPS position uncertainty

N_{vel} : GPS velocity uncertainty

The system matrix is given as;

$$\mathrm{F} = \begin{pmatrix} \mathrm{F}_{11} & \mathrm{F}_{12} & \mathrm{F}_{13} & \mathrm{F}_{14} & \mathrm{F}_{15} \\ \mathrm{F}_{21} & \mathrm{F}_{22} & \mathrm{F}_{23} & \mathrm{F}_{24} & \mathrm{F}_{25} \\ \mathrm{F}_{31} & \mathrm{F}_{32} & \mathrm{F}_{33} & \mathrm{F}_{34} & \mathrm{F}_{35} \\ \mathrm{F}_{41} & \mathrm{F}_{42} & \mathrm{F}_{43} & \mathrm{F}_{44} & \mathrm{F}_{45} \\ \mathrm{F}_{51} & \mathrm{F}_{52} & \mathrm{F}_{53} & \mathrm{F}_{54} & \mathrm{F}_{55} \end{pmatrix} \tag{E.7}$$

$$F_{11} = \begin{pmatrix} 0 & -\Omega\sin(L) - V_E / R_e \tan L & V_N / R_n \\ \Omega\sin(L) + V_E / R_e \tan L & 0 & \Omega\cos(L) + V_E / R_e \\ -V_N / R_n & -\Omega\cos(L) - V_E / R_e & 0 \end{pmatrix} \quad \text{(E.8)}$$

$$F_{12} = \begin{pmatrix} 0 & 1/R & 0 \\ -1/R & 0 & 0 \\ 0 & -\tan(L)/R & 0 \end{pmatrix} \quad \text{(E.9)}$$

$$F_{13} = \begin{pmatrix} -\Omega\sin(L) & 0 & -(V_E / R_E)^2 \\ 0 & 0 & -V_N /(R_N)^2 \\ -\Omega\sin(L) - V_E /(R_e(\cos L)^2) & 0 & V_E \tan(L)/R^2 \end{pmatrix} \quad \text{(E.10)}$$

$$F_{14} = -C_B^N \quad \text{(E.11)}$$

$$F_{21} = C_B^N . \tilde{a}^B \quad \text{(E.12)}$$

$$F_{22} = \begin{pmatrix} V_D / R_n & -2\Omega\sin(L) - V_E / R_e \tan L & V_N / R_n \\ -2\Omega\sin(L) - V_E / R_e \tan L & 1/R(V_N \tan(L) + V_D) & 2\Omega\cos(L) + 2V_E / R_e \\ -2V_N / R_n & -2\Omega\cos(L) - 2V_E / R_e & 0 \end{pmatrix} \quad \text{(E.13)}$$

$$F_{23} = \begin{pmatrix} V_E(2\Omega\cos(L) - V_E /(R_e(\cos L)^2) & 0 & (V_E{}^2 \tan(L) - V_D V_N)/R^2 \\ 2\Omega(V_N \cos(L) - V_D \sin(L)) + V_D V_N /(R_e(\cos L)^2) & 0 & V_E(V_N \tan(L) - V_D)/R^2 \\ 2\Omega V_E \sin(L) & 0 & (V_N{}^2 + V_E{}^2)/R^2 \end{pmatrix} \quad \text{(E.14)}$$

$$F_{25} = C_B^N . \tilde{w}^B \quad \text{(E.15)}$$

$$F_{32} = \begin{pmatrix} 1/R & 0 & 0 \\ 0 & 1/(R\cos(L)) & 0 \\ 0 & 0 & -1 \end{pmatrix} \quad \text{(E.16)}$$

$$F_{33} = \begin{pmatrix} 0 & 0 & V_N / R_n^{\,2} \\ 0 & 1/(R\cos(L)) & -V_E /(R^2 \cos(L)) \\ 0 & 0 & 0 \end{pmatrix} \tag{E.17}$$

$$F_{15} = F_{24} = F_{31} = F_{34} = F_{35} = 0_{3x3} \tag{E.18}$$

$$F_{41} = F_{42} = F_{43} = F_{44} = F_{45} = 0_{3x3} \tag{E.19}$$

$$F_{51} = F_{52} = F_{53} = F_{54} = F_{55} = 0_{3x3} \tag{E.20}$$

The system noise matrix can be simply written as;

$$G(x) = \begin{pmatrix} I_{3x3} & 0_{3x3} \\ 0_{3x3} & I_{3x3} \end{pmatrix} \tag{E.21}$$

For magnetometer and GPS aiding, measurement matrices can be expressed as follows, respectively;

$$H(x) = \begin{pmatrix} C_B^N B^B & 0_{3x3} & 0_{3x3} & 0_{3x3} & 0_{3x3} \end{pmatrix} \tag{E.22}$$

$$H(x) = \begin{pmatrix} 0_{3x3} & I_{3x3} & 0_{3x3} & 0_{3x3} & 0_{3x3} \\ 0_{3x3} & 0_{3x3} & I_{3x3} & 0_{3x3} & 0_{3x3} \end{pmatrix} \tag{E.23}$$

APPENDIX E

MATLAB CODE FOR MAGNETOMETER AND GPS AIDED NAVIGATION SIMULATION

Main.m

```
% Main Module

% clear all
% close all
% clc
% commandwindow

% Initiate the simulation parameters

INET_INPUT
% Start the simulation loop

% disp(' ')
% disp('---------------------- SIMULATION IS STARTED ----------------------')
Master = load('traj.dat') ;
```

```
% Outer Navigation Loop
i=1;
j=1;


for t=0:dt:(tmax-dt)
   % Calculate the Inertial Measurement Unit errors

[S_WB_IB_CORE,S_aB_SF_CORE] =
INET_IMUERROR(S_WB_IB,S_aB_SF, imu_bias_gyr_vector ,
imu_bias_acc_vector
,imu_F_scal_matrix,imu_G_scal_matrix,imu_rnd_gyr_vector,imu_rnd_acc_vecto
r);

[lat,lon,alt,velocity_vector,CL_B,phi,theta,psi,V_tot_ins]=
INET_ins(S_aB_SF_CORE ,S_WB_IB_CORE,CL_B, velocity_vector,lat,lon,alt
) ;



J=magfd(2005,1,M_h,90-M_Lat*180/pi,M_Lon*180/pi);

H= J(1:3)'*10^-5*1000;
B= S_CL_Bm'*H +INET_randgauss(0,[1 1 1]');

[Z1] = INET_MEASUREMENT_MAG_ONLY (H,B,BDOT, CL_B,
S_CL_Bm);
INET_ESTIMATION_AHRS(obs,Z_ahrs_vel,X,R,Rn_ahrs_vel,CL_B
,S_aB_SF_CORE, S_WB_IB_CORE, FAb, FAs, FGb
,FGs,M_CL_B,M_WB_IB,S_Latm ,velocity_vector,B,U,S_aB_SF_CORE);
```

```
%       [lat,lon,alt,       velocity_vector,CL_B,       phi,theta,psi,Ab,Gb,As,Gs]=
INET_FEEDBACK3a(lat,lon,alt, velocity_vector, phi,theta,psi,X);
%     disp(sprintf( ' Estimation Procedure is completed...'));
```

Magfd.m

```
function  J=magfd(DATE,ITYPE,ALT,COLAT,ELONG)
%  MAGFD
%  Function to compute Earths magnetic field
%  and components: X,Y,Z,T for a given latitude
%  and longitude, date and altitude.
%  Uses MATLAB MAT files sh1900.mat to sh2005.mat in 5 yr
%  intervals.
%
%  Usage: out=magfd(DATE,ITYPE,ALT,COLAT,ELONG);
%
%  DATE = date of survey (decimal years)
%  ITYPE=1 for geodetic to geocentric (USE 1)
%  ALT = altitude of survey relative to sealevel (km +ve up)
%  COLAT=90-latitude (decimal degrees)
%  ELONG=longitude of survey (decimal degrees)
%
%  Output array out contains components X,Y,Z,T in nanoteslas
%   X north component
%   Y east component
%   Z vertical component +ve down
%   T total field magnitude
%
%igrfyear=2000;
%igrffile='sh2000';
%DGRF=[1900:5:2000];
```

```
DGRF=[1900:5:2005];
igrfyear=2005;
igrffile='sh2005';
pl=0;
if DATE < 0, pl=1; end
DATE=abs(DATE);
% Determine year for base DGRF to use.
 if DATE < igrfyear,
  BASE=fix(DATE-DGRF(1));
  i=fix(BASE/5)+1;
  BASE=DGRF(i);
%   if pl==0,
%       fprintf('Using DGRF base year %f \n',BASE);
%   end
  eval(['load sh',num2str(BASE)])
  % loads agh and agh41 but now need to get
   iagh=agh;iagh41=agh41;
  % load next epoch
  eval(['load sh',num2str(DGRF(i+1))])
   eagh=agh;eagh41=agh41;
   dgh=(eagh-iagh)./5;dgh41=(eagh41-iagh41)./5;
   agh=iagh;agh41=iagh41;
   clear iagh iagh41 eagh eagh41
   T = DATE - BASE;
 else
%   if pl==0,
%       fprintf('Using IGRF base year %f \n',igrfyear);
%   end
  eval(['load ',igrffile])   % load in igrf data file
  T     = DATE - igrfyear;
 end
% combine spherical harmonic coefficients from first 8 degrees
```

```
% with degrees 9 and 10
 agh=[agh,agh41];
 dgh=[dgh,dgh41];
%
     D2R   = pi/180;
     R     = ALT;
     ONE   = COLAT*0.01745329;
     SLAT  = cos(ONE);
     CLAT  = sin(ONE);
     ONE   = ELONG*0.01745329;
     CL(1) = cos(ONE);
     SL(1) = sin(ONE);
     X     = 0.0;
     Y     = 0.0;
     Z     = 0.0;
     CD    = 1.0;
     SD    = 0.0;
     L     = 1;
     M     = 1;
     N     = 0;
if ITYPE == 1   % CONVERSION FROM GEODETIC TO GEOCENTRIC
COORDINATES
    A2    = 40680925.;  % squared semi major axis
    B2    = 40408588.;  % squared semi minor axis
    ONE   = A2*CLAT*CLAT;
    TWO   = B2*SLAT*SLAT;
    THREE = ONE + TWO;
    FOUR  = sqrt(THREE);
    R     = sqrt(ALT*(ALT + 2.0*FOUR) + (A2*ONE + B2*TWO)/THREE);
    CD    = (ALT + FOUR)/R;
    SD    = (A2 - B2)/FOUR*SLAT*CLAT/R;
    ONE   = SLAT;
```

```
   SLAT  = SLAT*CD - CLAT*SD;
   CLAT  = CLAT*CD +  ONE*SD;
end
   RATIO = 6371.2/R;
%
%      COMPUTATION OF SCHMIDT QUASI-NORMAL COEFFICIENTS  P
AND X(=Q)
%
     P(1)  = 2.0*SLAT;
     P(2)  = 2.0*CLAT;
     P(3)  = 4.5*SLAT*SLAT - 1.5;
     P(4)  = 5.1961524*CLAT*SLAT;
     Q(1)  = -CLAT;
     Q(2)  =  SLAT;
     Q(3)  = -3.0*CLAT*SLAT;
     Q(4)  = 1.7320508*(SLAT*SLAT - CLAT*CLAT);

NMAX=10; % Max number of harmonic degrees
NPQ=(NMAX*(NMAX+3))/2;
for K=1:NPQ,
 if N < M
   M     = 0;
   N     = N + 1;
   RR    = RATIO^(N + 2);
   FN    = N;
 end
 FM    = M;
 if K >= 5 %8,5,5
   if (M-N) == 0 %,7,6,7
      ONE   = sqrt(1.0 - 0.5/FM);
      J     = K - N - 1;
      P(K)  = (1.0 + 1.0/FM)*ONE*CLAT*P(J);
```

```
      Q(K)  = ONE*(CLAT*Q(J) + SLAT/FM*P(J));
      SL(M) = SL(M-1)*CL(1) + CL(M-1)*SL(1);
      CL(M) = CL(M-1)*CL(1) - SL(M-1)*SL(1);
   else
      ONE   = sqrt(FN*FN - FM*FM);
      TWO   = sqrt((FN - 1.0)^2 - FM*FM)/ONE;
      THREE = (2.0*FN - 1.0)/ONE;
      I     = K - N;
      J     = K - 2*N + 1;
      P(K)  = (FN + 1.0)*(THREE*SLAT/FN*P(I) - TWO/(FN - 1.0)*P(J));
      Q(K)  = THREE*(SLAT*Q(I) - CLAT/FN*P(I)) - TWO*Q(J);
   end
%
%    SYNTHESIS OF X, Y AND Z IN GEOCENTRIC COORDINATES
%
 end
 ONE   = (agh(L) + dgh(L)*T)*RR;

 if M == 0 %10,9,10
   X     = X + ONE*Q(K);
   Z     = Z - ONE*P(K);
   L     = L + 1;
 else
   TWO   = (agh(L+1) + dgh(L+1)*T)*RR;
   THREE = ONE*CL(M) + TWO*SL(M);
   X     = X + THREE*Q(K);
   Z     = Z - THREE*P(K);
   if CLAT > 0 %12,12,11
      Y = Y+(ONE*SL(M)-TWO*CL(M))*FM*P(K)/((FN + 1.0)*CLAT);
   else
      Y = Y + (ONE*SL(M) - TWO*CL(M))*Q(K)*SLAT;
   end
```

```
   L     = L + 2;
 end
   M     = M + 1;
end
%     CONVERSION TO COORDINATE SYSTEM SPECIFIED BY ITYPE
ONE   = X;
X     = X*CD +  Z*SD;
Z     = Z*CD - ONE*SD;
T     = sqrt(X*X + Y*Y + Z*Z);
J=[X,Y,Z,T];
%  END
```

IMUERROR.m

```
function [S_WB_IB_CORE,S_aB_SF_CORE] = INET_IMUERROR(S_WB_IB,S_aB_SF,imu_bias_gyr_vector , imu_bias_acc_vector
,imu_F_scal_matrix,imu_G_scal_matrix,imu_rnd_gyr_vector,imu_rnd_acc_vecto r)

%Function  to compute simulated IMU outputs
% S_WB_IB: reference gyro outputs
% S_aB_SF: reference accelerometer outputs
% imu_F_scal_matrix: Scale factor and misalignment error matrix for gyro
% imu_G_scal_matrix: Scale factor and misalignment error matrix for %accelerometer
% imu_bias_gyr_vector: Gyro bias vector
% imu_bias_acc_vector: Accelerometer bias vector
% imu_rnd_gyr_vector: Gyro noise vector
%,imu_rnd_acc_vector: Accelerometer noise vector
```

```
S_WB_IB_CORE = S_WB_IB+ imu_F_scal_matrix*S_WB_IB + imu_bias_gyr_vector + INET_randgauss(0,imu_rnd_gyr_vector);

S_aB_SF_CORE = S_aB_SF+ imu_G_scal_matrix*S_aB_SF + imu_bias_acc_vector + INET_randgauss(0,imu_rnd_acc_vector);
```

ESTIMATION.m

```
function [obs X Pe Phi U] = INET_ESTIMATION(obs,Z,X,R,Rn,CN_B ,S_aB_SF, S_WB_IB,M_CL_B,M_WB_IB ,Lat, velocity_vector,B,U)

global r_m_s states i
global dte CL_N deltaVx deltaVy deltaVz deltapitch deltaroll deltayaw deltaAccbias deltaAccscale deltaGyrbias deltaGyrscale deltaLat deltaLon deltah
persistent init_flag_est P Q

if isempty(init_flag_est)


   obs=zeros(states);
   U=zeros(states,1);
P = zeros(states,states) ;

% Covariance Related to deltavN
P(1,1) =  deltaroll  ;
P(2,2) = deltapitch ;
P(3,3) = deltayaw ;
% Covariance Related to gamma
```

```
P(4,4) = deltaVx;
P(5,5) = deltaVy;
P(6,6) = deltaVz ;

% Covariance Related to Accelerometer Bias Error

P(7,7) = deltaLat;
P(8,8) = deltaLon;
P(9,9) = deltah;



P(10,10) = deltaAccbias;
P(11,11) = deltaAccbias;
P(12,12) = deltaAccbias;

% Covariance Related to Accelerometer SF Error
P(13,13) = deltaAccscale ;
P(14,14)  = deltaAccscale ;
P(15,15)= deltaAccscale ;

% Covariance Related to Gyro Bias Error
P(16,16) = deltaGyrbias;
P(17,17) = deltaGyrbias;
P(18,18) = deltaGyrbias;

% Covariance Related to Gyro SF Error
P(19,19) = deltaGyrscale;
P(20,20) = deltaGyrscale;
P(21,21) = deltaGyrscale;

 U(1:3,1) = [ 0 0 0]' ;
U(4:6,1) = [ 0 0 0]';
```

```
U(7:9,1) = [ 0 0 0]' ;
U(10:12,1) = [ 0 0 0]' ;
U(13:15,1) = [ 0 0 0]' ;
U(16:18,1) = [ 0 0 0]' ;
U(19:21,1) = [ 0 0 0]' ;


   init_flag_est = 1 ;

end
F = getF(CN_B,S_aB_SF,S_WB_IB,FAb,FAs,FGb,FGs,Lat,velocity_vector);

G = getG(CN_B);
H = getH(CN_B,S_WB_IB,B);

Gm = getGm(CN_B,S_WB_IB) ;

% State Transition Matrix
 Phi =  expm(F*dte);


%Covariance Equations
X=X-U;
  X= Phi*(X);

P = abs((Phi*P*Phi' + G*R*G'));


Kn = P*H'* inv(H*P*H'+ Gm*Rn*Gm');


X=  X +Kn*(Z - H*X) ;
```

```
P= abs(((eye(21)- Kn*H)*P));
Pe=P;
U(1:3,1) = X(1:3) ;
U(4:21,1) = zeros(18,1);
```